Development of subject-specific musculoskeletal models for studies of lumbar loading

Michael Putzer

Vollständiger Abdruck der von der Fakultät für Bauingenieurwesen und Umweltwissenschaften der Universität der Bundeswehr München zur Erlangung des akademischen Grades eines

Doktors der Ingenieurwissenschaften
Dr.-Ing.

genehmigten Dissertation.

Gutachter:
1. Prof. Dr.-Ing. Ingo Ehrlich
2. Univ. Prof. Dr.-Ing. habil. Norbert Gebbeken

Die Dissertation wurde am 12.06.2018 bei der Universität der Bundeswehr München eingereicht und durch die Fakultät für Bauingenieurwesen und Umweltwissenschaften am 07.11.2018 angenommen. Die mündliche Prüfung fand am 29.11.2018 statt.

Acknowledgements

First and foremost, I would like to express my sincere gratitude to my advisor Professor Sebastian Dendorfer. He supported me since the beginning of my work in the laboratory for biomechanics as a master student. Your knowledge, guidance and motivation were invaluable to me to complete this work and the years as member of your laboratory team taught me countless things. Without you as a mentor I would not be where I am today. Thank you.

I would also like to express my sincere gratitude to my second advisor Professor Ingo Ehrlich. His commitment enabled the cooperative doctorate between the Ostbayerische Technische Hochschule Regensburg and the University of the Bundeswehr München. Our conversations helped and motivated me each and every time.

Furthermore, I want to thank Professor Norbert Gebbeken for his willingness to support this cooperative doctorate and for his valuable comments to my work. I highly appreciated each of our meetings.

Another thanks to Professor Michael Brünig for leading the Kolloquium and Andreas Kastenmeier for giving me his thoughts about my writings. I would also like to thank Klaus Bortenschlager for giving me the opportunity to complete this work at my new workplace.

I would also like to thank all my colleagues and students who accompanied me.

And at last, a very special thanks to my beloved wife Andrea for her continued patience and endless support throughout all the hard times during the completion of this work.

Abstract

Anatomical differences between individuals are often neglected in musculoskeletal models, but they are necessary in case of subject-specific questions regarding the lumbar spine. A modification of models to each subject is complex and the effects on lumbar loading are difficult to assess.

The objective of this thesis is to create a validated musculoskeletal model of the human body, which facilitates a subject-specific modification of the geometry of the lumbar spine. Furthermore, important parameters are identified in sensitivity studies and a case study regarding multifidus muscle atrophy after a disc herniation is conducted.

Therefore, a generic model is heavily modified and a semi-automatic process is implemented. This procedure remodels the geometry of the lumbar spine to a subject-specific one on basis of segmented medical images. The resulting five models are validated with regard to the lumbar loading at the L4/L5 level. The influence of lumbar ligament stiffness is determined by changing the stiffness values of all lumbar ligaments in eleven steps during a flexion motion. Sensitivities of lumbar loading to an altered geometry of the lumbar spine are identified by varying ten lumbar parameters in simulations with each model in four postures. The case study includes an analysis of the loading of the multifidus muscle and of the lumbar discs throughout various stages of disc herniation. This time each model performs four motions with two different motion rhythms.

The results indicate that lumbar motion and loading is dependent on lumbar ligament stiffness. Furthermore, subject-specific modelling of the lumbar spine should include at least the vertebral height, disc height and lumbar lordosis. The results of the case study suggest that an overloading of the multifidus muscle could follow disc herniation. Additionally, a subsequent atrophy of the muscles could expose adjacent levels to an increased loading, but these findings are highly dependent on the individual.

Kurzfassung

Anatomische Unterschiede zwischen Individuen bleiben in muskuloskelettalen Modellen oft unberücksichtigt, sind aber bei subjekt-spezifischen Fragen zur Lendenwirbelsäule (LWS) nötig. Eine entsprechende Anpassung von Modellen für jedes Subjekt ist aufwendig und die Auswirkungen auf die Belastung in der LWS sind schwierig abzuschätzen.

Ziel dieser Arbeit ist die Erstellung eines validierten, muskuloskelettalen Menschmodells, dessen Geometrie der LWS subjekt-spezifisch angepasst werden kann. Weiterhin werden wichtige Sensitivitäten des Modells identifiziert, sowie eine Fallstudie zur Atrophie des Multifidusmuskels nach einer Bandscheibenruptur durchgeführt.

Hierfür wird ein generisches Modell stark modifiziert und ein in großen Teilen automatisch ablaufender Prozess integriert, welcher die modellierte LWS auf Grundlage segmentierter computertomographischer Bilder subjekt-spezifisch anpasst. Die fünf damit erstellten Modelle werden hinsichtlich der Last der L4/L5 Bandscheibe validiert. Der Einfluss der Bändersteifigkeit wird mittels Variation der Steifigkeit aller Bänder in elf Schritten während einer Flexionsbewegung untersucht. Die Sensitivität der lumbalen Belastung bzgl. der Geometrie der LWS wird ermittelt, indem zehn Parameter der LWS in den fünf Modellen und in vier Haltungen variiert werden. Die Fallstudie beinhaltet die Analyse der Belastung der Multifidusmuskulatur und jene der Bandscheiben unter verschiedenen Degenerationsstufen. Dazu werden alle fünf Modelle mit vier Bewegungen sowie zwei Bewegungsrhythmen simuliert.

Die Ergebnisse zeigen eine Abhängigkeit der Bewegung und der Belastung von der Bändersteifigkeit. Sie lassen außerdem erkennen, dass für subjekt-spezifische LWS Modelle mindestens die Wirbelkörper- und Bandscheibenhöhe, sowie die Krümmung der LWS angepasst werden sollten. Die Fallstudie zeigt, dass eine Überlastung der Multifidusmuskulatur aufgrund einer Bandscheibenruptur auftreten kann. Die folgende Atrophie der Muskulatur kann die angrenzenden Bandscheiben einer erhöhten Belastung aussetzen. Allerdings ist dies stark vom Individuum abhängig.

Contents

List of acronyms and symbols

All acronyms and symbols, which are used throughout this thesis, are listed subsequently.

Acronyms

AF	annulus fibrosus
ALL	anterior longitudinal ligament
AMMR	AnyBody Managed Model Repository
AMS	AnyBody Modeling System
AP	anterior-posterior
API	application programming interface
BMI	body mass index
CNS	central nervous system
COM	centre of mass
COR	centre of rotation
CSA	cross-sectional area
CT	computer tomographic
DiH	disc height
EMG	electromyography
FCL	facet capsular ligament
FDK	force dependent kinematics
FE	finite element
IAP	intra-abdominal pressure
IDP	intradiscal pressure
ISL	interspinous ligament
ITL	intertransverse ligament
IVD	intervertebral disc
LF	ligamenta flava
LOR	lordosis angle
ML	medio-lateral
NP	nucleus pulposus
PA	posterior-anterior
PCSA	physiological cross-sectional area
PDL	pedicle length
PLL	posterior longitudinal ligament
RBF	radial basis function
ROM	range of motion
SPL	spinous process length
SR	spine rhythm

SSL	supraspinous ligament
STL	stereolithography
TPW	transverse process width
VBD	vertebral body depth
VBH	vertebral body height

Latin symbols

A	area, parameter
B	parameter
c	coefficient
$\mathbf{C}$	matrix of coefficients
d	depth
F	force
f	function
G	objective function
h	height
I	insertion node
k	factor, stiffness
L	bony landmark
l	length
$\mathbf{l}$	position vector of bony landmark
M	moment
m	mass
$\mathbf{M}$	matrix
N	normalization criterion, via node
n	normal
O	origin node
$\mathbf{o}$	origin point of radial basis function
P	parameter, pressure module
p	power, pressure
R	body fat percentage, ratio
r	ratio
s	scaling factor
$\mathbf{u}$	vector
V	volume
$\mathbf{v}$	vector
$\mathbf{w}$	vector
x	variable
y	variable

Greek symbols

α	rotation around first principle axis

β	rotation around second principle axis
ε	strain
γ	rotation around third principle axis
Φ	radial basis function
φ	angle
Θ	rotational displacement

Indices

a	anterior
BMI	body mass index
C	correction factor
c	compressive, compression
cont	contact
cor	centre of rotation
d	depth
def	default
Disc	lumbar disc
E	external
EX	extension
FE	flexion-extension
FL	flexion
h	height
I	internal
ID	intradiscal
inf	inferior
jnt	joint
l	length
lat	lateral
M	muscle
m	mass
mean	mean value
nom	nominal
p	penetration, posterior
rot	rotation
sbj	subject
slack	slack length
sup	superior
t	tension
v	vertex

1 Introduction

Low back pain is an increasing issue in the modern civilisation and it affects a large part of the population. People working in offices suffer from it as well as construction workers. This is emphasised by Bitzer et al. [11] who reported an increase of 50.2 % in hospitalisation between 2006 and 2014 because of low back pain. The cause for this may be the influence of a wide variety of behaviours of individuals like malnutrition and resulting obesity, heavy lifting without a proper technique, decreasing activity or simply bad or constrained postures during various activities.

An analysis of the causes or preservation of a repeated injury can be very difficult because of complex human body data acquisition. Particularly spinal loading mechanisms are difficult to determine with an experimental approach because spinal muscles consist of various muscle layers and measurements of the loading and activation of deeper muscle layers is nearly impossible without influencing the top ones. Nonetheless, this knowledge is essential to understand spinal loading mechanisms. Simulations with musculoskeletal models are an excellent tool to gather such data. They facilitate scientists and engineers to analyse the context of mechanical degeneration in the human body, enable them to conduct a retrospective analysis of an injury or allow for research to diminish or avoid pain and disease by optimising body posture and motion at workplaces. Thus, musculoskeletal simulations can be used to support ergonomics and rehabilitation or for the design of a new implant or implant technology. Even more, simulations have the advantage of safety to patients with a delicate health and offer the possibility of studying a lot of loading and failure modes.

Current available human musculoskeletal models are mainly generic with the possibility to scale them to a specific body height, weight and body fat percentage. However, there are manifold aspects in which the human lumbar spine distinguishes between individuals: bone or intervertebral disc geometry, material properties e.g. of ligaments or discs, lumbar lordosis, just to name a few examples. Several of those parameters may influence the loading modes of the lumbar spine in musculoskeletal models but this has hardly been investigated. Therefore, a novel musculoskeletal model with an integrated semi-automated process to morph the geometry of the lumbar spine to a subject-specific one is created and analysed throughout this thesis.

1.1 Objective of this thesis

This thesis is fundamental research regarding the musculoskeletal simulation of the lumbar spine, hence, subject-specific models are created and their sensitivity to different parameters is analysed. Finally, a case study is conducted. Figure 1.1 depicts an overview of the workflow which can be grouped into the following three steps:

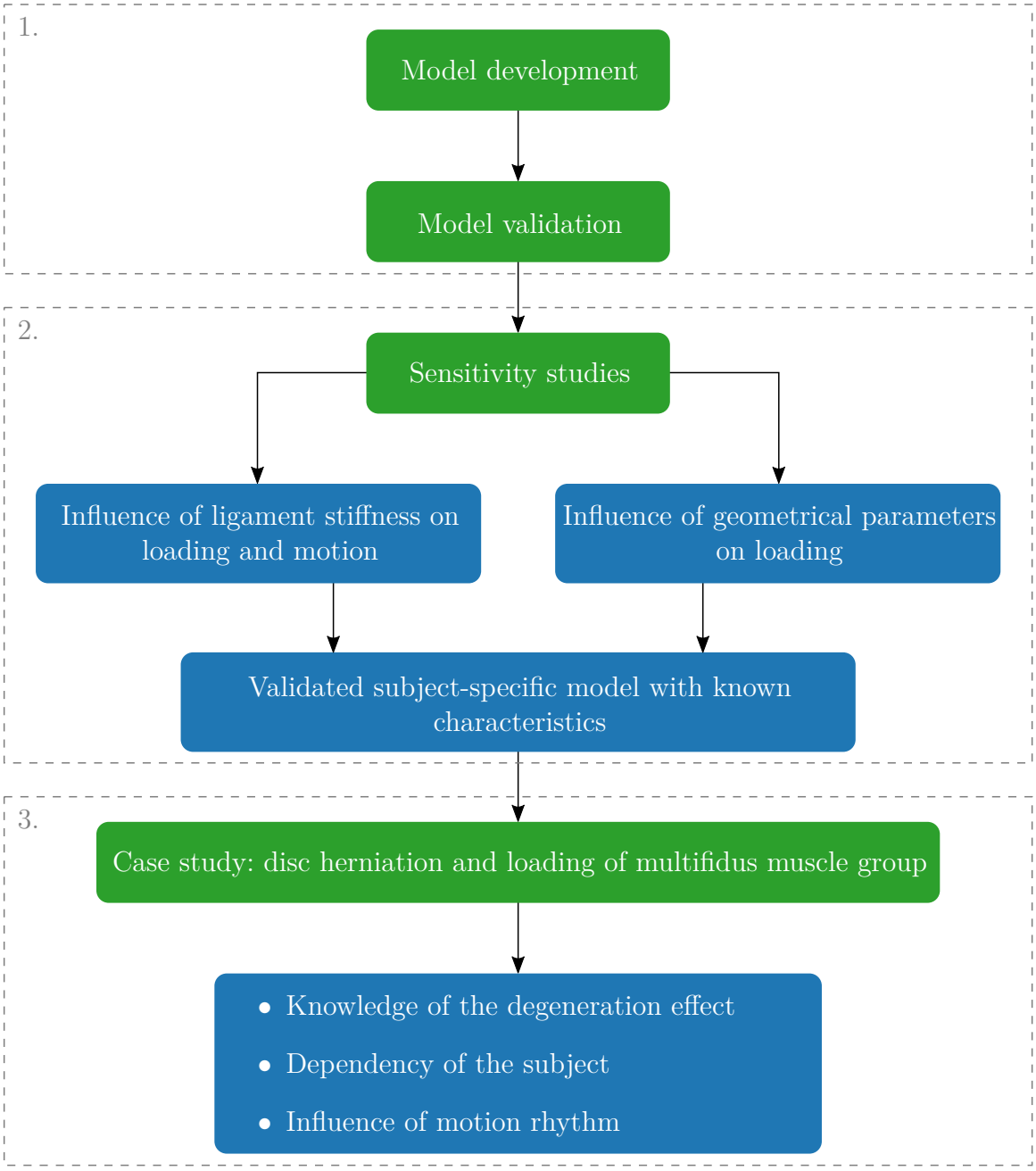

Figure 1.1: The chart shows the structure of this thesis with the main working packages (green) and respective results (blue).

1. Model development and validation,
2. evaluation of the sensitivity in specific areas,
3. application of the novel model to a real case.

The first step comprises the development of a musculoskeletal model with an exchangeable subject-specific lumbar spine and its validation with experimental data from literature. In the next step, the resulting validated model has to be evaluated in certain aspects to determine its sensitivity to different parameters. In this case, the studied elements are the ligament stiffness and lumbar geometrical parameters. The developed model in combination with the outcome of the sensitivity studies adds up to a validated model with known characteristics concerning the lumbar loading. Finally, this model is used in a case study regarding a disc herniation with following multifidus muscle atrophy and disc degeneration at an adjacent level.

A description of activities in every working package of the whole workflow (Figure 1.1) can be found subsequently:

Model development: The AnyBody Modeling System (AMS), a musculoskeletal modelling software, is utilised to build a new validated model of the lumbar spine which will be publicly available. This novel model is complemented with existing extremities, upper thorax and head from the AnyBody Managed Model Repository (AMMR) to a full musculoskeletal body model. The lumbar spine model itself includes vertebrae, facet joints, ligaments and discs as rotational joints with a specific stiffness. In addition, a subject-specific approach is used for the geometry of the lumbar vertebrae and their relative positions and orientations. The subject-specific modifications are not hard-coded instead they are based on parameters, hence it is possible to easily import data of different subjects. Furthermore, the contact between the facet joints of the lumbar spine are modelled as a surface contact. The disc stiffness is implemented with a linear relationship and the option to switch to a non-linear version. The relative motion of the lumbar vertebrae can be driven by a predetermined rhythm or the AMS computes the motion based on a quasi-static equilibrium of the lumbar forces. As stated above, the whole model is created with portability in mind. This ensures, that the anthropometry of the model can be easily modified and that the model can be applied to other tasks than those of this study.

Model validation: Published experimental data form the basis for the validation process. This data comprises various measurements of healthy subject's intradiscal pressures (IDPs) in different poses and with various loading conditions. Furthermore, the progress of the IDP over different motions is used to validate the model.

Sensitivity studies: In the next step, the sensitivity of the new lumbar spine model is assessed to determine the necessary level of modification for a subject-specific model. Of special interest is the effect of the stiffness of all lumbar ligaments on the kinetics and kinematics during flexion as well as the sensitivity of lumbar loading to changes of specific vertebral and spinal dimensions. The analysis regarding the former sensitivity includes simulations with flexion motions, body heights and

weights of three different subjects and it is focused on lumbar forces, moments and range of motions. The latter sensitivity study is conducted with five different models, each with an individual lumbar geometry, body weight and height. Here, the disc force between the forth and fifth lumbar vertebra is examined with the models in four basic postures and with various sizes of lumbar dimensions.

Case study: The models are used to understand the underlying degeneration effect of multifidus muscle atrophy following disc herniation. Therefore, a ruptured disc in various severity levels is modelled in the previous five models with the multifidus muscle group either activated or deactivated. The resulting changes in the loading of the multifidus muscle group and adjacent disc levels are evaluated. Furthermore, the influence of a specific spinal motion pattern on lumbar loading and multifidus muscle forces are determined. On the one hand, this case study gives knowledge about the underlying degeneration effect and, on the other hand, the influence of different subjects and spinal motion rhythms on lumbar loading are elaborated.

1.2 Outline of this work

The structure of this thesis is as follows. Chapter 2 explains technical terms used throughout this work and gives an overview of the current knowledge about the functional anatomy of the lumbar spine. It includes a review of the literature in terms of the examined case study, which concerns disc herniation and multifidus muscle atrophy. The chapter is complemented with information about currently available musculoskeletal models that concern the topics of this thesis. Chapter 3 contains a description of the utilised musculoskeletal modelling system, the AnyBody Modeling System (AMS), with technical terms of its elements, a brief explanation of its solver and special options. The following Chapter 4 contains the main work of this thesis, the development of a novel lumbar spine model with subject-specific geometry and method of validation. Additionally, the applied methods of the sensitivity studies and the case study are presented. The following chapter 5 includes the results of the model validation as well as the outcome of the studies. Those results are discussed in Chapter 6 and a brief summary and outlook are given in chapter 7.

2 The functional anatomy of the lumbar spine and regarding studies

The first sections of this chapter provide information about technical terms concerning the field of anatomy. The succeeding sections contain an overview of the functional anatomy in the area of the lumbar spine. These sections include the current knowledge about role and functionality of the described matter. Finally, an overview regarding state of the art musculoskeletal models of the lumbar spine is given.

2.1 Positions, directions and planes

There are several expressions which simplify a description of an anatomical position or direction as well as whole portions of the body. The latter is enabled by the definition of anatomical planes, as shown on the left side in Figure 2.1, each of which divides the body into two symmetrical halves. The sagittal plane separates the body into a left and a right part, while the coronal or frontal plane does this for the front half and the back half. The third plane, the axial plane, splits the body into an upper and a lower half.

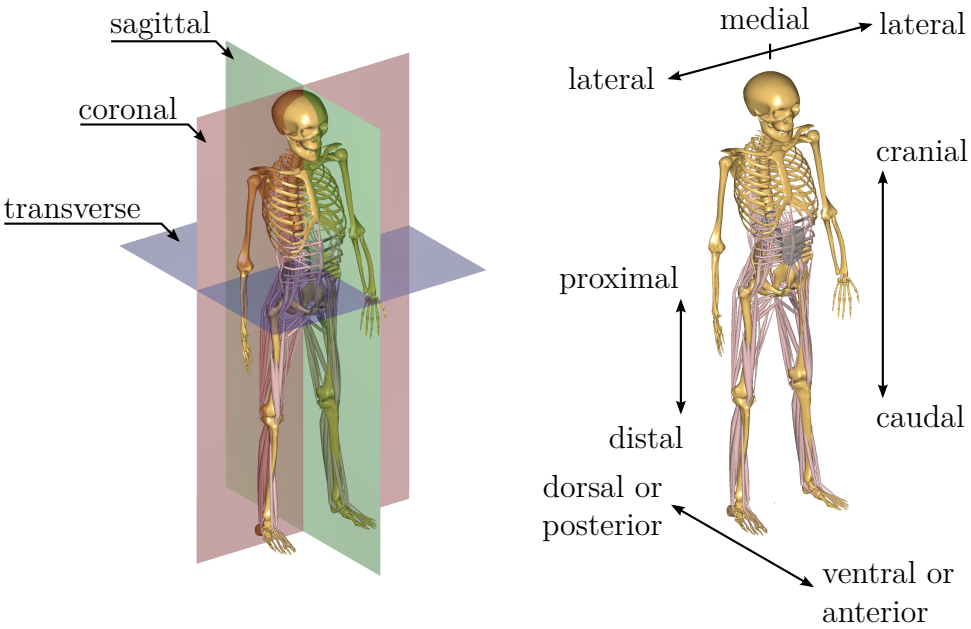

Figure 2.1: There are three principal planes which divide the body into two halves (left) and various anatomical directions and positions (right).

There are a lot of terms for anatomical positions and directions but this thesis will concentrate on the ones described in this paragraph. The right part of Figure 2.1 depicts a selection of phrases for various positions. A superior or inferior position means above or below something whereas an anterior position implies one located in front of something. Towards the rear or behind is called posterior. Medial positions mean locations toward the mid-line or away from the side. The opposite of this would be the lateral side, meaning away from the mid-line or toward the side. A proximal position is located close to the centre of the body while a distal position is contrary to that. Positions ventral indicate the ones toward the belly and dorsal positions are located towards the back. Further positions would be cranial and caudal. The first one means towards the head while the second one signifies towards the tail. All these terms describing anatomical positions, and combinations of them, are employed to form directional phrases, e.g. medio-lateral (ML) means from the mid-line to the outside or anterior-posterior (AP) denotes from front to back. Swapping the two positional terms leads to a reversed direction, for example posterior-anterior (PA) stands for 'from back to front'.

2.2 Motions and postures

The human anatomy allows countless motions and postures, however, this work is limited to only a few basic ones, such as flexion. It is a bending motion of a joint and is used for various movements throughout the body, e.g. flexion at the elbow means to move the forearm towards the upper arm. This work solely concentrates on studies about the spine, and hence, all terms will be explained within this scope. Therefore, flexion describes a forward bending motion of the trunk. The opposite movement is extension, which stretches a joint, and means moving the trunk backwards. Both motions occur exclusively in the sagittal plane. The corresponding postures are called flexed or extended. Furthermore, bending the trunk sidewards is called lateral bending (posture: lateral bended). While this motion happens in the coronal plane, axial rotation (posture: axial rotated) is carried out in the axial plane and describes a rotation about the vertical axis of the body. Another term for this motion is torsion. Figure 2.2 shows the explained motions or postures used throughout the studies.

2.3 Additional medical terms

The term in vivo is used for processes which occur in a living entity like a human, animal or plant. Contrary to that, in vitro describes studies made outside of a living organism, for example in a test tube or petri dish. Furthermore, the term in silico is employed for tasks carried out with the help of a computer, i.e. simulations. Another frequently used term is 'landmark' or 'bony landmark'. Every bone has a certain shape with protuberance, grooves, corners and edges, which serve as a guide to specific locations. These conspicuously irregularities are called bony landmarks.

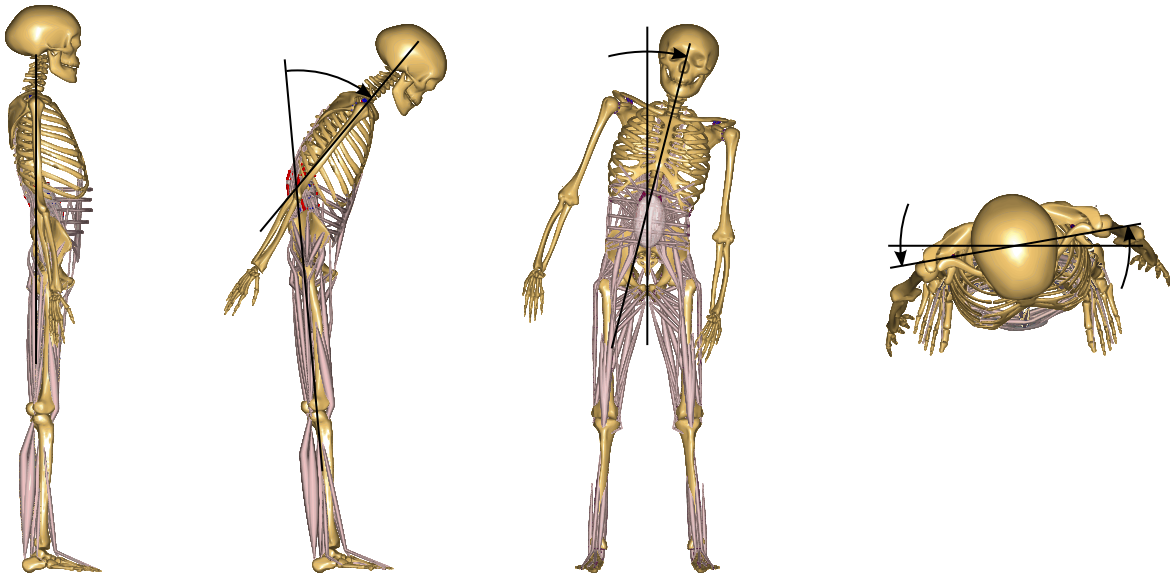

Figure 2.2: Selection of four basic postures used throughout this work (from left): upright standing, flexed, lateral bended and axial rotated.

2.4 Spinal column

The human spine consists of 24 vertebrae, grouped in three main clusters, the sacrum and the coccyx. Starting from the top, the first set is named the cervical spine and consists of seven vertebrae. It is followed by a group of twelve vertebrae, the thoracic spine, and another set of five vertebrae. The latter one is called lumbar spine. From a lateral view, the spine has several curves in which the lumbar spine has an inward curvature. This is also called a lordotic curvature or (lumbar) lordosis. The opposite of lordosis is kyphosis. It is suggested to specify the lordosis angle by Cobb method [7]. Usually, this technique specifies an angle, that is measured between a line at the upper endplate of the first lumbar vertebra and a line at the upper endplate of the sacrum. The mentioned regions, the spinal curvature as well as the Cobb angle are marked in Figure 2.3. The inferior end of the spine forms a joint at the sacrum level with the ilium of the pelvis and is called the sacroiliac joint. This connection is rather stiff due to very strong ligaments [84].

A spinal motion segment comprises two adjacent vertebrae, an intervertebral disc (IVD) and various ligaments.

2.5 Vertebrae

Every vertebra in each section is labelled with a character and a number, starting from the cranial end. Literature shows various labels but in the further course of this work the labelling reads as follows: C1 to C7 for vertebrae of the cervical spine, the ones of the thoracic spine are labelled with T1 to T12 and the vertebrae of the lumbar spine are labelled with L1 to L5.

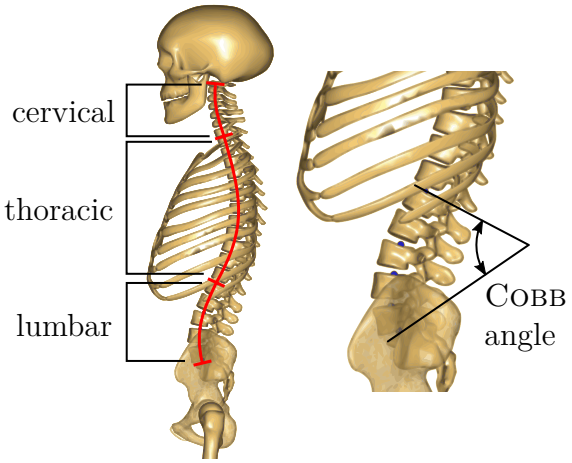

Figure 2.3: The spine in a natural shape (highlighted in red) with various spinal regions (left). Additionally, the lordosis angle measured with Cobb technique is depicted (right).

Each vertebra itself is divided into the vertebral body and the posterior parts. The latter includes seven processes, two pedicles and two laminae which form the vertebral arch. This arch in combination with the posterior side of the vertebral body encloses the spinal canal. It is also called the vertebral foramen. Following the arch from anterior to posterior, the vertebral body is connected to the transverse process by the pedicles, followed by the superior and inferior articular processes, the laminae and the most posterior part in form of the spinous process. The surfaces at the end of the superior and inferior articular processes are the facet joint surfaces. Figure 2.4 depicts the views from lateral and superior positions on a vertebra with all parts labelled. The vertebral dimensions were subject of several anatomical studies and the results of mean values have been published [10, 61, 62, 85].

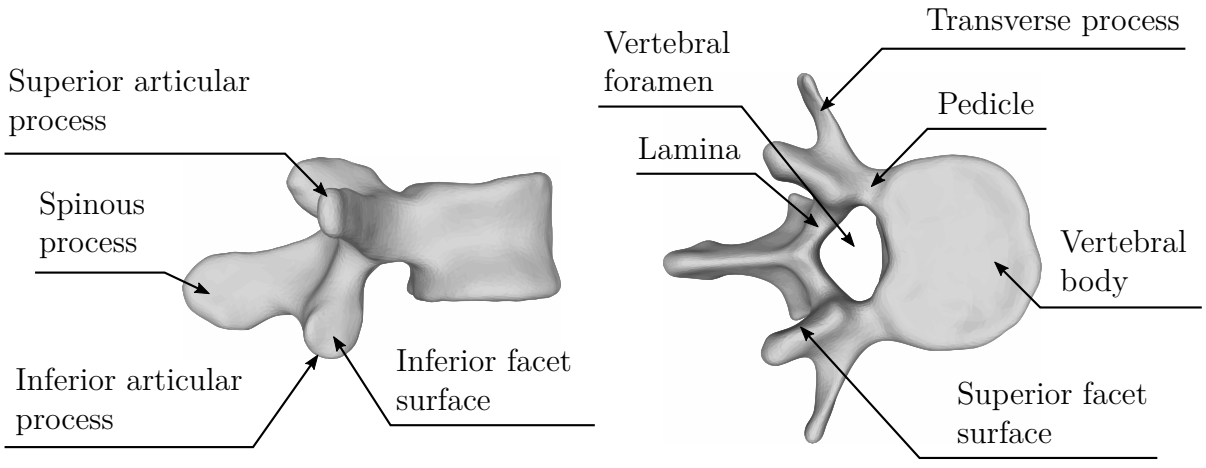

Figure 2.4: Views from lateral (left) and superior (right) position on a lumbar vertebra with all anatomical parts labelled.

2.6 Intervertebral disc

An intervertebral disc (IVD), located between the superior and inferior endplates of the vertebral bodies, connects adjacent vertebrae. It consists of two parts: the annulus fibrosus (AF) which contains the pressurised nucleus pulposus (NP). The AF is a circular fibrous structure comparable to a ligament. It connects two vertebrae and transmits tensile forces, while the NP is the gelatinous centre and resists compressive forces. The NP is incompressible because of the contained water. This water content changes in dependency of the loading throughout various activities due to diffusion of water and nutrients for the IVD [82]. As a consequence, high pressure, e.g. resulting from a standing posture, forces diffusion of water out of the NP and reduces the height of the IVD [50, 100]. Additionally, a high mechanical stress degenerates a disc much faster [53] which in turn decreases segmental stiffness, the height of the disc and load bearing abilities [100, 108]. Mechanical properties of the IVD, like its rotational or translational stiffness, were determined in various studies [83, 99]. It was reported that a healthy IVD has a much higher resistance to motions than one with a radial tear [83]. Furthermore, the stiffness of the discs increases with its size where significant parameters are its depth and width [51].

2.7 Facet joints

The facet joints are positioned bilateral between each end of the superior articular processes of an inferior vertebra and the inferior articular processes of the superior vertebra (Figure 2.5). The orientation of their contact surfaces are nearly vertical in the lumbar part. They consist of various bony, ligamentous and cartilaginous tissues. The bony parts are the mentioned ends of the articular processes which are covered with the cartilaginous tissues. These tissues are acting as sliding surfaces, whereas the ligamentous capsules are providing guidance and connection of the specific adjacent articular processes while they also wrap up the whole joint. These joints provide two functions: first, they transfer a

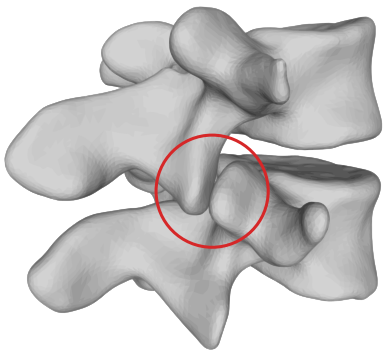

Figure 2.5: Posterior-lateral view on two adjacent vertebrae. Together, they form a motion segment and one of its bilateral facet joints is highlighted. Only the bony structure is present, which is usually covered by soft tissues like cartilaginous sliding surfaces and facet capsules.

portion of the load which is applied to the spine and second they limit excessive motion. The load transmissive function is increasing stability of the spinal column, and therefore, is giving the joints a stabilising role. This task is defective after removal of even a single joint in course of a surgery [2, 89]. Intervertebral shear forces and certain amounts of the compressive forces are transferred through them, provided the lumbar spine is in a lordotic posture [3]. This supports the load bearing of the intervertebral discs and results in additional loading if a disc's soft tissue is removed. Such a degeneration could almost double the loading of the facet joints [39]. The basic orientation of the joints does not affect intradiscal pressure or facet joint forces but an asymmetric orientation of the left and right side, as it can be in some subjects, could change it [41]. The function of limiting excessive motion is mostly active in axial rotation and extension but the capsular ligament limits flexion, too [1, 3, 36, 81, 89, 91]. However, contact between facet surfaces is also established in a lateral bended posture [81].

2.8 Ligaments

The lumbar vertebrae are connected by six different ligaments. The following lists the ligaments in order of their occurrence from an anterior-posterior direction: anterior longitudinal ligament (ALL), posterior longitudinal ligament (PLL), ligamenta flava (LF), intertransverse ligament (ITL), interspinous ligament (ISL) and supraspinous ligament (SSL) (Figure 2.6). The ALL runs alongside the anterior side of all vertebral bodies, nearly covering their complete width. Its collagen fibres are firmly attached to the bone, but the connection between disc and ligament is rather loose. On the opposite side of the vertebral bodies and through the vertebral foramen runs the PLL. It is much more narrow than the ALL at the bony level and its width increases slightly at disc level. The connection to the vertebral body is located at the superior and inferior posterior rim. The laminae of the superior and inferior vertebrae are the attachment points for the LF. These ligaments fill the space between the adjacent vertebral arches and cover up the spinal canal. The fourth ligament listed, the ITL, runs vertical and bilateral from the tips of the transverse processes of adjacent vertebrae. The last two ligaments link the spinous processes together. While the ISL interconnects the superior and inferior surfaces of two spinous processes, the SSL only runs from the tips of the spinous processes and is attached to the most posterior side of ISL.

All lumbar ligaments support the IVD and the facet capsules in their role as passive stabilisers of the spine. They share some functions with the IVD and the facet capsules. Their main function, stabilising the spinal column, is achieved by limiting the range of motion (ROM) [16, 36]. For example, the ALL counters extension while posterior ligaments mainly resist a flexion motion [36, 81]. ALL and PLL are not loaded during lateral bending or axial rotation [81]. In addition, their stabilising function reduces the forces exerted by the erector spinae muscle. Han et al. [32] reported this fact and concluded that 'individual muscle forces and their patterns were considerably affected by ligament stiffness'.

As stated above, ligaments are passive elements, and they only contribute to spinal stability if they are stretched. They solely transfer tensile forces which act at the ac-

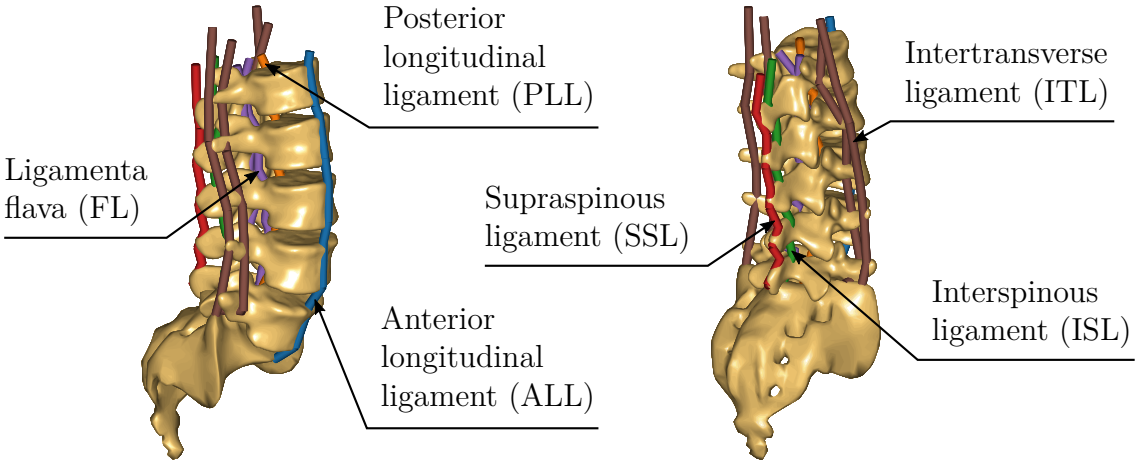

Figure 2.6: Illustration of a modelled lumbar spine including its ligaments' courses. All elements of the same colour represent a ligament. A few of them are depicted with more than a single string because they cover a wider area of the bone.

cording attachment points. Consequently, ligaments remain loose and do not produce any forces if they are compressed. The tensile characteristic of most ligaments is determined by extracting specimens of several cadavers and subjecting them to tensile test [15, 55, 67]. Additionally, these publications include individual mean stiffness values, which are defined by a linear regression line in the linear section of the force-deflection curve.

2.9 Muscles and stabilisation

There are different types of muscles in the human body: smooth, cardiac and skeletal muscles. In this work, the term muscle always describes skeletal muscles. They allow the body to move. Such muscles include a contractile element and two tendons which connect it to the bone. The contractile element consists of muscle fibres. These fibres are bundled and surrounded by a connective tissue. This tissue in combination with the contractile element is called muscle fascicle.

Usually, a muscle has two attachment points, one at each end. For this reason, the intermediate muscle tissue slides over the underlying bone or can even detach from it which is dependent on the joint's position. The muscle forces are transferred to the connecting bones in the muscle's line of action. The distances between attachment points and joint are the lever arms of the muscle. The term moment arm describes the perpendicular distance of a muscle's line of action to the joint. An optimal moment arm is present if the moment arm corresponds to the lever arm. There are some muscles with additional attachment points. They work like deviation points and affect the line of action as well as the moment arms of the muscles.

A muscle has two important functions with regard to musculoskeletal models: on the one hand, they provide the necessary forces to drive a joint, hence, enable body motion

and, on the other hand, muscles are very important to stabilise the body [9, 40]. For example, a flexion motion is not counteracted adequately by the ligaments, therefore, muscles have to work as stabilisers [16, 70]. An important role plays the multifidus muscle because it is a major stabiliser of the lumbar spine [97, 98]. It contributes to spinal orientation as well as to intersegmental motions by controlling intervertebral shear and torsion [31, 48, 54]. Additionally, the superficial fascicles stabilise the spine during flexion because they act contrary to the motion [48]. However, a co-activation of the psoas and multifidus, meaning an activity of agonist and antagonist, could destabilise the spine in flexion while it increases stability in axial rotation and lateral bending [70].

Multifidus muscle atrophy can be caused by different events: a reduction of multifidus cross-sectional area (CSA) is reported after a prolonged bed-rest [8] or it is often delineated that a degeneration of the multifidus muscle is connected to disc herniation [18, 23, 37, 38, 42]. One reason for a locally shrinking CSA of the muscle may be an impaired nerve root due to a disc rupture [106] but most of the time this is confined to a single side only. Whereas bilateral atrophy can be seen with disc herniation alone [18, 38, 42]. A long-term indication of multifidus muscle atrophy may be fat infiltration, yet, this occurs frequently in subjects with low back pain [44], after long physical inactivity [93] and it increases with age [86].

Disc degeneration further affects the muscle recruitment pattern: published results of a computational study show a decreasing activity of the multifidus musculature after disc degeneration [43]. Pain at the lower back could also lead to an altered muscle recruitment pattern; actually, a difference in muscle activity of an affected and unaffected side could be measured [19]. But even in a healthy condition, the activation of muscles is a highly individual matter [95].

In addition, the recruitment pattern has an influence on lumbar loading, too [101]. Furthermore, it is known, that tension of the musculature strongly affects the lumbar forces [107] and could increase the loading over all lumbar segments [12]. Especially, the multifidus could strongly affect this loading because it has a large physiological cross-sectional area (PCSA), hence, it contributes with a high magnitude to lumbar loading [12].

2.10 Lumbar loading and kinematics

The prediction and determination of lumbar loading is a very complex matter because of the manifold factors which are influencing it. It depends on body height and weight [6, 34] and differs heavily between various postures and activities [102]. External loads and especially lifting weights, even small ones, could change the forces in the lumbar spine by a large amount, too [77, 96]. Furthermore, simulations with a parametric and simplified finite element (FE) model of a lumbar motion segment determined the disc geometry and the position of the facets as major parameters regarding lumbar loading [58]. Direct measurement of lumbar loading or IDP in a healthy subject is very challenging, hence, only limited data is available and it is spread over a wide range [56, 80, 92, 102, 103].

Also, there was only some data published about subjects with back problems [80] and post-surgery [74–78, 90].

This data about IDP does provide knowledge about the loading of the anterior column of the spine but it is not directly comparable to a compressive force F_c as it is computed in musculoskeletal simulations. Therefore, an approximation of the form

$$F_c \approx p_{ID} \cdot A_{Disc} \cdot k_C \tag{2.1}$$

can be used to convert values [22, 57]. p_{ID} is the measured IDP, A_{Disc} represents the cross-sectional area of the according disc and k_C is an individual correction factor which is necessary to consider the shape and material properties of a subject's disc. It has to be determined in in vitro experiments. Literature indicates a range between 0.55 and 0.77 [22].

Furthermore, lumbar motion patterns can differ in each individual. Even reports about the ROM of lumbar motion segments are contradictory [46, 66], hence, each individual could have a special spine rhythm but with similar patterns in the motion sequences. Gatton and Pearcy [29] described four sequences which were determined in various flexion tasks. These motion patterns ranged from movement starting with the top vertebrae and ending with the lower ones to the exact opposite. A hybrid form, were the mid portion of the lumbar spine moved at last as well as motion of all segments at the same time was observed, too. The L5/S1 segment seems to contribute the least to the overall motion [4, 64]. A basic motion is not only performed with rotation of the vertebrae around the main axis because there is always the tendency to move in an additional direction. This is described as coupled motion and it is present in all tasks: flexion is coupled with lateral bending and axial rotation [66], axial rotation with lateral bending [87, 88] and flexion [26]. Coupled motions are also reported for lateral bending [45]. The orientation of the coupled motion does not necessarily have to be unidirectional and could change over the lumbar levels [88]. A herniated disc does not alter the coupled motions fundamentally, but they could differ in their range [45]. Furthermore, lumbar kinematics are also age-related, as the ROM seems to decrease for older subjects [13].

2.11 Musculoskeletal models of the lumbar spine

In recent history, numerical models have been used intensively to analyse various issues concerning the lumbar spine. They can be divided into two main groups: FE models and rigid body models. Most FE models are limited to the lumbar spine or a motion segment but often include sophisticated material models, detailed vertebral geometry and disc as well as ligaments [22, 59, 99]. A few FE models even consider muscles forces in the simulations [27, 107]. All loads that result from the rest of the body, from motions or from external factors have to be assumed or approximated. Rigid body models, by contrast, usually include the whole lumbar spine, larger parts of the human body or even the full body. Musculoskeletal models extend this by a multitude of muscles.

The work published by De Zee et al. [21] describes a detailed rigid body model of the lumbar spine for the AMS, an inverse dynamic simulation software, that computes muscle forces by an optimisation algorithm. This musculoskeletal model is free to use and it includes the pelvis, sacrum, all lumbar vertebrae and the thorax as a single lumped mass. All geometry was based on a specific subject (175 cm body height, 72 kg body weight), but everything was modelled symmetrical to the sagittal plane and the vertebrae were without mass and inertia. The whole model was fixed at the pelvis. The lumbar joints were implemented as spherical joints with hard-coded positions according to Pearcy and Bogduk [65]. Eight groups of muscles were considered in the model: multifidus muscle, erector spinae, psoas major, quadratus lumborum, rectus abdominus, obliquus externus and obliquus internus. Each group included a different number of fascicles (Table 2.1) that represent its various parts or layers. The courses of the individual muscle fibres were based on varying published data. The abdominal muscles required the rectus sheath for a realistic modelling, hence, this was implemented as a rigid body without mass and inertia properties. In addition, a model of the intra-abdominal pressure (IAP), in an experimental state at this time, was added. Besides the implementation of the transversus muscle, which was required for this, the IAP was modelled as a constant volume with attachments to the pelvic floor and bottom of the thorax. As soon as the transversus muscle was activated, it compressed the volume, which, in turn, presses on its attachments. This resulted in a force that straightens up the body. Intervertebral motions were controlled by the spine rhythm, that distributed flexion-extension, axial rotation or lateral bending, measured between pelvis and thorax, over all lumbar joints. This rhythm did not enable coupled motions but executed a basic movement solely around the according axis. The model was validated by the maximal moment in extension at the L5/S1 level and the IDP when holding a weight at a certain distance. Both validation simulations resulted in values that corresponded to the according published values. The model of De Zee et al. [21] was a first step for a general musculoskeletal model of the lumbar spine that could be applied to numerous tasks. It considered the contribution of muscles to the stabilisation of the spine during different motions. However, validation was not extensively and had to be enhanced. Moreover, it lacked lumbar ligaments and facets, but these elements play an important role in limiting motions, and they also stabilise the lumbar spine. Possibly, the muscles had to exert higher forces in order to compensate these missing passive elements which could raise spinal loading. Furthermore, influences of the lower body also were neglected and the vertebral geometry was limited to the symmetrical structure.

The above described model of the lumbar spine became the base model in the repository of the AMS. Galibarov et al. [28] continued the development of this model. They added six lumbar ligaments as single elements per level from T12 to the sacrum: the ALL, PLL, ISL, SSL, ITL and LF. The attachment points of all ligaments corresponded to anatomical landmarks found in literature and a linear elastic material model was used for these elements. Stiffness properties were derived from reported data [15, 67]. The addition of ligaments required a decrease of the disc stiffness, because their contribution was previously considered in these properties. Furthermore, Galibarov et al. [28] implemented the usage of the force dependent kinematics (FDK) solver at all lumbar joints. This new method to compute the orientation of joints is explained in Section 3.3. Basically, this

Table 2.1: A list of the number of fascicles per muscle group of the model of De Zee et al. [21] and the additional muscles of the model of Han et al. [35]. Each number considers both sides of the body, where applicable.

De Zee et al. [21]		Han et al. [35]	
Muscle group	No. of fascicles	Muscle group	No. of fascicles
Multifidus (lumbar)	38	Latissimus dorsi	10
Erector spinae	58	Simispinalis	18
Psoas major	22	Multifidus (thoracic)	24
Quadratus lumborum	10	Serratus posterior inferior	4
Rectus abdominus	1	Intertransversarii	22
Obliquus externus	12	Rotatores	22
Obliquus internus	12		
Transversus	5		

technique computed the orientation of the joints based on an equilibrium of all forces. Validation of this improved model was not included, instead the application of FDK was presented by adding elements with two different stiffness values between the pedicles of the L4/L5 level. These elements altered the spinal kinematics. The pre-defined spine rhythm, used previously, could not show a difference in kinematics due to an added stiffness. This new approach was a large step to subject-specific modelling of the lumbar spine because properties of the individual, like lumbar stiffness, divergent positions of attachment points or limiting structures such as the facets, could now alter the spinal motion pattern. However, this model still lacked an application of a subject-specific geometry and facet joints. Also, the inter-individual influence of lumbar shapes and properties on model output was still unknown. A more advanced version of this model is used as basis for the model development in this work.

Han et al. [35] used the full body model of the AMS that includes the detailed spine of De Zee et al. [21], legs, arms and skull. They expanded this model with missing muscles (Table 2.1 right), ligaments and a non-linear disc stiffness. Similar to Galibarov et al. [28], the ALL, PLL, ISL, SSL, ITL and LF were added. In addition, the capsular ligament was also implemented. All ligaments were modelled as tensile elements with a non-linear characteristic and experimental data was used to calibrate the according coefficients. The non-linearity of the disc stiffness was also based on experimental data. In addition, the heights of the discs were modified according to published mean values. Furthermore, the spinal rhythm of the flexion-extension motion was adapted to measurements of various subjects. Validation included a comparison with implant forces and IDP measurements as well as with predicted compression forces and muscle activation patterns. Most results showed a good agreement with the experimental data. Han et al. [35] concluded that all short muscles, passive elements and IAP should be added to a model, especially if predictions of lumbar loading during movements with a large ROM or with weighted activities are intended. However, no information about the PCSA of the short muscles were given and to my current knowledge no other studies are available that cover the

missing informations.

Christophy et al. [17] also created a generic musculoskeletal model of the lumbar spine. Similar to De Zee et al. [21], it included the five lumbar vertebrae, a rigid pelvis, sacrum and the thorax as a single lumped part. Masses and inertia properties were set according to reported data and the positions of the lumbar joints were determined by Pearcy and Bogduk [65]. Each joint was modelled with six degrees of freedom and a pre-defined spine rhythm that reduced the input to the angles of flexion-extension, axial rotation and lateral bending between the T12 vertebra and the sacrum. The joints lacked a stiffness model, no ligaments or facet joints were defined and the utilised OpenSim software prevented an accurate modelling of the IAP. However, the muscle apparatus, that consisted of the erector spinae, rectus abdomini, psoas major, quadratus lumborum, multifidus, latissimus dorsi and internal as well as external obliquus, was modelled with high detail. This musculoskeletal model did not use the simple muscle model, instead an advanced version of the Hill-type model was applied. The basic Hill-type muscle model simulates a muscle by a non-linear spring element, which represents the tendon, followed by a passive elastic spring in parallel with an active contractile element. The latter two elements represent the muscle itself. Both, muscle and tendon, can enclose an angle, the pennation angle. This muscle model is usually implemented by force-length and force-velocity curves and additional scaling factors. All necessary data was collected from several published studies, however, they showed inconsistencies. In order to receive consistent data, all published data was normalised to the erector spinae. Further assumptions and approximations were necessary to complete all scaling factors and physiological parameters for the advanced muscle model. In addition, muscle activation patterns had to be specified manually. This demonstrates, that an application of such an advanced muscle model is difficult and the authors caution that the simulated joint and muscle forces have to be interpreted very carefully.

3 The simulation software

The AMS, also referred to as AnyBody (AnyBody Technology, Aalborg, Denmark), is a software tool to analyse musculoskeletal problems with the help of inverse dynamics. Compatible musculoskeletal models and motions are created with its text-based and object-orientated programming language (AnyScript). A model comprises rigid bodies for bones, joints as well as passive and active force elements like ligaments and muscles. The created models used throughout this work are completed with a few parts provided by the repository which is shipped with the AMS. A typical workflow for a simulation is as follows: create or modify model, apply motions to the model, define output and simulate the case. The main advantages why AnyBody has been used for these studies are that the created models are freely available and that the software is able to solve under-determined systems. The latter is essential because every realistic musculoskeletal model in an inverse dynamic simulation represents an under-determined system. This fact is caused by the presence of more than one muscle which generates the force or moment for a specific motion. For example, inducing flexion at the elbow joint would theoretically require only a single muscle between the upper arm and the forearm but in fact there are more muscles, e.g. the biceps brachii and the brachialis. Both contribute directly to the flexion motion [82]. This leads to a problem that has to be solved in the computations and is explained in the according section.

3.1 Mechanical elements

The following sections describe various elements of a musculoskeletal model and their functions in the AMS. However, the explanations only cover subjects necessary to understand the software's application in this work. Precise information, especially about properties of classes, objects and available in-depth knowledge about some of their underlying concepts, can be found in the reference manual and the tutorials delivered with the software.

3.1.1 Rigid bodies

Even though most pictures from musculoskeletal models simulated in the AMS present realistic bone geometries, only coordinate systems, also referred to as reference frames, and various properties are used in computations. In AMS terms rigid bodies are called segments, and the according object requires a defined mass and the principal moments of inertia which are approximated as an ellipsoid. The deviation moments of inertia are set to zero if not declared otherwise. All properties of a segment and local definitions of other objects are related to its local reference frame which is placed at the centre of mass (COM) by default. Figure 3.1 shows a realistic bone geometry of an upper arm, the humerus, from a lateral view with scaled representation of its moments of inertia as

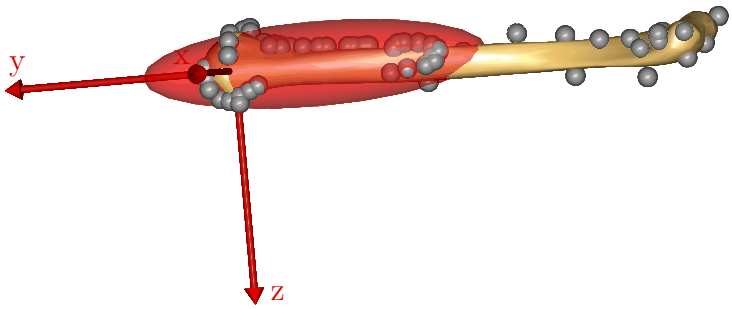

Figure 3.1: The actual bone geometry (yellow) is usually used for a better representation of the model. Computations in the AMS utilise coordinate systems as reference frames (red), mass, moments of inertia (red ellipsoid) and nodes (grey).

an ellipsoid and the actual reference frame. The according deviation moments of inertia are modified because the ellipsoid is not centred in the local reference frame. The grey points in this picture are nodes which are used to define attachment points for muscles and ligaments, joint positions, etc. This is necessary to model realistic moment arms of the various elements. Nodes are always created in the current reference frame and each node is a reference frame for itself. Furthermore, the relative position between the parent reference frame and the node's one stays always the same. Hence, the angular velocity and acceleration of the node are identical to those of its owner.

3.1.2 Joints and Drivers

Simulations with an inverse dynamic approach require that the examined musculoskeletal model is determined kinematically. This implies that the defined system provides the exact same amount of constraints as there are degrees of freedom of rigid bodies, aka segments. There are two ways to add constraints to a model: joints and drivers, in which a joint is a combination of drivers and measurements.

The subsequent description of these elements is based upon the following example of a simple hinge joint between two objects, a segment and the global reference system. The latter is a basic requirement for all models and such a global coordinate system is always fixed. In this example model, the segment is created with a mass of 1 kg and principal moments of inertia which resemble a stick. With the remaining parameters (deviation moments of inertia) left at their defaults, the segment's COM is located in the centre of the ellipsoid. All translations and rotations of the rigid body should be locked except its rotation around the global z-axis. The final assembly is shown in Figure 3.2.

In the AMS, measurements evaluate different quantities like distances, angles or the length of a path between two segments or reference systems. A kinematic driver is used to force a measurement to a specific value or characteristic, thus it limits the available number of degrees of freedom and enables motions in the model. The previously described example of a hinge joint illustrates this. Such a joint shall be modelled between the fixed

global reference system and a single segment. Two measurements between the global reference system and the segment, a linear and a rotational measurement, are necessary to determine the exact position of the segment. The linear measurement returns the distances in the x, y and z directions while the rotational measurement returns the angles around the axes. Both measurements are used as input to a so-called measure organiser. This object outputs a selection of its input variables. In this example all input variables are selected except the rotation around the z-axis. The output of the measure organiser, the five selected values, is used as input to a kinematic driver, for example a simple driver. This object provides a motion with a constant acceleration, hence, the starting distance and angle as well as the (rotational) velocity and the constant acceleration between the two objects can be specified. In case of the intended hinge joint, all these values are set to zero. Therefore, the segment is located and orientated in the same way as the global reference system but with a single degree of freedom left, the rotation around the z-axis. The according source code can be found in the Appendix A.1. The outlined procedure enables a generation of every conceivable joint configuration, however, it is also possible to use basic predefined joints, e.g. an AnyRevoluteJoint (hinge joint).

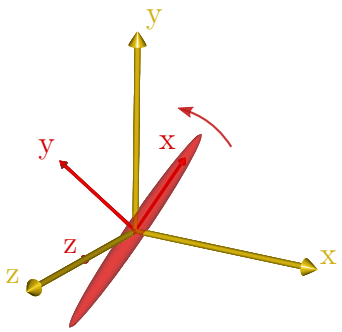

Figure 3.2: A simple example of a hinge joint in AnyBody. The segment (red ellipsoid and coordinate system) is rotating (indicated by arrow) around the z-axis of the global reference system (yellow coordinate system).

The above example and every available joint for itself are not determined kinematically and therefore a simulation run is not possible. Additional degrees of freedom, in the above case the rotation around the z-axis, have to be constrained. Generally, this can be achieved by the creation of an individual measure organiser and driver which control the remaining degrees of freedom. Regarding the example, the existing driver and the measure organiser could be modified. The commented source code for the latter possibility can be found at the end of Appendix A.1.

Moreover, force generating objects are needed for motions in an inverse dynamic simulation. Besides elements described in the further course of this chapter, drivers also have the capability to act as a force generating object by applying reaction forces or moments to the model.

3.1.3 Passive elements

Passive elements are components which only provide force in dependence of a positional variable. A ligament represents such a passive element. One major attribute of a ligament is, that it only generates a force when it is elongated. This means, there is zero force as long as the current length of the ligament is below or equal to its undeformed length also called the slack length. This is rather important because it raises the requirement of a calibration of models and will be explained later. The creation of a ligament requires two things: a definition of the pathway and a ligament model that defines the characteristics.

Basically, the AMS uses ligament models with a non-linear characteristic and it computes the ligament force by

$$F = c_0 + c_1 \cdot \varepsilon + c_2 \cdot \varepsilon^2 + c_4 \cdot \varepsilon^4 \tag{3.1}$$

with ε representing the current strain of the ligament and coefficients c_i which are determined by the software. These coefficients are computed in such a way that the definition of the ligament model is met. Necessary parameters for the definition of a ligament model are the slack length l_{slack}, a nominal strain value ε_{nom} and the according nominal force value F_{nom}, whereas the latter two describe the nominal point. These three parameters define the general stiffness of the ligament

$$k_{\text{nom}} = \frac{F_{\text{nom}}}{\Delta l_{\text{nom}}} \qquad \text{with} \qquad \Delta l_{\text{nom}} = \varepsilon_{\text{nom}} \cdot l_{\text{slack}} \tag{3.2}$$

which represents the basic gradient of the ligament's force-length relationship. The ligament object includes two additional parameters c_{slack} and c_{nom} to alter this gradient of the ligament force when it reaches its slack length and the nominal point, respectively. Both parameters can be set to any value of an interval from zero to one and they interpolate the curve's slope by

$$k(l = l_{\text{slack}}) = c_{\text{slack}} \cdot \frac{F_{\text{nom}}}{\Delta l_{\text{nom}}} \qquad \text{and} \qquad k(l = l_{\text{nom}}) = c_{\text{nom}} \cdot \frac{F_{\text{nom}}}{\Delta l_{\text{nom}}}. \tag{3.3}$$

With default values of $c_{\text{slack}} = 1$ and $c_{\text{nom}} = 1$, the ligament shows a linear elastic behaviour above the slack length because the stiffness is constant at any time. This fact eliminates the non-linear terms of Equation 3.1, results in coefficients

$$c_0 = 0 \qquad \text{and} \qquad c_1 = \frac{F_{\text{nom}}}{\varepsilon_{\text{nom}}} \tag{3.4}$$

and provides a much simpler condition of

$$F = \frac{F_{\text{nom}}}{\varepsilon_{\text{nom}}} \cdot \varepsilon \qquad \text{with} \qquad \varepsilon \geq 0 \tag{3.5}$$

to compute the ligament force.

Usually, ligament properties are reported as a stiffness value and an according strain value, hence, the nominal stiffness is missing. A conversion of Equation 3.2 to the

form

$$F_{\text{nom}} = k_{\text{nom}} \cdot \varepsilon_{\text{nom}} \cdot l_{\text{slack}} \tag{3.6}$$

solves this problem, because all three components on the right side of this equation can be derived from literature (k_{nom} and ε_{nom}) or the values can be determined prior to the simulation (l_{slack}).

Apart from the definition of a ligament model, the pathway of the desired ligament has to be declared. This route is created between reference systems, nodes or segments. The simplest ligaments, which are used throughout this study, are linking two nodes from different segments, and they result in a single element per ligament. The current total length l of a ligament is always determined by

$$l = |[OI]| \tag{3.7}$$

which is the shortest path between its origin O and insertion I. If the definition of the ligament route contains additional nodes, so-called via nodes N, beside the origin and insertion, the shortest paths between consecutive nodes are measured and summarised to the total ligament length. This results in a total ligament length of

$$l = |[ON_1]| + \sum_{i=1}^{n} |[N_i N_{i+1}]| + |[N_n I]| \tag{3.8}$$

where n represents the number of via nodes in the ligament definition. The order of node declaration in the ligament object determines the route of the ligament.

Both, the ligament's pathway and its model, influence the orientation and magnitude of the ligament force. The computed force affects segments which own the first and last connection point and it acts along a line defined by the according element. In addition, via nodes also transfer forces to their segments but the orientation of those forces is defined by a line bisecting the angle which is formed by the adjacent elements of the ligament.

Ligaments only transfer tensile forces, hence, there is no force output if the strain is negative. As a consequence, it is important to determine an appropriate slack length. Therefore, the model has to be set into a defined posture at which the forces in the ligaments are supposed to be zero. The length of each ligament with the model in this position is assigned to the slack length parameter of the according ligament model. This procedure is called calibration of the model.

Another passive element which has to be modelled in a musculoskeletal model is the stiffness of joints, e.g. the stiffness of a spinal disc. There is a single force generating element that is used for rotational and translational stiffness alike. The characteristic, linear or non-linear, is defined by a function of any form. Usually, it is a linear stiffness factor, due to the availability of published data, and it is multiplied with the negative displacement or rotation of the joint. This results in a force or moment acting contrary to the motion. The according positional values can be easily acquired with a measurement object.

3.1.4 The active elements: muscles

Similar to a ligament, a muscle is created with a muscle model and its pathway. In contrast, however, it is an active element which provides a force to induce a certain motion. Throughout this study, a basic muscle model, without passive element properties, is used.

This model, often referred to as simple muscle model, characterises a muscle only with a constant muscle strength. The strength reflects the maximum force that the muscle can generate. This force is determined in experimental measurements with the according joint in a static condition meaning that the muscle's length remains constant. It is also called the maximal isometric strength and is obtained via measuring the PCSA of the muscle and its specific tension in the mentioned experiments. Moreover, it is possible and reasonable that a scaling factor dependent on the analysed subject affects the muscle strength. Realistic values for the PCSA as well as the specific tension of the muscle can be obtained from literature and the basic model from the AMMR already includes decent ones.

As stated at the beginning of this section, the creation of muscles is similar to the creation of ligaments, meaning that it is necessary to determine a muscle model and a pathway. The muscle model, that is used for the conducted studies, has been covered above and pathways are created analogue to the definition of ligaments via nodes. Usually, a muscle progresses over certain bony landmarks without a tight attachment, therefore, more than two nodes have to be used for a realistic modelling. The origin and insertion points of the muscle, the first and the last node on the list of the according object, are special: the muscle is rigidly attached to them and they transmit forces to their segments in the muscle's line of action. However, all other nodes, specified in the object, transfer forces only in the direction of the bisector of the angle which is spanned by the muscle at this point. There is no frictional force between the muscle and touched segments. A detachment of the muscle tissue from surrounding bone in case of an inversion of the angle is not possible with this kind of modelling, hence, the influence of the muscle on the segment is always present.

A frictionless wrapping muscle is used, for the case that muscle detachment is required. Such a muscle can wrap around a specified volume. The wrapping path is defined by the surface of the volume element, e.g. a cylinder. The program routine searches for the shortest path between the origin and insertion of the muscle and wraps around the surface if it blocks the way. The shortest path is not the shortest one between the two nodes, it refers to the shortest path with respect to the surface of the volume. Ideally, an initial location is defined from where the solver should start its search for the path around the surface to ensure a correct progression of the muscle around the volume.

The briefly explained muscle is the one mostly used throughout this work. However, there is one occasion where a different variant, namely the general muscle object, is applied. In fact, a realistic muscle is only able to pull but the software offers a muscle model which leaves the decision of the force direction to the user, hence it is possible to implement a muscle which is able to produce a pushing force. Such a muscle model

is used to model the abdominal pressure described in publication of De Zee et al. [21].

3.1.5 Surface contact

A surface contact can only be realised between two surfaces which are formatted as stereolithography (STL) surface files. A STL file approximates the surface of a three-dimensional object by triangles, only. Basically, the surface contact object computes the contact moments and forces based on penetration volume V_p and a specific pressure module P by

$$F_\mathrm{cont} = P \cdot V_\mathrm{p}. \tag{3.9}$$

This general expression is converted to a form where the individual contact force of each vertex is computed by

$$F_\mathrm{v} = P \cdot A_\mathrm{v} \cdot d_\mathrm{v} \cdot n_\mathrm{v}. \tag{3.10}$$

In this equation, A_v is the area of a vertex. It is one third of the sum of all triangles connected to the vertex. d_v is the penetration depth of the vertex and n_v is the normal of the vertex. The vertex's penetration depth is defined as the shortest distance between the vertex and the closest point on the surface of the other object. A vertex is only considered in contact if the penetration depth lies within a user defined range. The individual contact moment for every vertex is computed by

$$M_\mathrm{v} = F_\mathrm{v} \cdot l_\mathrm{v} \tag{3.11}$$

where l_v is the distance between the vertex and the reference frame of the according surface object.

$$F = \sum F_\mathrm{v} \qquad \text{and} \qquad M = \sum M_\mathrm{v} \tag{3.12}$$

compute the total contact forces and moments between the two surfaces. They are applied to the reference systems of the objects during the simulation.

3.2 Solving an under-determined system: activation of muscles

As stated in the introduction to this chapter, a musculoskeletal model is an under-determined system leading to an infinite number of solutions. That is because there are much more muscles in the body than are kinematically necessary. For example, a flexion motion of the forearm is not performed with the force of a single muscle. Instead, the biceps brachii and the brachialis muscle are the main contributors to this movement. Further issues in simulating the human body concern the modelling of muscles which are acting contrary to the principal motion. From a mechanical point of view, it would be sufficient to activate the agonist, the muscle responsible for the motion. In the previous example of arm flexion, an activation of the biceps muscle would be sufficient to perform the motion but the triceps muscle located at the opposite side of the

biceps is also activated during this movement [30]. This co-contraction of the antagonist, the muscle which counteracts the motion, is known as the LOMBARD'S paradoxon and was formerly discovered when rising from a sitting to a standing posture [47]. Here, the hamstring as well as the quadriceps muscle group contract even though they are actually antagonistic muscles. Another problem is that muscles are only able to generate pulling forces which is causative for additional constraints in solving musculoskeletal models.

Basically, solving an inverse dynamic system means solving a linear system of equations. In case of a musculoskeletal model in the AMS, such a system is of the form

$$\mathbf{M}\mathbf{v} = \mathbf{v}_{\mathrm{E}} \qquad \text{where} \qquad \mathbf{v} = \begin{bmatrix} \mathbf{v}_{\mathrm{I}} \\ \mathbf{v}_{\mathrm{M}} \end{bmatrix} \tag{3.13}$$

and comprises a vector $\mathbf{v}_{\mathrm{E}}$ of external forces and inertia forces, a vector $\mathbf{v}_{\mathrm{M}}$ of forces in muscles, a vector $\mathbf{v}_{\mathrm{I}}$ of internal forces in joints and a rectangular matrix of coefficients $\mathbf{M}$. Considering the special issues resulting from musculoskeletal models as stated above, the numerical solver has to be designed to overcome these limitations. The main problem is the determination of the activation patterns of muscles. It is assumed that there is an underlying criterion in the central nervous system (CNS) behind muscle recruitment because electromyography (EMG) measurements showed similar patterns of muscle activation for specific motion sequences, especially with trained ones, rather than random activation of muscles [14]. Hence, this whole issue is expressed as an optimisation problem where the objective function

$$G(\mathbf{v}_{\mathrm{M}}) \tag{3.14}$$

has to be minimised [20]. Additionally, the model's linear system of equations and the fact that muscle forces are limited to positive values need to be considered. In this equation G stands for an optimisation function of various forms. The recruitment of muscles is basically computed with

$$G = \sum_{i=1}^{n_{\mathrm{M}}} \left(\frac{F_i}{N_i} \right)^p \qquad \text{and} \qquad F_i \geq 0, \quad i = 1, \ldots, n_{\mathrm{M}} \tag{3.15}$$

as published by RASMUSSEN et al. [71] where n_{M} represents the number of muscles in the model, F is a muscle force and N is a normalisation factor. Usually, the muscle strength is used as normalisation factor in ANYBODY and the power p of the function determines muscle synergism.

Linear muscle recruitment with power $p = 1$ results in activation of a minimum number of muscles in the model in such a way that only muscles with an optimal moment arm and muscle strength are recruited for the workload [71, 79]. A power $p > 1$ will always result in some muscle synergism, meaning that even muscles with low muscle strengths or an unfavourable moment arm contribute a small amount and a power $p > 2$ produces large muscle synergism with the goal to keep the activation of each muscles as minimal as possible [94]. This has to be taken into account while choosing a value

for the power. Furthermore, the polynomial muscle recruitment in Equation 3.15 requires

$$\frac{F_i}{N_i} \leq 1, \quad i = 1, \ldots, n_{\mathrm{M}} \tag{3.16}$$

as a restriction to prevent overloading muscles and a very high power of the criterion increases time for a numerical solution [71].

Rasmussen et al. [71] introduced another way how to do muscle recruitment in the AMS by using the min/max criterion. The definition of this criterion is as follows:

$$G(\mathbf{v}_{\mathrm{M}}) = max\left(\frac{F_i}{N_i}\right), \quad i = 1, \ldots, n_{\mathrm{M}}. \tag{3.17}$$

In brief, this criterion shares the external loads over all muscles 'in such a way that the maximum relative muscle force is as small as possible' [71]. From a physiological point of view this is reasonable because it is kind of a minimum fatigue criterion, meaning muscles with maximum relative loading fatigue at first. Hence, contribution of all muscles to an activity reduces the maximal loading of a single one. Rasmussen et al. [71] showed that this criterion is comparable to the use of a high power polynomial criterion but without the numerical difficulties. Nevertheless, the problem with a high order polynomial criterion remains where a muscle could be activated much faster than a realistic muscle is able to.

3.3 Force dependent kinematics

Actually, inverse dynamic simulations require an integral definition of the kinematics of a model. In case of a model of the human body it can be very difficult to acquire all the data necessary. Especially, kinematics related to structures below several layers of soft tissue are hard and even more, small motions in joints which depend on the current forces acting in the joint are nearly impossible to obtain. These shortcomings can be met with a method published by Andersen et al. [5], the FDK method.

A joint or a driver partly is a collection of reaction forces which constrains the motion of an object, hence, they remove degrees of freedom of the model. Basically, the FDK solver of the AMS replaces such a restriction with an elastic element, in other words, it allows motion dependent on a reaction force. Therefore and because of the iterative process that is used by the FDK solver to determine the new value of the concerning translation, rotation or driver attribute, the FDK option can only be used for small motions. FDK locally suspends the inverse dynamic approach which is usually used for the positioning. Instead, the translational or rotational position of the concerned constraint is based on a quasi-static equilibrium of forces and introduced FDK reaction forces. As noted in Figure 3.3, the iterative loop starts with the joint located at its initial position and an inverse dynamic analysis is executed. The resulting forces are employed as input to compute the quasi-static equilibrium. As long as the residue of the numerically solved equilibrium equations falls below a specified tolerance, the process will repeat with an

increased displacement in the concerning direction. Otherwise the joint is at its final position.

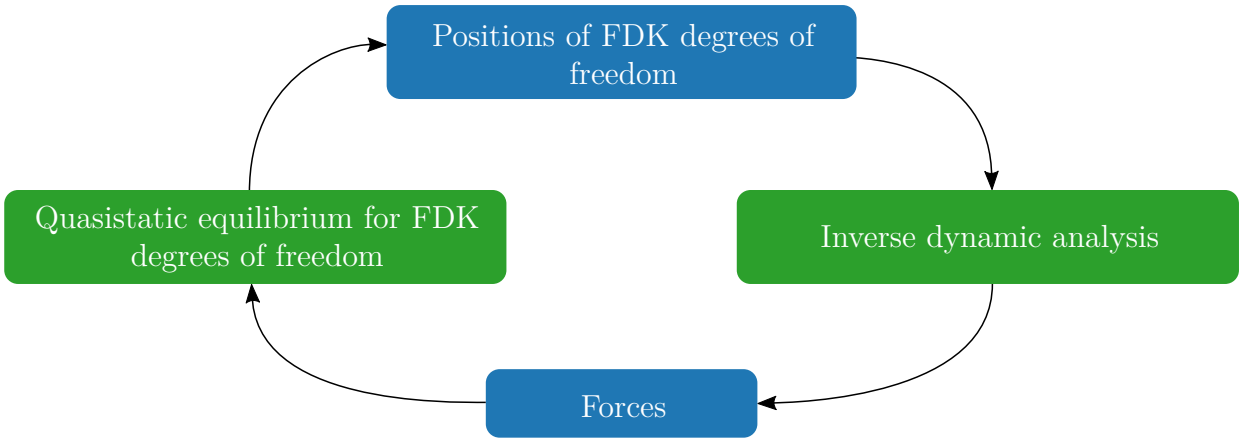

Figure 3.3: This is the iterative loop which is applied to compute the positions of joints with an activated FDK option. Green boxes are active items and the blue boxes represent resulting data.

3.4 Customisation of models

On the one hand, each individual is different from another one, and on the other hand, a lot of products should fit for a large variety of people. For example, ergonomic analyses can either be conducted with a 50th percentile model or with a wide variety of subject-specific data, if computation time is not an issue. The subject-specific data can be provided by anthropometric databases. Although anthropometric data of a standard database cover a large variety of body dimensions, subject-specific data could show an exotic combination of values. Moreover, there are applications where only one specific subject has to be simulated, e.g. pre-simulations to a subject-specific implant. Therefore, customisation of musculoskeletal models is necessary but dependent on the application. As a consequence, there is not a single model to fit all applications and each musculoskeletal model has to be customised in different factors to the current needs. These factors comprise anthropometric factors like height, weight and body fat percentage or the individual bone shape, muscle strength and motion patterns.

3.4.1 Scaling laws

There are different ways to customise the generic model, which roughly corresponds to the 50th percentile European male, using standard tools of the AMS. A basic set are the scaling laws. They change a body model in terms of body height, body weight, the body fat percentage and muscle strength. These scaling laws can be divided into two main groups and their main distinctive feature is the source of input data: the subject's segment lengths (Figure 3.4). Each length is either measured as a joint to joint distance or it is taken between specific bony landmarks, visible through the soft tissue. Furthermore,

the external dimensions for the latter method have to be measured in an upright standing posture with the upper arms close to the sides of the body and the forearms flexed by 90°.

Regardless of the chosen method, an extensive amount of data of the subject would be required to create a subject-specific model but these data is rarely available, and especially during the studies for this thesis it was not the case. Therefore, there are default values ready for use for all segment lengths and the modified lengths of the bones are acquired by scaling. This leads to a two-step modification of the model in terms of scaling. First, each segment length of the subject is determined and second, these new lengths are used to scale each part of the model. The characteristic of this scaling is controlled by the selected scaling law. There are three different scaling methods available, each considers a different selection of properties: segment lengths, segment lengths and masses or segment lengths, masses and fat percentage.

The first scaling law is a uniform one because it scales sizes of each segment proportionally in all three directions according to the specified segment length. Without detailed knowledge about the subject's segment lengths, those measurements are determined by multiplying the initial segment length with a scaling factor. This scaling factor is calculated as the ratio between the body height of the subject h_{sbj} and the default model h_{def} by

$$s = \frac{h_{\mathrm{sbj}}}{h_{\mathrm{def}}}. \tag{3.18}$$

Afterwards, the modified length of each segment l_{sbj} and the default value of each segment length l_{def} are utilised to quantify an individual scaling factor for every single segment i by

$$s_{\mathrm{l},i} = \frac{l_{\mathrm{sbj},i}}{l_{\mathrm{def},i}}, \qquad i = 1, \ldots, n \tag{3.19}$$

which is then applied to the according section of the model and alters each segment in all three directions uniformly. Additionally, the body mass is distributed between all segments considering distribution data published by Winter [105]. The scaling of muscle strength is also linear and differs between segments, too. The corresponding scaling factor for each segment i depends on segment masses and is determined by

$$s_{\mathrm{M},i} = \left(s_{\mathrm{m},i}\right)^{\frac{2}{3}}, \qquad s_{\mathrm{m},i} = \frac{m_{\mathrm{sbj},i}}{m_{\mathrm{def},i}} \qquad \text{and} \qquad i = 1, \ldots, n \tag{3.20}$$

with m_{sbj} as a segment mass of the subject and m_{def} as a segment mass of the default model.

The second scaling law extends the first one by using lengths and masses to determine all sizes of the model. While the lengths are only scaling segments in their main direction (Figure 3.4), the masses do this for the remaining two. As before, each scaling factor is calculated as ratio between the subject's value and default value, except the factor influencing muscle strength. This value is determined by the ratio between the scaling factors of mass and length.

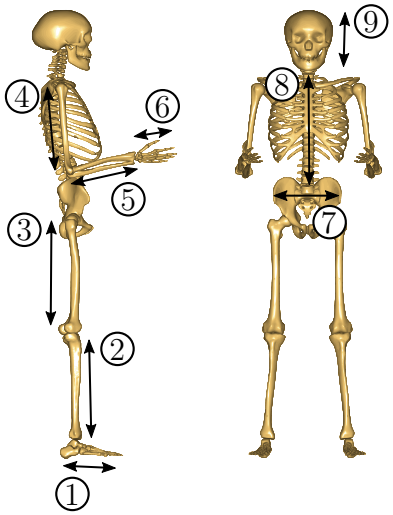

Figure 3.4: Indicated is the main direction of each segment. The labels correspond to the declaration in Table 3.1.

Table 3.1: The length for each listed segment can be modified and is considered in the scaling laws. The numbers correspond to the labels in Figure 3.4.

No.	Segment	No.	Segment	No.	Segment
1	Foot	4	Upper Arm	7	Pelvis
2	Shank	5	Lower Arm	8	Trunk
3	Thigh	6	Hand	9	Head

The third method of scaling adds the body fat percentage as an additional input parameter to the existing two (body height and body mass). The scaling laws described before adapt muscle strength according to the body height and weight, however, in reality, the body fat percentage influences muscle strength, too. Basically, this third scaling law works exactly like the previous one but with an altered method to determine the muscle strength. In this third case, the body fat percentage is considered. Each segment's scaling factor is calculated by

$$s_{\mathrm{M},i} = \frac{s_{\mathrm{m},i}}{s_{\mathrm{l},i}} \cdot \frac{1 - R_{\mathrm{other}} - R_{\mathrm{sbj}}}{1 - R_{\mathrm{other}} - R_{\mathrm{def}}} \tag{3.21}$$

with R_{sbj} as the subject's body fat percentage, R_{def} as the default body fat percentage and R_{other} representing the share of mass of the remaining tissue and bones [72]. Typically, this last value is set to 0.5. It is either possible to input the body fat percentage manually or to use the standard implementation which utilises the body mass index (BMI) and calculates fat percent based on an estimation from literature [25].

3.4.2 Morphing

Another way to customise a model is to scale segments on basis of subject-specific data from clinical images. This technique is called morphing. As aforementioned, the sources of this process are medical images, e.g. computer tomographic (CT) scans of a bone. These images are utilised to create a detailed three-dimensional surface model of the bone. This in turn is the basic information to scale the corresponding bone of the musculoskeletal model via transformation functions. The concept of morphing will be used in the generation of the models for this work, therefore the workflow will be explained thoroughly in the following chapter.

3.5 Model repository

The AMMR provides a generic human body model which can be used throughout a study and several example applications are included. It is structured into the application file tree and the body file tree. The latter contains the standard body model and this model can be used as a whole or in parts. Two different versions (1.4.1 and 1.6.1) of the AMMR are used throughout this work because the models are updated to conform the guidelines of the repository prior to the multifidus study. This change does not alter the behaviour or characteristics of the models. It merely improves the usability.

4 Material and methods

In course of this study, a model framework is created which morphs and scales parts of a generic model according to subject-specific data. Subsequently, three different studies are conducted utilising these models. This chapter describes model creation, structure and implementation of the studies.

4.1 Model development

A main goal of this thesis is to create a publicly available basic human musculoskeletal model of the full body for simulation in the AMS with an incorporated semi-automatic process to set up a subject-specific model at load time. An individual model is considering a subject-specific geometry of the lumbar spine including an adapted disc stiffness, body weight and body height. Input only requires each lumbar vertebrae as a surface geometry, data about bony landmarks of every lumbar vertebra, body weight and body height.

The overall workflow for the creation of subject-specific models is split into two main parts, as depicted in Figure 4.1. The first step is to program a basic musculoskeletal full body model, further referred to as basic model, which uses processed subject-specific data as input (Figure 4.1, right). Therefore, a generic model from the AMMR is heavily modified in the following sections: ligaments, discs and joints of the lumbar spine as well as all lumbar vertebral geometry including the facet joints. Modifications of the ligaments are confined to the alteration of attachment points and material models. The discs and joints are changed with regard to the stiffness model and position, respectively. Facet joints are implemented as a surface contact between the actual geometry to consider subject-specific limits of the ROM. All geometric modifications are carried out in a semi-automatic morphing process. This process morphs and repositions the lumbar vertebrae, all lumbar joints and all related attachment points of ligaments and muscles based on a three-dimensional representation of the lumbar vertebrae and their relative position to each other. It allows a fast switching between the different datasets and utilises the individual geometry of the lumbar spine. Furthermore, an existing scaling option is used to adjust the body height and weight.

Processing of the subject-specific data is necessary to use it as input for the basic model (left part of Figure 4.1). The first step is segmentation of the CT images to obtain the lumbar spine as a surface geometry. A sequence of CT images contains greyscale images. Each image represents a cross-sectional area of the scanned part of a subject in case of medical CT images. The process of segmentation identifies and marks all necessary segments of an image. More precisely, each pixel of the areas of interest is labelled and all pixels with the same label represent a single object or part, e.g. a vertebra or only the cortical bone, the hard outer layer, of a vertebra. After labelling is finished,

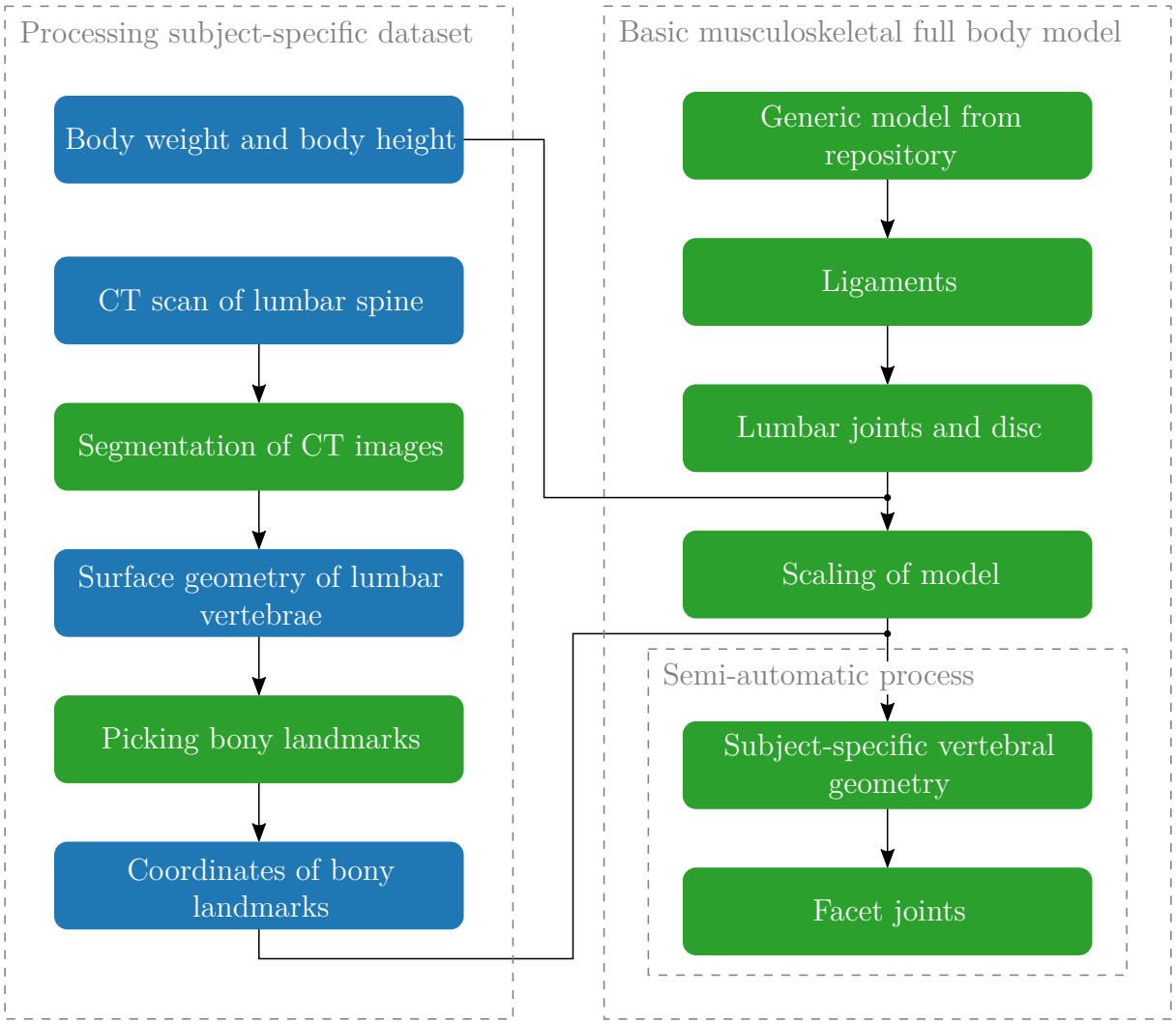

Figure 4.1: The model creation is split into two main work packages. The right part shows the workflow applied to create a basic musculoskeletal model of the full body. The processing of every subject-specific dataset is outlined on the left part. Using a processed subject-specific dataset as input for the basic model results in a musculoskeletal full body model with a subject-specific geometry of the lumbar spine. The green boxes are work steps and blue boxes represent input or result data.

the software computes a three-dimensional representation of the selections. In case of model development, only the bony part of the lumbar spine is necessary to obtain three-dimensional models of the vertebrae. Finally, coordinates of several bony landmarks of the vertebrae are extracted from the surface geometry of each lumbar vertebra. All results of processing the subject-specific dataset are used as input for the semi-automatic process described above.

4.1.1 Subject data

Out of 15 data sets, five are selected based on an adequate image resolution in cranial-caudal direction of the CT scans of the lumbar part. Every set includes information about age, weight, height and sex of the subjects beside the images. All subjects are male. The mean age is 57.3 ± 4.4 yr with the age of subject one unknown, the range of the body weight is rather large with a mean value of 93.2 ± 17.7 kg and the mean height is 176 ± 6 cm. Additionally, each subject's lordosis angle is measured and the individual cross-sectional area of the L4/L5 lumbar disc is determined. The measurement of the lordosis angle is performed with the COBB method and it results in a mean angle of $53.4 \pm 5.7°$. The determination of the cross-sectional area of the disc is carried out by approximating an ellipse at the middle of the disc's height. For that purpose the major and minor axes are measured from the lateral and frontal CT scans. In case of subject one only transversal scans are available, wherefore those images are used to determine the area. Every measurement is performed three times and the mean value is used to calculate the disc's cross-sectional area. The mean disc size of all subjects is $1834 \pm 169\,\mathrm{mm}^2$. All individual values are summarised in Table 4.1. Even though, each subject's lumbar spine shows age-related degenerations, however, none of them had any surgery on the lower back. In particular the L5/S1 lumbar disc of subject one shows severe degenerations and signs of a beginning degeneration in the remaining lumbar discs. Subject four has a severe degeneration at the L4/L5 lumbar level.

Table 4.1: Additional information about the subjects.

Subject	Age	Sex	Weight (kg)	Height (cm)	Disc area* (mm^2)	Lordosis† (°)
1	n/a	m	70	168	1623	60
2	64	m	86	177	1791	53
3	58	m	97	178	2136	43
4	55	m	124	174	1769	57
5	52	m	89	185	1852	54

* approximated by an ellipse, † measured by Cobb method

4.1.2 Segmentation of computer tomographic images

All datasets include various CT image sequences and each image collection which contains only a part of the lumbar spine is discarded. Additionally, all CT recordings with outshining sections of the lumbar spine due to metallic objects like stents in blood vessels are also neglected. The remaining image sequences are inspected and a single one per subject is selected for segmentation. The selection criteria include the image resolution in all spatial directions and the overall image quality. Therefore, care is taken that the image resolution is as high as possible and that there is as little image noise as possible. Then, the three-dimensional surface geometry of each lumbar spine is created via segmentation. This task is performed with the software Simpleware ScanIP (Version 5, Synopsys Inc., Mountain View, USA). At the beginning, a CT image sequence is cropped to

the lumbar part only. Afterwards, filtering of the images facilitate a better differentiation between bones and soft tissues like discs or ligaments. Thereby, no information is lost because only the outer bony structures of the vertebrae are necessary for modelling. However, the remaining noise in the images prevents a complete automation of the segmentation process, hence, the edges of each vertebra are mostly selected by hand. A tool, which selects connected pixels over all slices of the CT scans and based on each pixel's colour information, is used to catch most surfaces within the selected edges. Finally, the software is utilised to find and remove all remaining holes in the surface geometry. After finishing the segmentation procedure, every lumbar vertebra is exported as an individual STL file. With regard to further processing in the AMS, it is essential to use a single global reference system for every vertebra per subject.

4.1.3 Picking bony landmarks

Several bony landmarks of a vertebra are required for positioning and morphing purposes in the AMS. Therefore, the x-, y- and z-coordinates of a total of 40 bony landmarks per vertebra are recorded in a specific order using a tool of the software MeshLab

Table 4.2: Listing of bony landmarks recorded for every lumbar vertebra. The locations are depicted in Figure 4.2.

No.	Location	No.	Location
1	superior attachment point of ALL	21	posterior peak of superior right facet
2	mid attachment point of ALL	22	superior peak of superior right facet
3	inferior attachment point of ALL	23	lateral peak of left TP
4	mid of superior vertebral endplate	24	mid of anterior side of left TP
5	superior attachment point of PLL	25	mid of posterior side of left TP
6	mid attachment point of PLL	26	lateral peak of right TP
7	inferior attachment point of PLL	27	mid of anterior side of right TP
8	mid of inferior vertebral endplate	28	mid of posterior side of right TP
9	superior left lateral end of VB	29	inferior peak of inferior left facet
10	left lateral end at mid of VB	30	inferior peak of inferior right facet
11	inferior left lateral end of VB	31	superior attachment point of ISL
12	superior right lateral end of VB	32	posterior attachment point of SSL
13	right lateral end at mid of VB	33	left mid of posterior end of SP
14	inferior right lateral end of VB	34	right mid of posterior end of SP
15	mid of superior side of left pedicle	35	mid superior peak of lamina
16	mid of medial side of left pedicle	36	inferior anterior crest of SP
17	posterior peak of superior left facet	37	mid of inferior left facet surface
18	superior peak of superior left facet	38	mid of inferior right facet surface
19	mid of superior side of right pedicle	39	mid of superior left facet surface
20	mid of medial side of right pedicle	40	mid of superior right facet surface

ALL: anterior longitudinal ligament, ISL: interspinous ligament, PLL: posterior longitudinal ligament, SP: spinous process, SSL: supraspinous ligament, TP: transverse process, VB: vertebral body

(www.meshlab.net). This landmark file is generated for every vertebra of each model. Table 4.2 provides the sequential list of all the locations of interest, Figure 4.2 depicts the landmarks at an example geometry. The acquired data is imported to the model with the help of a Python script (Appendix A.2.1) and usage of the Python hook (Appendix A.2.2) provided by the application programming interface (API) of the AMS.

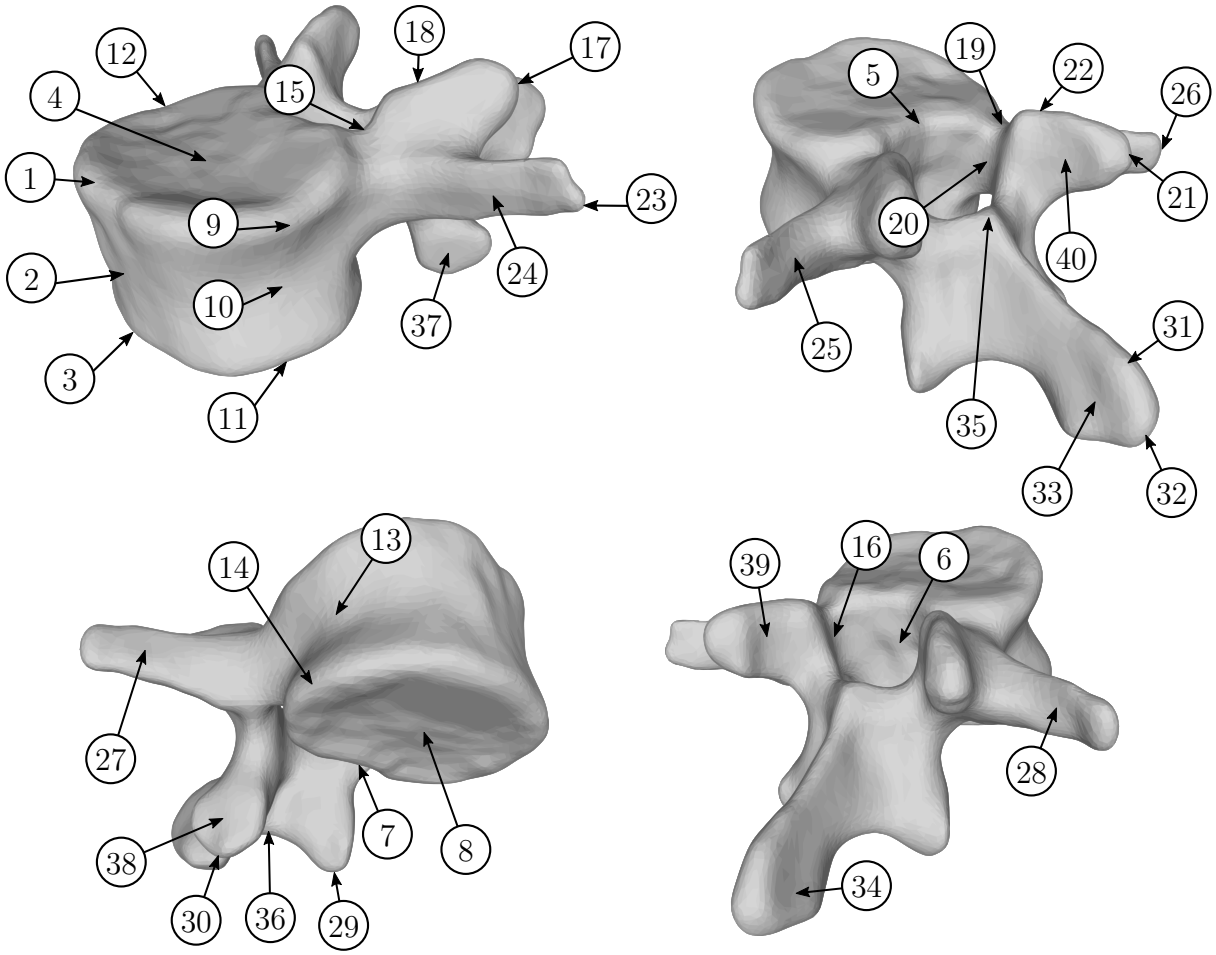

Figure 4.2: Illustration of a vertebra labelled with the number of the recorded bony landmark according to Table 4.2.

4.1.4 Generic model from the repository

As mentioned at the beginning of this chapter, the basic model is created by reworking the detailed spine model from the AMMR and extending it with other body parts of the generic full body model of the repository (Figure 4.3). Only a short overview of this generic model is given here, covering the most important information with regard to this thesis.

The generic full body model includes the following parts: both legs and arms, a skull, an upper thorax and an articulated generic lumbar spine. This spine model is based on

Figure 4.3: The generic full body model from the AMMR including the initial spine model and musculature for the trunk and legs.

the one published by Galibarov et al. [28], which in turn is an improved version of the model of De Zee et al. [21]. All shapes of the model's body parts are symmetrically to the sagittal plane. The upper thorax includes the cervical spine, the thoracic spine, all ribs and the sternum as a single lumped part. Every other bone is modelled as an individual segment except the small bones of hands and feet. These bones are cumulated in a single segment.

The five lumbar vertebrae and the sacrum are connected via spherical joints, which are centred between the vertebral bodies. Each mass of a vertebra is determined by a fifth of the lumbar share that is specified in the distribution data of Winter [105]. The inertia properties are set to ones representing a sphere and the centre of mass is located at the centre of the vertebral body. The disc stiffness is modelled with a three-dimensional rotational stiffness with a linear relationship according to literature data [83]. The inverse dynamic analysis can be run with either the spine rhythm or FDK at those spherical joints. It has to be noticed, that the switch from one to another changes the order of the rotation axis from x, y, z, to z, y, x.

Ligaments are modelled at the lumbar spine only and with linear characteristics based on published data [15, 67]. The following ligaments are present in the generic model: ALL, PLL, LF, ITL, ISL and SSL. Aside from the LF and ITL, they are represented by a single element connecting the inferior and superior landmark of two adjacent vertebrae at each lumbar level. The LF is implemented with two elements at a lumbar motion segment whereas the ITL comprises four elements per vertebral pair, two at each side of the vertebrae. All six ligament groups are completed with a linear elastic material model per group and per lumbar level.

All muscles of arms, neck, breast and shoulder girdle are excluded. The following muscle groups, all close to the lumbar part, are incorporated: multifidi (thoracic and lumbar), erector spinae, psoas major, quadratus lumborum, obliquus externus, obliquus internus, semispinalis, rectus abdominis, spinalis and transversus abdominis. They are accompanied by most leg muscles. All implemented leg muscles are listed in Table A.1. Each muscle is modelled by a number of fascicles and as an active element with a constant strength. The strength is defined by the PCSA and the specific tension of the muscle

for each fascicle. This simple model of muscles is chosen, because the more sophisticated models require input data that is scarcely available. The muscles span from their origin to insertion over various so-called via-points, which also transfer forces to the connected segments. The direction of this transmission is the bisecting line of the enclosed angle. Only the iliopsoas muscle of the legs is modelled as a wrapping muscle to enable a detachment of the muscle if hip flexion is present.

Moreover, the preliminary model of the intra-abdominal pressure (IAP) is included in the generic model. This is realised by creating a constant volume in the abdomen which extends in cranial-caudal direction when the transversus muscle compresses it and therefore generates a force on the bottom of the thorax and the pelvic floor. This results in an extensor function of the intra-abdominal pressure. The IAP is limited to a value of 26 600 Pa as measurements indicated [24].

All basic motions or postures used throughout the studies are defined by the driver controlling the relative orientation between the pelvic and the thoracic segment. For this purpose, this driver manages the angles between the according reference systems. Angles of zero degree around the three spatial axes correspond to an upright standing posture and a negative flexion angle determines an extension. Positive values for lateral bending or axial torsion tilt or twist the thorax to the left side, while negative values move it to the right side.

4.1.5 Ligaments

Modifications of the ligaments are confined to the intertransverse ligament and the ligamenta flava at each lumbar level. Figure 4.4 depicts a motion segment with the according elements representing the connective tissue. These ligaments are modelled with multiple elements, because they are located on the left and right side of a vertebra and they cover a larger area. Every single element of the two ligaments is created with an individual model to consider different values for the calibrated slack length. All other material-specific parameters are transferred from the original ligament model and correspond to literature data [15, 67]. These modifications are implemented as a model option.

4.1.6 Lumbar joints

Each centre of rotation (COR), originally centred between adjacent vertebral endplates, is relocated in the sagittal plain according to mean values (Table 4.3) reported by Pearcy and Bogduk [65]. This data was published as a fraction of the vertebral depth (VBD) and height (VBH) of the inferior bone of the motion segment, hence, the joint locations are modelled with analogue dependencies.

Figure 4.5 shows the underlying process which includes multiple vector additions. This is caused by the fact that joint creation requires two nodes, each in one of the segments

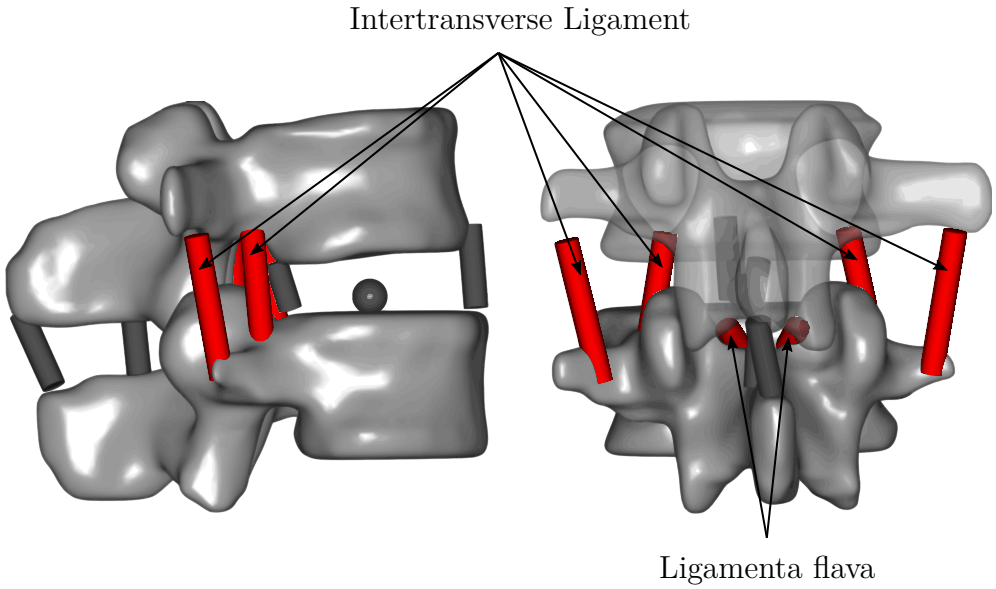

Figure 4.4: The picture shows a lateral and posterior view of a lumbar motion segment with its ligaments. Both modified element groups representing the two ligaments are labelled and highlighted in red. The view on the ligamenta flava is obstructed by the articular processes in the left part of the image.

which have to be connected. Beginning with the inferior segment, the first step is to calculate vectors of the vertebral depth $\mathbf{v}_{\mathrm{VBD}}$ and height $\mathbf{v}_{\mathrm{VBH}}$ by

$$\mathbf{v}_{\mathrm{VBD}} = \mathbf{l}_{1,\mathrm{inf}} - \mathbf{l}_{5,\mathrm{inf}} \qquad \text{and} \qquad \mathbf{v}_{\mathrm{VBH}} = \mathbf{l}_{7,\mathrm{inf}} - \mathbf{l}_{5,\mathrm{inf}}. \tag{4.1}$$

The position vectors of the superior attachment points of the ALL ($\mathbf{l}_{1,\mathrm{inf}}$) and PLL ($\mathbf{l}_{5,\mathrm{inf}}$) are used in the calculation for the vertebral depth, whereas, the vertebral height is calculated based on the position vectors of the superior and inferior attachment point of the PLL ($\mathbf{l}_{5,\mathrm{inf}}$ and $\mathbf{l}_{7,\mathrm{inf}}$). The first index of a landmark's position vector shows the number of the bony landmark in accordance with Table 4.2, while the second index denotes the corresponding vertebra of the motion segment, either the superior or inferior one. Pub-

Table 4.3: Mean values of joint positions for every lumbar level given as a fraction of the vertebral depth and height of the inferior bone of the motion segment.

Level	x_{mean}	y_{mean}	Comment
T12/L1	0.50	-0.02	Position from generic model; no literature data available.
L1/L2	0.43	0.03	Literature data [65]
L2/L3	0.40	-0.04	
L3/L4	0.38	-0.05	
L4/L5	0.41	-0.04	
L5/S1	—	—	Not modified.

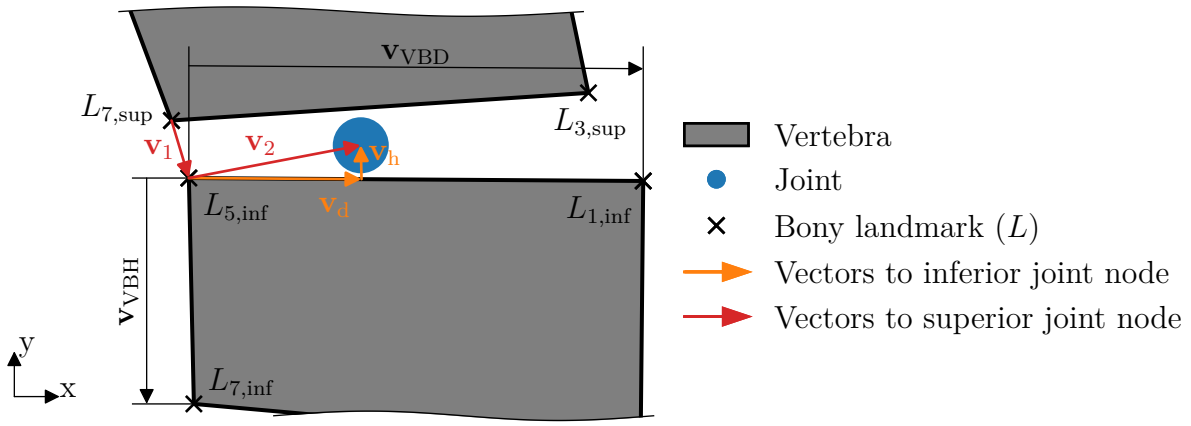

Figure 4.5: The method which is developed for positioning of the joints: locations of joint nodes of the inferior vertebrae were calculated (orange) via published mean values [65] and the vertebral height and depth. Whereas the coordinates of the joint nodes of the superior vertebrae where dependent on vertebral landmarks and the previous calculation (red).

lished mean values x_{mean} and y_{mean} multiplied with the vectors of vertebral depth $\mathbf{v}_{\mathrm{VBD}}$ and height $\mathbf{v}_{\mathrm{VBH}}$, respectively, form the basis for a vector

$$\mathbf{u} = \mathbf{v}_\mathrm{d} + \mathbf{v}_\mathrm{h} = x_{\mathrm{mean}} \cdot \mathbf{v}_{\mathrm{VBD}} + y_{\mathrm{mean}} \cdot \mathbf{v}_{\mathrm{VBH}}, \tag{4.2}$$

that indicates the joint's position relative to the inferior segment's superior attachment point of the PLL $L_{5,\mathrm{inf}}$. A vector addition with the position vector of this attachment point ($\mathbf{l}_{5,\mathrm{inf}}$) as starting location results in the final position of the inferior joint node

$$\mathbf{v}_{\mathrm{jnt,inf}} = \mathbf{l}_{5,\mathrm{inf}} + \mathbf{u} \tag{4.3}$$

relative to the concerning vertebra. The relative location of the joint node of the upper segment is defined by

$$\mathbf{v}_{\mathrm{jnt,sup}} = \mathbf{l}_{7,\mathrm{sup}} + \mathbf{v}_1 + \mathbf{v}_2 = \mathbf{l}_{7,\mathrm{sup}} + (\mathbf{l}_{5,\mathrm{inf}} - \mathbf{l}_{7,\mathrm{sup}}) + \mathbf{u}. \tag{4.4}$$

Basically, this definition consists of three parts: the first term $\mathbf{l}_{7,\mathrm{sup}}$ describes a vector to the location of the inferior attachment point of the PLL belonging to the upper segment. Then the path continues along the PLL to the lower vertebra and is completed with the vector $\mathbf{u}$ to the joint node.

4.1.7 Lumbar discs

The stiffness model of the lumbar discs, which is implemented in the repository's model, is modified and a new non-linear stiffness model is created. While the modification removes a bug in the original implementation, the new model considers a subject's body height in the stiffness. Furthermore, the orientation of every lumbar disc is determined at any time during simulation to be able to compute the correct shear and compression shares

from the joint reaction forces.

Bugfix to linear stiffness model

The linear disc stiffness model is adapted to the usage of a different order of rotation when switching from the spine rhythm to FDK. A conditional statement tests the current used option (spine rhythm/FDK) and activates a stiffness model corresponding to the current order of rotation. Prior to this modification, the flexion-extension and lateral bending parameters were misapplied when the FDK option was active.

Non-linear stiffness model

A new non-linear characteristic for the rotational disc stiffness is added to complement the linear one. It is implemented to the model as an option and can be activated with a switch. This characteristic is based on the publication of Weisse et al. [99] which provides a non-linear stiffness model of the form

$$k_{\text{rot}} = P_1 \cdot P_2 \cdot e^{P_2 \cdot \Theta} \tag{4.5}$$

where Θ represents the current rotational displacement. The two parameters P_1 and P_2 are depended on the direction of rotation and consider either the presence or the absence of the posterior ligaments and facets. They were determined for the four basic motions flexion, extension, lateral bending and axial rotation. Table 4.4 lists the values for both parameters and configurations. The distinction between absence or presence

Table 4.4: Parameters P_1 and P_2 required for different configurations to model the new non-linear rotational disc stiffness [99].

Motion	P_1 (Nm)	P_2 (deg^{-1})	Ligaments & facets
Flexion	1.840	0.178	present as individual elements with a stiffness value
Extension	1.390	0.137	
Lateral bending	3.240	0.182	
Axial rotation	1.320	0.453	
Flexion	1.080	0.340	stiffness included in disc stiffness
Extension	2.080	0.296	
Lateral bending	4.520	0.190	
Axial rotation	4.150	0.490	

of the posterior ligaments and facets is also added the model. If all lumbar ligaments are included in the model as elements with stiffness properties, the first set of values according to Table 4.4 is used for the parameters P_1 and P_2. Otherwise, the contribution of the ligaments to the lumbar stiffness is considered in the disc stiffness by applying the second set of values.

The lumbar disc stiffness is realised in the model as a moment which acts at a joint and in the opposite direction of the current vertebral rotation. The rotation can be split

into the rotations around the principal axes. Therefore, the stiffness values for axial rotation, rotation around the cranial-caudal axis, and lateral bending, rotation around the anterior-posterior axis, are determined by

$$M = -1 \cdot k_{\mathrm{rot}} \cdot \Theta \cdot s \tag{4.6}$$

where k_{rot} is computed according to Equation 4.5, Θ is the current rotational displacement around the concerning axis and s is a scaling factor. This factor considers the body height and is described in the next section. The stiffness for a flexion or extension movement is integrated in a slightly different manner because each according coefficient k_{rot} is calculated with different parameters but both motions rotate around the same axis. The equation is of the form

$$M = -1 \cdot (A \cdot k_{\mathrm{FL}} \cdot \Theta_{\mathrm{FE}} + B \cdot k_{\mathrm{EX}} \cdot \Theta_{\mathrm{FE}}) \cdot s \tag{4.7}$$

where k_{FL} represents the coefficient k_{rot} for a flexion motion and k_{EX} the one for an extension movement. Θ_{FE} is the current rotation around the flexion-extension axis. The parameters A and B simply describe the present direction of rotation as flexion or extension by setting one of them to a value of one and the other one to zero. The direction of rotation is determined by comparing the current value of Θ_{FE} with a predefined position that indicates the turning point. Here, it is 0°.

While the linear model of the disc stiffness is not scaled with the body height, the new non-linear characteristic is always combined with the subsequent scaling method that considers the body height. In addition and analogous to this rotational disc stiffness, a translational stiffness is implemented in the model. However, this extension is not validated to the current date and it is not used in the studies, hence, a description can be found in the Appendix A.4.

Scaling of disc stiffness

The scaling mechanism for the non-linear disc stiffness is based on a publication regarding changes of disc stiffness during adolescent growth [51]. This report provides the relative increase of disc stiffness in dependence of the relative growth of vertebral dimension for the four basic motions flexion, extension, axial rotation and lateral bending. It identified the endplate depth and width as main contributors to a change of stiffness. Therefore, a scaling factor, based on these two parameters, is developed.

Initially, a mean vertebral depth $\overline{VBD}$ and width $\overline{VBW}$ of the L4 and L5 lumbar vertebra is computed from landmark data of the active model. This step is repeated with data published by Weisse et al. [99] ($\overline{VBD_{\mathrm{W}}}$ and $\overline{VBW_{\mathrm{W}}}$). Next, the ratios between the two data sources are calculated by

$$r_{\mathrm{VBD}} = \frac{\overline{VBD}}{\overline{VBD_{\mathrm{W}}}} - 1 \qquad \text{and} \qquad r_{\mathrm{VBW}} = \frac{\overline{VBW}}{\overline{VBW_{\mathrm{W}}}} - 1 \tag{4.8}$$

to obtain the percentaged changes in size between active and literature model. Both ratios are utilised to proportion the reported variations of stiffness which result from the

Table 4.5: Relative changes of stiffness Δk_{VBD}, Δk_{VBW} and related dimensional alterations ΔVBD, ΔVBW from literature [51].

Motion	Δk_{VBD} (%)	Δk_{VBW} (%)	ΔVBD (%)	ΔVBW (%)
Flexion	28.2	3.2	18.2	8.0
Extension	20.1	1.6		
Axial rotation	23.9	4.9		
Lateral bending	10.9	15.8		

changes of vertebral dimensions to the current model. This is realised by

$$R_{\mathrm{VBD}} = r_{\mathrm{VBD}} \cdot \frac{\Delta k_{\mathrm{VBD}}}{\Delta VBD} \qquad \text{and} \qquad R_{\mathrm{VBW}} = r_{\mathrm{VBW}} \cdot \frac{\Delta k_{\mathrm{VBW}}}{\Delta VBW} \tag{4.9}$$

where Δk_{VBD} and Δk_{VBW} represent the relative increases of stiffness caused by the growth of the vertebral depth ΔVBD and vertebral width ΔVBW. Table 4.5 lists the according values for all motions. A combination of Equations 4.8 and 4.9 results in a scaling factor for every movement direction with

$$\begin{aligned} s_n &= 1 + R_{\mathrm{VBD},n} + R_{\mathrm{VBW},n} \\ &= 1 + \left(\frac{\overline{VBD}}{\overline{VBD_{\mathrm{W}}}} - 1 \right) \cdot \frac{\Delta k_{\mathrm{VBD},n}}{\Delta VBD} + \left(\frac{\overline{VBW}}{\overline{VBW_{\mathrm{W}}}} - 1 \right) \cdot \frac{\Delta k_{\mathrm{VBW},n}}{\Delta VBW} \end{aligned} \tag{4.10}$$

as a general formulation. The index n indicates parameters that change with the direction of rotation. Finally, this scaling factor is applied to the computation of disc stiffness of every lumbar level as described in the previous section.

Orientation of discs

The orientation of the discs in all spatial directions is determined by the reference system of segments $S_{S1/L5}$ to $S_{T12/L1}$. These segments are without mass and inertia. In the further course of this thesis, they are called virtual segments. They are placed in the centre between adjacent PLL attachment nodes and are aligned along bisecting lines of the angles between according vertebral endplates. Drivers ensure that these positions will be kept and that the segment's orientation will correctly follow the rotation of the disc.

This target is realised in three steps: constraining the segment's translational position, drive the rotation around medio-lateral as well as vertical axis and finally determine the orientation of the anterior-posterior axis. This technique constrains all six degrees of freedom of each virtual segment.

The position of a virtual segment is determined by two vectors which describe the translations between the segment itself and the superior or inferior vertebra. These vectors

are calculated by

$$\mathbf{u}_{\text{sup}} = \mathbf{v} - \mathbf{l}_{7,\text{sup}} \qquad \text{and} \qquad \mathbf{u}_{\text{inf}} = \mathbf{v} - \mathbf{l}_{5,\text{inf}} \tag{4.11}$$

where $\mathbf{l}_{7,\text{sup}}$ and $\mathbf{l}_{5,\text{inf}}$ represent the position vectors of the PLL landmark node of the superior as well as the inferior vertebra and $\mathbf{v}$ is the position vector of the virtual segment. All these vectors are specified in the global reference system. In the next step, both vectors $\mathbf{u}_{\text{sup}}$ and $\mathbf{u}_{\text{inf}}$ are equalised in quantity and are reversed in direction. This constrains the translational movement of the virtual segment and centres it between the PLL landmark nodes. The according mathematical relationship is of the form

$$\mathbf{u}_{\text{sup}} + \mathbf{u}_{\text{inf}} = \begin{bmatrix} x_{\text{sup}} \\ y_{\text{sup}} \\ z_{\text{sup}} \end{bmatrix} + \begin{bmatrix} x_{\text{inf}} \\ y_{\text{inf}} \\ z_{\text{inf}} \end{bmatrix} = \begin{bmatrix} 0 \\ 0 \\ 0 \end{bmatrix}. \tag{4.12}$$

This context is modelled by utilising a simple kinematic driver, that uses a linear combination of translational measurements as input, for the constraints. The object, which handles such a linear combination, requires a matrix of coefficients as input. This matrix is derived from a slightly altered mathematical formulation of Equation 4.12 of the form

$$\underbrace{\begin{bmatrix} 1 \cdot x_{\text{sup}} + 0 \cdot y_{\text{sup}} + 0 \cdot z_{\text{sup}} + 1 \cdot x_{\text{inf}} + 0 \cdot y_{\text{inf}} + 0 \cdot z_{\text{inf}} \\ 0 \cdot x_{\text{sup}} + 1 \cdot y_{\text{sup}} + 0 \cdot z_{\text{sup}} + 0 \cdot x_{\text{inf}} + 1 \cdot y_{\text{inf}} + 0 \cdot z_{\text{inf}} \\ 0 \cdot x_{\text{sup}} + 0 \cdot y_{\text{sup}} + 1 \cdot z_{\text{sup}} + 1 \cdot x_{\text{inf}} + 0 \cdot y_{\text{inf}} + 1 \cdot z_{\text{inf}} \end{bmatrix}}_{\text{linear combination of measurements}} \underbrace{= \begin{bmatrix} 0 \\ 0 \\ 0 \end{bmatrix}}_{\text{constraint of driver}} \tag{4.13}$$

and results in a matrix of coefficients with the form

$$\mathbf{C}_{\mathbf{u}} = \begin{bmatrix} 1 & 0 & 0 & 1 & 0 & 0 \\ 0 & 1 & 0 & 0 & 1 & 0 \\ 0 & 0 & 1 & 0 & 0 & 1 \end{bmatrix}. \tag{4.14}$$

Rotations β and γ around the medio-lateral and vertical axis of the segment are controlled with the y- (vertical) and z-components (horizontal in medio-lateral direction) of another two vectors $\mathbf{w}_{\text{sup}}$ and $\mathbf{w}_{\text{inf}}$. They determine the translations between the closest ALL attachment nodes of the adjacent vertebrae and the virtual segment by

$$\mathbf{w}_{\text{sup}} = \mathbf{v} - \mathbf{l}_{3,\text{sup}} \qquad \text{and} \qquad \mathbf{w}_{\text{inf}} = \mathbf{v} - \mathbf{l}_{1,\text{inf}}. \tag{4.15}$$

Each vector is calculated by utilising the position vector of the according landmark ($\mathbf{l}_{3,\text{sup}}$ and $\mathbf{l}_{1,\text{inf}}$) and the position of the virtual segment $\mathbf{v}$. Furthermore, they are determined in the local reference system of the virtual segment. Both vectors are then constrained by

$$\mathbf{w}_{\text{sup}} + \mathbf{w}_{\text{inf}} = \begin{bmatrix} 0 \\ y_{\text{w,sup}} \\ z_{\text{w,sup}} \end{bmatrix} + \begin{bmatrix} 0 \\ y_{\text{w,inf}} \\ z_{\text{w,inf}} \end{bmatrix} = \begin{bmatrix} 0 \\ 0 \\ 0 \end{bmatrix}. \tag{4.16}$$

This affects only the two specified components by forcing the vectors to an equal length in the coronal plane and mirroring them at the transversal plane. As before, linear measurement objects provide the two vectors while a linear combination of the selected components is used as input to a simple kinematic driver. This driver models the constraints that orientate the medio-lateral and vertical axis of the virtual segment. The mathematical background of this procedure is of the form

$$\underbrace{\begin{bmatrix} 0 \cdot x_{\mathrm{w,sup}} + 0 \cdot y_{\mathrm{w,sup}} + 0 \cdot z_{\mathrm{w,sup}} + 0 \cdot x_{\mathrm{w,inf}} + 0 \cdot y_{\mathrm{w,inf}} + 0 \cdot z_{\mathrm{w,inf}} \\ 0 \cdot x_{\mathrm{w,sup}} + 1 \cdot y_{\mathrm{w,sup}} + 0 \cdot z_{\mathrm{w,sup}} + 0 \cdot x_{\mathrm{w,inf}} + 1 \cdot y_{\mathrm{w,inf}} + 0 \cdot z_{\mathrm{w,inf}} \\ 0 \cdot x_{\mathrm{w,sup}} + 0 \cdot y_{\mathrm{w,sup}} + 1 \cdot z_{\mathrm{w,sup}} + 1 \cdot x_{\mathrm{w,inf}} + 0 \cdot y_{\mathrm{w,inf}} + 1 \cdot z_{\mathrm{w,inf}} \end{bmatrix}}_{\text{linear combination of measurements}} \underbrace{= \begin{bmatrix} 0 \\ 0 \\ 0 \end{bmatrix}}_{\text{constraint of driver}} \tag{4.17}$$

and it results in a matrix of coefficients with the form

$$\mathbf{C}_{\mathrm{w}} = \begin{bmatrix} 0 & 0 & 0 & 0 & 0 & 0 \\ 0 & 1 & 0 & 0 & 1 & 0 \\ 0 & 0 & 1 & 0 & 0 & 1 \end{bmatrix} \tag{4.18}$$

which is used in the definition of the object representing a linear combination of vectors.

Finally, the virtual segment's remaining unconstrained rotation α around the anterior-posterior axis is fixed. Therefore, the angles α_{PLL}, β_{PLL}, γ_{PLL} between the reference systems of the inferior and superior vertebra's PLL landmarks are measured in global coordinates and their bisector is used to constrain the free rotation. The implementation is similar to the one described above, but this time the basic formulation is

$$\underbrace{\begin{bmatrix} 1 \cdot \alpha_{\mathrm{PLL}} + 0 \cdot \beta_{\mathrm{PLL}} + 0 \cdot \gamma_{\mathrm{PLL}} - 2 \cdot \alpha + 0 \cdot \beta + 0 \cdot \gamma \end{bmatrix}}_{\text{linear combination of measurements}} \underbrace{= \begin{bmatrix} 0 \end{bmatrix}}_{\text{constraint of driver}}. \tag{4.19}$$

It is important to ensure that the matrix of coefficients $\mathbf{C}_{\alpha}$ corresponds to the output of the rotational measurement object in terms of the order of rotations. The outlined procedure is implemented with a rotation sequence of the form z, y, x, therefore, the matrix of coefficients is

$$\mathbf{C}_{\alpha} = \begin{bmatrix} 0 & 0 & 1 & 0 & 0 & -2 \end{bmatrix}. \tag{4.20}$$

4.1.8 Scaling of model

As mentioned in Section 4.1.4, a scaling method from the repository is used to further adapt the model to the subjects. The selected method requires body height, body weight and body fat percent as input parameters and is described in Section 3.4.1. However, the BMI is employed to calculate the body fat percentage because of missing data. It is defined by

$$R_{\mathrm{BMI}} = \frac{m}{(h)^2} \tag{4.21}$$

with the body mass m in kilograms and the body height h in metres.

4.1.9 Subject-specific vertebral geometry

The subject-specific shape of the lumbar spine and its vertebrae is derived from CT images. Therefore, the generic geometry of each lumbar vertebra is morphed to a subject-specific one in four iterations. The applied workflow for the morphing procedure is depicted in Figure 4.6 and it does not change between the different lumbar vertebrae. It

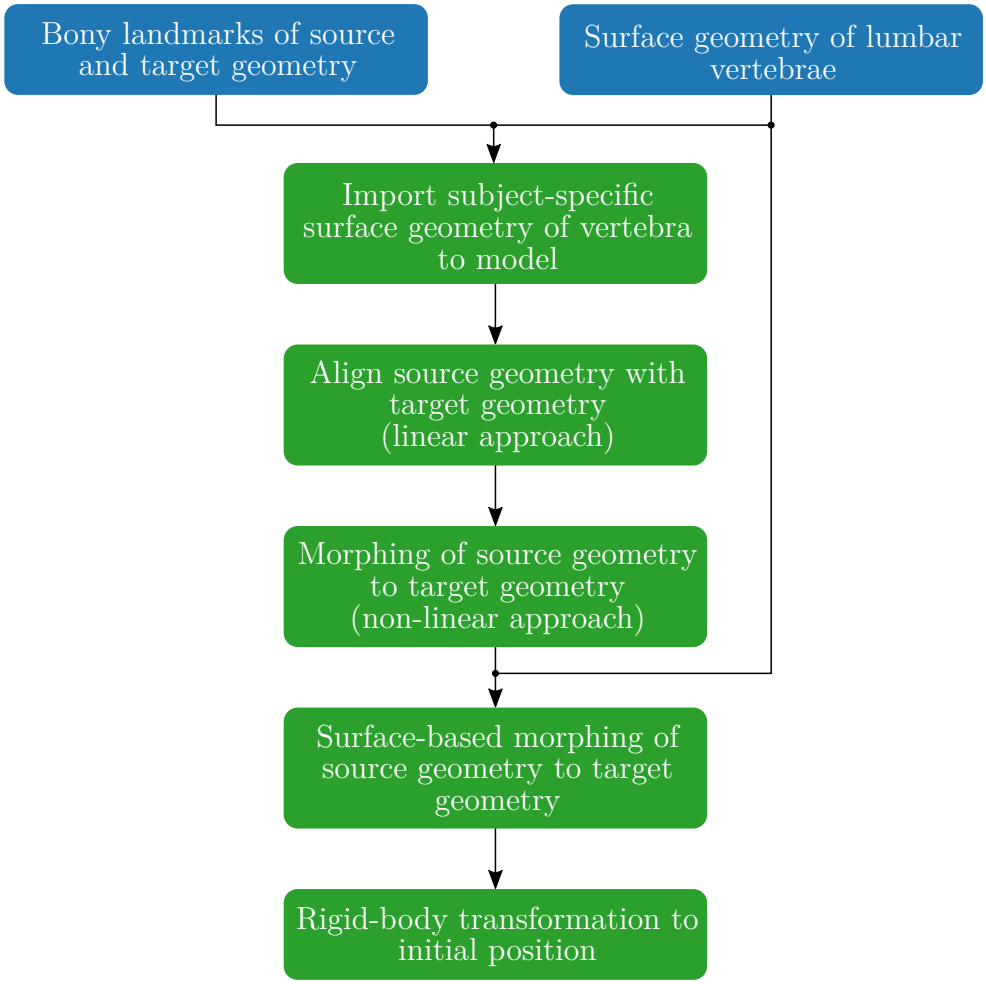

Figure 4.6: The morphing procedure of a single vertebra involves four different transformations. They are executed one after another. Blue boxes represent input data and green boxes are actions.

is designed as a function which can be executed for every lumbar vertebra and it facilitates the import of a subject-specific vertebral geometry for any number of lumbar levels. The AMS does not provide such a functionality, hence, a workaround is used. The workflow is repeated in individual files for every lumbar vertebra and only the input data is adapted to each level. This data comprises the naming of and references to the AnyScript objects as well as landmark data of the generic geometry and the subject-specific geometry. The morphing procedure itself requires the generic and subject-specific

geometrical objects as source and target. If not stated otherwise, source related content is everything regarding the generic model, while each object denoted as target belongs to the subject-specific geometry.

The first step of the workflow is to import target and source landmarks to matrices in the model. Whereas the latter are statically included, all target landmarks are loaded from a file via a PYTHON script as aforementioned. Furthermore, all target landmarks need to be scaled because CT images are usually recorded in millimetres.

The first of four morphing functions has a linear characteristic and moves the source geometry to the target's location based on the landmark data. It utilises translation, rotation, skewing and scaling of the geometry. All in all, it creates a linear transformation with twelve degrees of freedom and a least-squares method using source and target landmarks. This results in a relocated and slightly modified source geometry with the source landmarks close to the positions of the target landmarks. However, both geometries still show major differences.

A non-linear morphing function, based on radial basis functions (RBFs), is applied to improve this. It enables a better approximation of the target surface because it also considers local features. RBFs are usually used to approximate a function and their main characteristic is that their values depend only on the distance to their origins. Here, a RBF of a thin-plate type

$$\Phi = r^2 \cdot \ln(r) \qquad \text{with} \qquad r = \|\mathbf{v} - \mathbf{o}\| \tag{4.22}$$

is used. It is well suited for approximations with a higher number of origin points (landmarks). The approximation itself is performed by linear combinations of the RBFs

$$f(\mathbf{v}) \approx \sum_{i=1}^{n} c_i \cdot \Phi(\|\mathbf{v} - \mathbf{o}_i\|) \tag{4.23}$$

with n as the number of origin points and c as RBF coefficients. These coefficients are automatically determined because the morphing function is applied with an implicit specification. In this way the target and source landmarks provide the information for the coefficients' determination and the resulting interpolation between target and source produces a surface with a good fit at the locations of the landmarks. Additionally, a bounding box is used to further improve this morphing, especially for the attachment points of muscles and ligaments because these points are extrapolated (they are not covered by the landmarks). The bounding box adds extra points to the approximation. These points are the corners of the box and points on the faces. The latter are determined by a division factor which is set to two in all three directions. The size of the bounding box is defined by the specified landmarks and it is influenced by a scaling factor. This scaling factor is also set to two in all directions.

To catch as much detail as possible, an additional morphing function, using the vertebral surface, is employed. Basically, this method matches the previous one but instead of specifying source and target landmarks, this functionality generates this information based on two specified STL files. STL files represent a surface geometry by triangles,

as mentioned earlier. The morphing function uses the polygonal surface information to automatically pick a specified number of points (set to 500) on the source surface. Afterwards, vertices of the target surface with the smallest distance to these points are determined. Both informations are then used to create another RBF approximation with the other settings equal to the previous ones.

At last, the morphed shape of each vertebra is moved to the corresponding location in the model by a final linear rigid body transformation. In case of the L5 vertebra, this final transformation is constructed by simply using target and source landmarks as starting and final location, respectively. This particular step differentiates between the L5 lumbar vertebra and all other lumbar vertebrae. This distinction is necessary, because the information about the subject's lumbar lordosis has to be preserved. Therefore, the location of the L5 vertebra is used as foundation for the repositioning of the other four lumbar vertebrae. For this purpose, an interim conversion is constructed because this offers the option to modify the vertebra's position with additional parameters which is required for the parameter studies, for example a parametrised disc height. It is realised by using the superior and inferior landmarks of the ALL and PLL (landmark numbers 1, 3, 5 and 7 in Table 4.2) of the L5 target geometry as origin and the same landmarks as destination but after applying the complete subject-specific transformation chain. Without an additional parametrisation due to the parameter studies, it results in a transformation matrix equal to the one for the final transformation of the L5 vertebra. Consequently, the interim conversion is used to transform the target points of the remaining four vertebrae and the result is specified as the destination for the linear rigid body transformation, while the untransformed target points represent its origin. Thereby, the vertebrae L1 to L4 are moved to their proper position in the model and the subject-specific lumbar lordosis is preserved.

The four described transformations for every lumbar vertebra need to be executed one after another because each one requires the improved output of the preceding morphing function as input. Therefore, a collective transformation function, invoked at the creation of any concerning lumbar object, starts the morphing process.

4.1.10 Facet joints

The contact between facet joints is modelled by a surface contact function. This function utilises STL files to compute the contact forces between the surfaces. In order to keep the computational cost as low as possible, only the absolute necessary sections of a vertebra are considered. Therefore, a separate STL file of every facet of the lumbar vertebrae L1 to L5 is created with the open source software MeshLab. The facets are separated from the vertebra by slicing the individual facet and closing occurring holes. Afterwards, those newly constructed geometries are scaled and imported at a new reference node located at the central point of the according vertebral body. Just as the surface geometry of the vertebrae, the facet surfaces have to be shifted from their imported location to the correct one in the model with linear rigid body transformations. Therefore, the L5 vertebra's facets are relocated by a linear rigid body transformation with the target landmarks of the vertebra as origin and the source landmarks as the destination. The different handling

of the L5 vertebra and the remaining ones is also necessary, hence, the facets of the other four lumbar vertebrae are transformed by the same final linear rigid body transformation as the vertebrae. This moves every facet to its corresponding position but retains an offset of the import location, the distance between the import location of the vertebra and the newly created node at the central point of the vertebral body. This known offset is corrected by another rigid body transformation.

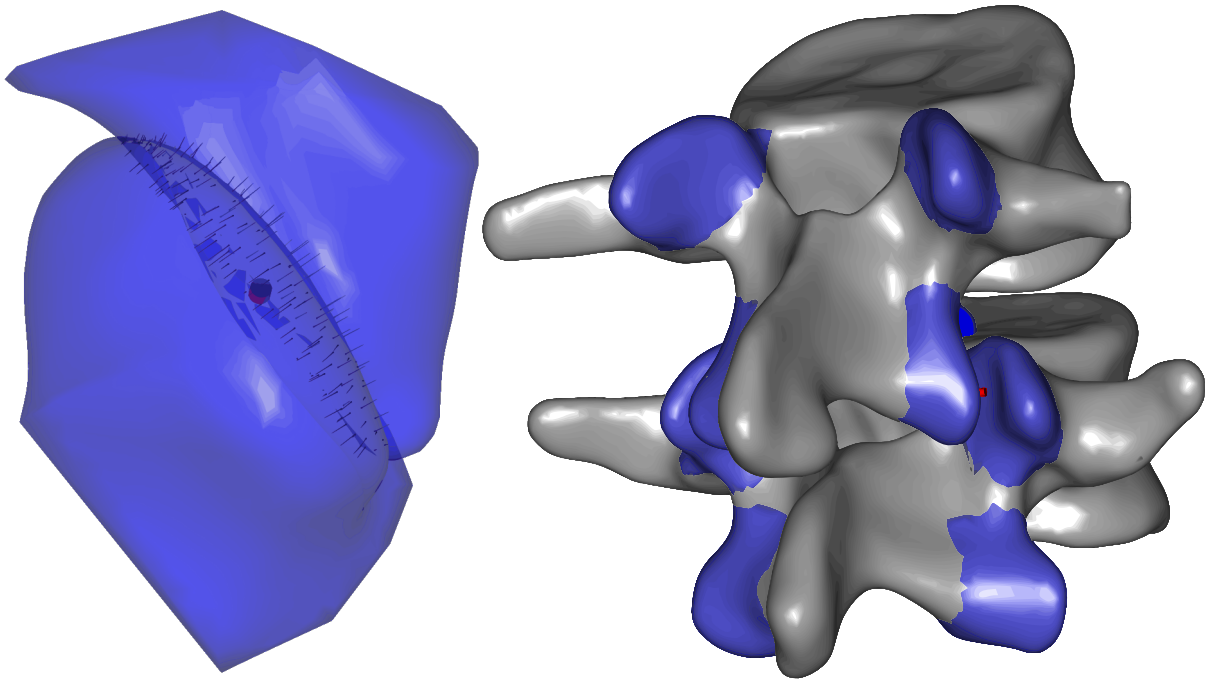

Figure 4.7: A pair of adjacent facet surfaces are shown on the left. They are in contact and according force vectors are also displayed as well as the modelled facet capsular ligament. The right part depicts a motion segment with the imported geometries of facets (blue) for surface contact after applying all necessary transformations.

Adjacent facets are then referenced in a surface contact function that computes the contact forces and moments based on the penetration depth of vertices and a pressure module. This module is set to a tuned value of $500\,\mathrm{MN/m^3}$. Moreover, the mesh refinement options for master and slave surfaces are set to four. As the name suggests, this option refines the mesh that is created by the vertices, in order to have a good density of contact points. Figure 4.7 shows the final results when two adjacent facets are in contact (left) and facets in combination with their vertebrae (right).

The facet capsular ligament (FCL) is modelled between two nodes, which are positioned around the centre of a line connecting the mid landmarks of a pair of facets. The landmark's numbers are 37 to 40 as listed in Table 4.2. Furthermore, the material properties of the FCL (Table 4.6) are adjusted according to data published by Pintar et al. [67]. Because of different central locations of adjacent facet surfaces of the various subjects and the initialising sequence of a model in the AMS, the subsequently described method is implemented to achieve a preset length of the FCL.

Table 4.6: Material properties of the FCL according to published values [67].

Lumbar level	Stiffness N/mm	Strain %
L1/L2	42.5	90.4
L2/L3	33.9	70.0
L3/L4	32.3	52.7
L4/L5	30.6	47.9

The first step is to create a segment without mass and inertia properties for every single facet. Afterwards, these segments are linked to the according landmarks on the facets with three artificial ligaments using a generic ligament class. Each ligament represents one of the three spatial directions. The usage of a ligament for the distance quantification is essential, because only the length of a ligament can be calibrated. To ensure that these artificial ligaments do not change the kinetics of the model, their properties are adjusted to produce no forces. Their only purpose is to set the location of the virtual segments during calibration. While calibrating, segments are relocated with the help of drivers. A single driver adjusts the relative position of the segment to its according facet surface landmark in all three spatial directions. This is achieved by applying a linear combination of values of the following linear measurements to the driver: measurements between segment and landmark as well as between the two landmarks of adjacent facet surfaces. The linear combination determines the centre between those two landmarks and the driver sets both segments around this location to keep an adjustable gap between them (2 mm by default). A successful calibration procedure then returns the vector between a facet surface landmark and a virtual segment by the calibrated lengths of the according artificial ligaments. Finally, these values are utilised by drivers that constrain the segments to their landmarks. This technique is implemented to determine the attachment nodes' position during the calibration run.

4.1.11 Calibration

Calibration is done in an upright standing posture. Hence, the rotation of the lumbar joints is adjusted to zero. This results in a neutral position corresponding to that during the scanning. For all other connections, the default values are retained. The calibration procedure comprises all modelled ligaments including the artificial ones.

4.1.12 Parametrisation

All parametrisation of the lumbar geometry is confined to the position and orientation of nodes without affecting the displayed geometry of a bone. Table 4.7 lists all parametrised anatomical dimensions which are available in the model, while the following sections give detailed information about the particular implementation. For a better illustration the parameters are also shown in Figure 4.8.

Table 4.7: List of all lumbar geometrical parameters with their according abbreviation.

No.	Parameter	Abbreviation
1	Vertebral body width	VBW
2	Vertebral body height	VBH
3	Vertebral body depth	VBD
4	Transverse process width	TPW
5	Spinous process length	SPL
6	Pedicle length	PDL
7	Disc height	DiH
8	Interfacet width	IFW
9	Interfacet height	IFH
10	Lumbar lordosis	LOR

General

As stated in the introduction to this section, only nodes are affected by the parametrisation. Initially, the orientation of the lumbar vertebrae has to be determined because their reference systems are orientated in accordance with the global reference system, hence, individual transformation matrices have to be constructed to achieve a parametrisation that is aligned with each vertebra's orientation. Otherwise, a modification would not follow the object's shape.

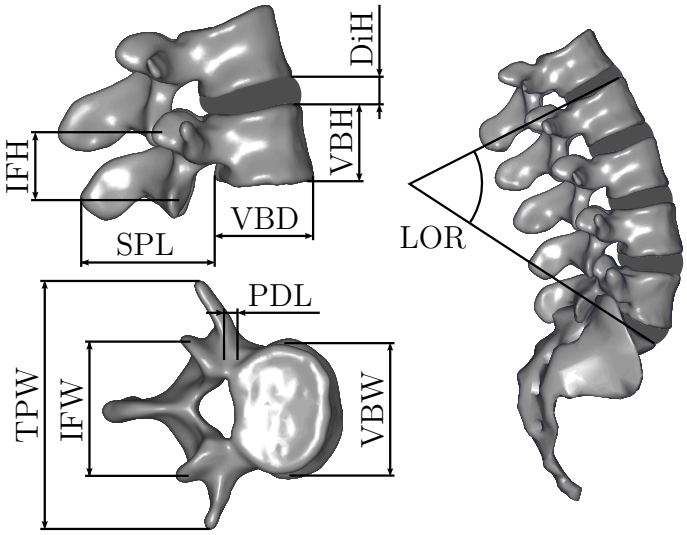

Figure 4.8: All anatomical parameters which could be modified in the model. The abbreviations are listed in Table 4.7.

The AMS computes an initial rotational transformation matrix for every segment. This matrix corresponds to the initial orientation of the segment and it is already available when the model is loaded. This is important because the position of a node is defined at this stage and it can not be modified at a later stage. Therefore, this initial rotational

transformation matrix is used to transform a modification of nodes to the corresponding reference system. Virtual segments with zero mass, zero inertia properties and without a connection to the body model by drivers are utilised to provide the necessary information. The orientation of these segments corresponds to the inclination in the sagittal plane of the lumbar vertebrae when the model is loaded. It is determined by the upper vertebral endplate at each lumbar level. The landmarks of the superior attachment points of the PLL and ALL are used to calculate the according rotational displacement around the medio-lateral axis.

A majority of the defined parameters influences the shape of the lumbar vertebrae without affecting the positions of the vertebral bodies (the central point/COM of the body stays at its position). For this reason, the information about the orientation of each vertebra in combination with the value of the parameter is sufficient to create the desired effect, e.g. increase the width of the vertebral body. Just the following parameters require further modifications in the model.

Disc height

An adjustable disc height is created by modifying every inferior joint node location. Therefore, a vertical unit vector for each lumbar vertebra is introduced. It indicates the selected shifting direction of the concerning joint nodes. As in the definition of these nodes, bony landmarks are used to compute the unit vectors. Figure 4.9 illustrates the whole process to increase or decrease the disc height at every lumbar level.

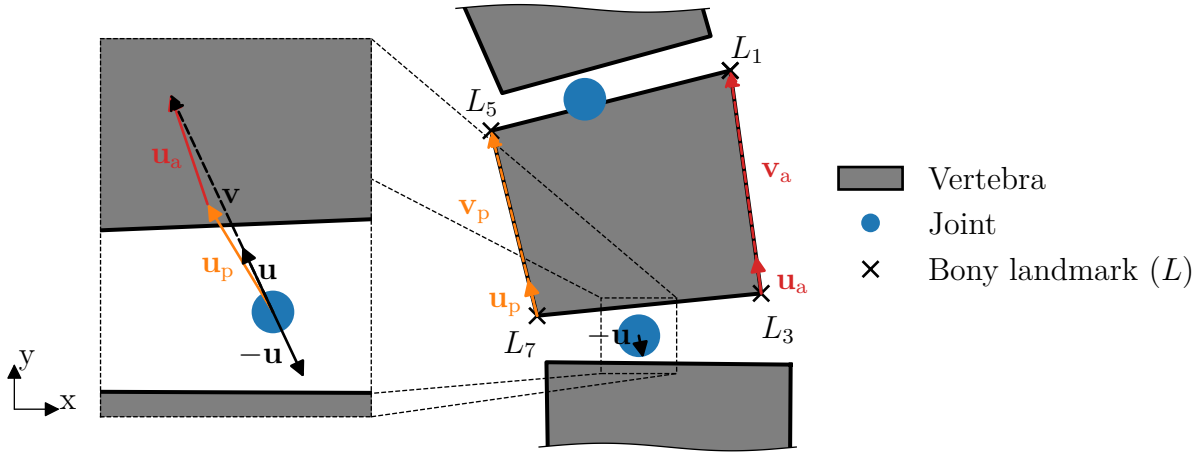

Figure 4.9: An illustration of the process to determine the unit vector used to reposition the inferior joint node of a lumbar vertebra for parametrisation.

The position vectors of the superior and inferior landmarks $\mathbf{l}$ of the ALL and PLL define

two unit vectors

$$\mathbf{u}_\mathrm{a} = \frac{\mathbf{v}_\mathrm{a}}{|\mathbf{v}_\mathrm{a}|} \qquad \text{with} \qquad \mathbf{v}_\mathrm{a} = \mathbf{l}_1 - \mathbf{l}_3 \qquad \text{and} \tag{4.24}$$

$$\mathbf{u}_\mathrm{p} = \frac{\mathbf{v}_\mathrm{p}}{|\mathbf{v}_\mathrm{p}|} \qquad \text{with} \qquad \mathbf{v}_\mathrm{p} = \mathbf{l}_5 - \mathbf{l}_7 \tag{4.25}$$

which are used to determine the selected direction to modify the inferior joint node. A vector addition of both

$$\mathbf{v} = \mathbf{u}_\mathrm{p} + \mathbf{u}_\mathrm{a} \tag{4.26}$$

returns another vector $\mathbf{v}$, describing the direction for the modification. The associated unit vector

$$\mathbf{u} = \frac{\mathbf{v}}{|\mathbf{v}|} \tag{4.27}$$

in conjunction with the parameter value is used to shift the location of the joint node and changes the disc height. Only the inferior joint node of a vertebra is repositioned to respect the adapted position of all lumbar joints.

Vertebral body height

The method for the modification of the vertebral body height is closely related to the previous one utilised for the alteration of the disc height, thus, the created unit vectors are also applied here. In contrast to the changes of the disc height, both (superior and inferior) joint nodes of a segment are shifted along the associated unit vector but in opposite directions. All other nodes, which have to be modified (e.g. attachment nodes of ALL and PLL), are moved along the vertical axis of the according vertebra. All superior nodes of the vertebral body are shifted in cranial direction while all concerned inferior nodes are moved in caudal direction. The corresponding axes are represented by the reference systems of the previously described virtual segments. This method guarantees an even distribution of the specified height change to the upper and lower part of the vertebral body.

Lumbar lordosis

The variable LOR affects the lumbar spine as a whole. This given change of the lumbar lordosis is equally distributed over five levels starting with the L4/L5 level and continuing upwards. It is programmed by affecting the current transformation matrices of the according spinal joint. Each joint is rotated about a fifth of the specified angular change.

Disc stiffness

The L4/L5 lumbar disc stiffness can be adjusted as a percentage. The three-dimensional stiffness vector is affected as a whole by a variable in a range between 0 and 1.

Multifidus muscle strength

Multifidus muscles are parametrised in such a way that fascicles crossing the L4/L5 lumbar level are either enabled or disabled. An implemented switch turns them operational or sets their strength close to zero rendering them inactive. This option changes the behaviour of the left and right part of the muscle group simultaneously.

4.2 Validation

The validation of the models is founded on the comparison of computed IDP with literature data and encloses the following three steps: checking of absolute values in an upright standing posture, lining up the progression of the IDP throughout motions and comparison of the relative changes between postures proportioned to an upright standing pose. These three validation steps are executed prior to the sensitivity studies and the case study, because their model configuration is different. Overall, three configurations are used. The first configuration is composed of the AMMR in Version 1.4.1, lumbar discs with a linear stiffness model, ligament groups calibrated as a whole and the surface contact between facets but yet without facet capsular ligaments. It is used in the sensitivity studies. The other two configurations utilise a similar set-up with the AMMR in Version 1.6.1, the advanced implementation of the disc stiffness and the ligaments (non-linear model and individually calibrated ligaments) as well as facet capsular ligaments and the surface contact between facets. They only differ in their spinal motion rhythm, with the second configuration using force dependent kinematics and the third one is adjusted to utilise the pre-defined spine rhythm. Both configurations are used in the case study. Table 4.8 shows a comparison of these configurations.

Table 4.8: Overview of the three validated model configurations.

Option	Config 1	Config 2	Config 3
AMMR version	1.4.1	1.6.1	1.6.1
Disc stiffness model	Linear	Non-linear	Non-linear
Ligament calibration	Groups	Individual	Individual
Surface contact of facets	Active	Active	Active
Facet capsular ligament	None	Active	Active
Spinal kinematics	FDK	FDK	Pre-defined spine rhythm
Application	Sensitivity studies	Case study	Case study

The settings of the AMS are adjusted as follows throughout all validation simulations. The gravity is set to $9.81\,\mathrm{m/s^2}$, the polynomial muscle recruitment is used with a power of three and an activation of muscles above 100 % is also allowed. If the latter is the case in a simulation run, it is considered in the evaluation of the results. The FDK solver is configured with a maximal residue of 0.5 N for the computation of the quasi-static equilibrium of all concerning forces. Furthermore, the number of iterations to reach this tolerance is limited to 600 to maintain a reasonable computation time. These AMS

settings are summarised in Table 4.9 and all unmentioned options are set to their default values. Some of these AMS settings in the validations may differ from the settings used in

Table 4.9: Customised solver options for validation simulations.

Option	Value
Type of muscle recruitment	Polynomial
Power of polynomial criterion	3.0
Limit activation of muscles	Off
Force dependent kinematic solver	On
Limit of FDK iterations	600
FDK force tolerance	0.5

the studies, however, they mostly affect the computational time with a sufficient precision of the results.

4.2.1 Absolute values

The computed IDP at the L4/L5 lumbar level is compared to various reported experimental data [80, 92, 102]. Therefore, each model is set up in an upright standing posture that represents the relaxed standing pose used in the experiments. Furthermore, all configurations are investigated.

The simulations return reaction forces of the joint while data in literature is reported as an IDP, hence, the resulting values are approximated with

$$p_{\mathrm{ID}} \approx \frac{F_{\mathrm{c}}}{A_{\mathrm{Disc}} \cdot k_{\mathrm{C}}}. \tag{4.28}$$

This equation represents a rearrangement of Equation 2.1 with F_{c} as the compressive component of the simulated joint reaction force, A_{Disc} as the cross-sectional area of the disc and k_{C} as an individual correction factor. In combination with the first configuration of the model described above, the vertical component of the L4/L5 joint reaction force is used as compressive force. The components of this force vector are aligned with the global coordinate system because the actual orientation of the disc is not available at this time. During the other two approaches, the vector of the L4/L5 joint reaction force is transformed with the rotational transformation matrix obtained from the corresponding virtual segment described in Section 4.1.7. This way, the coordinate system of the joint reaction force is aligned to the actual orientation of the disc and the y-component of the force vector corresponds to the acting compressive force of the disc. The disc's cross-sectional area of all five subjects is listed in Table 4.1 and the correction factor ranges from 0.55 to 0.77 with a mean value of 0.66 according to Dreischarf et al. [22] because individual correction factors are not available.

4.2.2 Progression of intradiscal pressure

The three basic motions extension (15°) to flexion (40°), axial rotation (−12° to 12°) and lateral bending (−15° to 15°) are simulated with each model in the previously described configurations. All motions are divided into eleven discrete steps if the FDK solver is applied and into seven discrete steps if the spine rhythm is used. The step size of the FDK simulations in combination with a non-linear model of the disc stiffness and the extension to flexion motion is kept variable to receive a sufficient number of successful simulation runs. Again, each model's IDP is approximated by Equation 4.28. The mean value of 0.66 is used as correction factor, because this part of validation solely concentrates on the progression of the IDP. Apart from that, the procedure to determine the compressive force remains the same as described in the previous section. The calculated progression of the IDP is compared to data of a single subject reported by Wilke et al. [103]. This data is not available in computer processable form and, hence, it is digitised using the software Plot Digitizer (Version 2.6.8, plotdigitizer.sourceforge.net).

4.2.3 Changes on intradiscal pressure between postures

The simulations consider the following postures (Figure 4.10): upright standing, standing with the trunk flexed forward, seating in a relaxed position, seating with back straight and without back support, standing with a weight close to the body, standing with a weight in hands distant from the thorax, lifting a weight with flexed lumbar spine and lastly, lying in a supine position. Each model is set up in every single one of these pos-

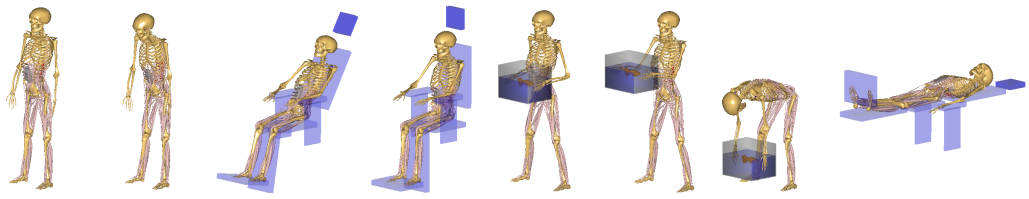

Figure 4.10: The models are configured to adopt the shown postures for validation purposes. Those stances are named as follows: upright standing, standing flexed forward, sitting relaxed, sitting straight without support, standing lift close, standing lift stretched arms, lifting a weight, lying on the back (from left to right).

tures with all previously specified configuration states. Afterwards, the resulting IDPs are normalised to the upright standing posture to facilitate a comparison between the different subjects. The simulated results are also compared to normalised values of reported IDPs from experiments [56, 80, 92, 102, 103]. A brief description of every used posture will be given hereafter, while more information about the applied settings can be found in Table A.3 in the Appendix A.5.

Standing

The standing pose is the one which is used as starting position in nearly every study. All values of the posture driver are set to zero. In medio-lateral direction the model's centre

of mass is aligned between the feet, while in posterior-anterior direction it is shifted 5 cm in front of the ankles. Moreover, rotation about the medio-lateral axes of the ankle joints is not constrained.

Standing flexed forward

The standing pose with the trunk flexed forward is based on the standard pose and differs only in the flexion-extension angle. The according value is set to $-50°$ while all other values remain at zero.

Sitting relaxed

The models are placed in the chair from the publicly available AMMR model 'SpinePressureSeatingRelaxed'. Therefore, the same approach is applied which means that additionally to the established connection between pelvis and seat, the feet, footrest, trunk and backrest are also connected to it. A connection is active, if the distance between the connection node of the segment and the rectangle segment of the seat model fall below 5 cm. Reaction forces at the connecting nodes are realised by artificial muscles with a very high strength. Additionally, the driven inclination angle of the backrest replaces the flexion-extension driver of the body model.

Sitting straight without support

For this position a similar approach to the relaxed posture is taken. It mainly differs at the backrest and legrest inclination angles (Table A.3). Both are adapted to position the model in a straight seating pose. Furthermore, the artificial muscles between trunk and backrest are set to zero, so that the model is not supported by the backrest.

Standing with weight close to the body

Basically, the model in an upright standing posture is modified to hold a weight of 20 kg in between its hands. The weight's COM is set to a height of 1.2 m and an anterior-posterior distance of 25 cm between the model's centre of mass and the box centre.

Standing with weight in extended arms

The model described in the previous section is changed in a few points: the anterior-posterior distance between centre of mass of the model and the box is set to 45 cm. Additionally, some joint angles of the arms are adjusted (Appendix A.5).

Lifting a weight

The model with the weight close to the body is modified to one lifting the same weight from the ground. Therefore, the lumbar flexion is set to 45° and the position of the box is determined by the arms. The according angles are modified to obtain a natural posture of the arms. All joint angles can be found in the Appendix A.5.

Lying on the back

The relaxed seating posture is modified to a lying one by mainly adjusting the seat's joint angles. Backrests, legrests and armrests are set into a horizontal position at the same height, while a model-specific footrest position determines the exact posture of the legs. Contact forces between model and seat are specified according to the description in the relaxed seating simulations but without a support at the foot rest.

4.3 Studies

The following sections give detail about the set-up of the two sensitivity studies as well as the case study. Both sensitivity studies have already been published [68, 69]. It has to be noted that each study is conducted with a different version of the model due to its increasing complexity in the course of this thesis. The subsequent sections include a description of every utilised model state based on the explanations in the previous sections.

4.3.1 Influence of ligament stiffness on loading and motion

The design of this study is depicted in Figure 4.11. The study itself is based on fluoroscopic recordings of three subjects provided by Ortho Kinematics, Inc. (Austin, Texas). This data is used to calculate subject-specific CORs, which are verified by data from Pearcy and Bogduk [65]. The provided and calculated data is used to construct three models. Each model performs a flexion motion in the simulation with a ROM adapted to the experimental data. In course of the sensitivity study, the stiffness of the lumbar ligaments is changed in eleven steps and forces, moments as well as the ROMs are evaluated. The simulations are conducted with the AMS in version 5.3.0.

Subject data

Fluoroscopic recordings are a sequence of lateral radiographic images of a controlled motion. In this case the subjects execute an extension to flexion movement. The captured images, 180 per dataset, include the lumbar vertebrae from L3 to S1. Additional data files provide informations about the coordinates of all corners of rectangles that approximate the vertebral body, the body height and body weight of each subject (Table 4.10). All participants gave a written informed consent about the usage of the

Table 4.10: Body height and body weight of the three subjects who executed the extension-flexion motion while being recorded.

Subject	Body height	Body weight
1	175 cm	76 kg
2	173 cm	79 kg
3	178 cm	86 kg

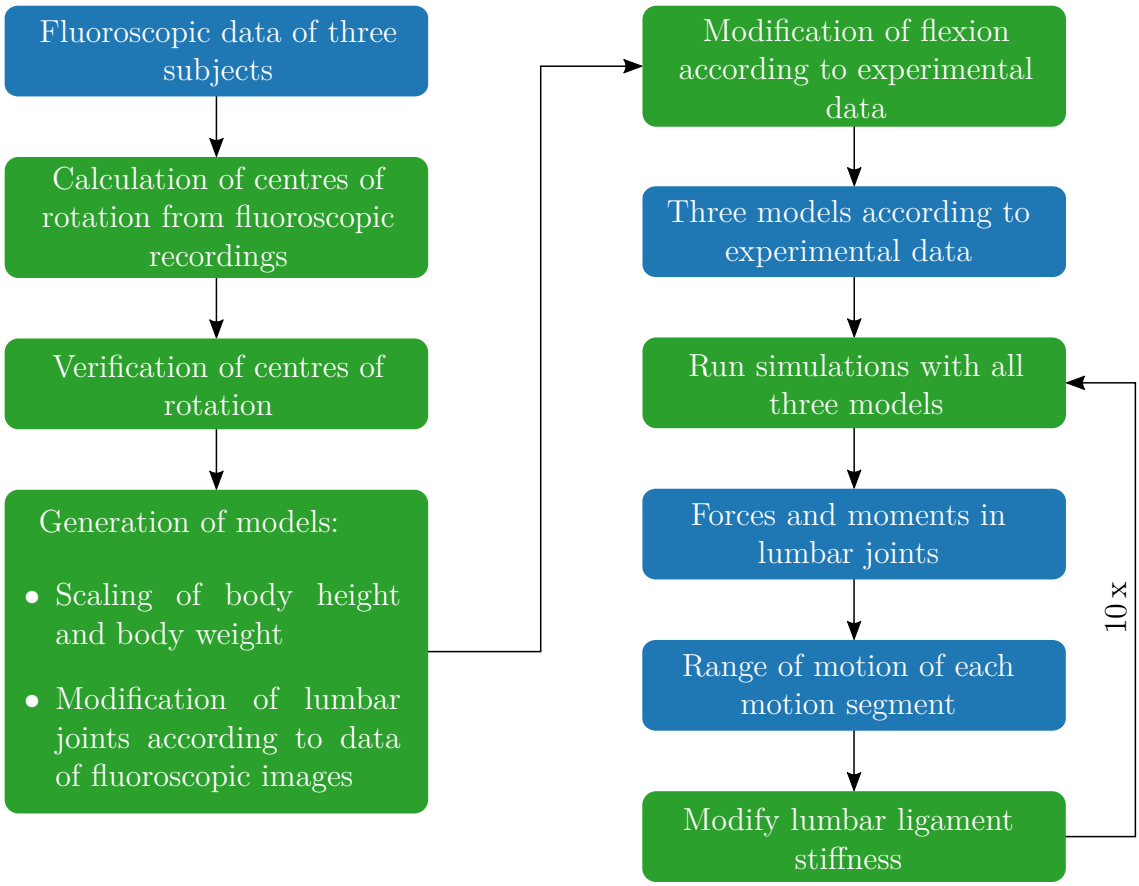

Figure 4.11: An overview of the study regarding the influence of ligament stiffness on lumbar loading and motion. The blue boxes represent result or input data and green boxes are actions.

generated data.

At first, positions of the COR of the available lumbar levels L3/L4, L4/L5 and L5/S1 are calculated. The following technique developed by Panjabi [60] is utilised for this. The coordinates (x, y) of two points on the upper vertebra per motion segment are measured at two different points in time. In the particular cases, the superior corners of each previously described rectangle are used. These points correspond roughly to the landmarks L_1 and L_5. The first and last image of each set are used. All measurements are taken with respect to the same fixed coordinate system. Its origin is located at the posterior corner on the superior side of the sacrum. The four measurements per level are

$$L_1 = (x_1, y_1), \quad L_1' = (x_2, y_2), \quad L_5 = (x_3, y_3) \quad \text{and} \quad L_5' = (x_4, y_4) \tag{4.29}$$

with L_1, L_5 as the first measurements and L_1', L_5' as the second ones. The coordinates of

a COR $(x_{\text{cor}}, y_{\text{cor}})$ are calculated by

$$x_{\text{cor}} = \frac{(y_4 - y_3) \cdot a - (y_2 - y_1) \cdot b}{2 \cdot c} \qquad \text{and} \qquad y_{\text{cor}} = \frac{(x_2 - x_1) \cdot b - (x_4 - x_3) \cdot a}{2 \cdot c} \tag{4.30}$$

where

$$\begin{aligned} &a = x_2^2 - x_1^2 + y_2^2 - y_1^2, \qquad b = x_4^2 - x_3^2 + y_4^2 - y_3^2 \qquad \text{and} \\ &c = (x_2 - x_1) \cdot (y_4 - y_3) - (x_4 - x_3) \cdot (y_2 - y_1). \end{aligned} \tag{4.31}$$

Basically, this procedure superimposes the start and final position of every motion segment and constructs perpendicular bisectors of the lines between the two chosen points. The point of intersection of these bisectors is the position of the according COR. The resulting positions are verified with data of a flexion motion published by Pearcy and Bogduk [65].

Individual body models

The starting point for the models used in this study is a subject-specific model based on the lumbar geometry of subject one in combination with the following model options: a linear disc stiffness, ligaments calibrated in groups, inactive FCL but activated surface contact between the facets and an active FDK solver. Furthermore, the calculated CORs of L3/L4 and L4/L5 together with the body heights and weights of the subjects are used to construct three individual models. Hence, the configured models are scaled with the data provided (Table 4.10) and the lumbar joint's COR at the L3/L4 and L4/L5 level are relocated to the positions calculated from the fluoroscopic images. Moreover, each model's flexion movement, meaning initial and final position, was adapted to the subject's scope.

Configuration of simulations

The intervals of variation of each ligament stiffness are taken from published experimental studies [15, 67]. They are listed in Table 4.11. The reported ranges, defined by the mean

Table 4.11: Mean values and standard deviations in N/mm defining the studied intervals of all lumbar ligament stiffness. There were no deviations for the ITL available.

	T12/L1	L1/L2	L2/L3	L3/L4	L4/L5	L5/S1
ALL	32.9 ± 20.9	32.4 ± 13.0	20.8 ± 14.0	39.5 ± 20.3	40.5 ± 14.3	13.2 ± 10.2
PLL	10.0 ± 5.5	17.1 ± 9.6	36.6 ± 15.2	10.6 ± 8.5	25.8 ± 15.8	21.8 ± 16.0
ISL	12.1 ± 2.6	10.0 ± 5.0	9.6 ± 4.8	18.1 ± 15.9	8.7 ± 6.5	16.3 ± 15.0
SSL	15.1 ± 6.9	23.0 ± 17.3	24.8 ± 14.5	34.8 ± 11.7	18.0 ± 6.9	17.8 ± 3.8
LF	24.2 ± 3.6	23.0 ± 7.8	25.1 ± 10.9	34.5 ± 6.2	27.2 ± 12.2	20.2 ± 8.4
ITL	50.0	50.0	50.0	50.0	50.0	50.0

Table 4.12: The solver was set to the listed status. Only important and all custom values are specified.

Option	Value
Type of muscle recruitment	Polynomial
Power of polynomial criterion	3.0
Limit activation of muscles	On
Force dependent kinematic solver	On
Limit of FDK iterations	200
FDK force tolerance	0.001

values and standard deviations, are divided into ten equal sections, resulting in a step size of 10 % and eleven individual steps. Those values are used to conduct eleven simulations for each of the three constructed models. In a single run, all lumbar ligament stiffness values over all lumbar levels are set to the same percentage.

The publications are lacking values for the lumbar ITL, hence, mean values of the ligament at the T7/T8 level are used. Due to missing standard deviations, this ligament is not varied throughout the studies.

Every simulation is conducted with gravity and an active FDK solver. The force tolerance is reduced to 0.001 N to achieve a very precise positioning of the lumbar vertebrae and the number of iterations is set to 200 to keep the computation time in reasonable time frame. Furthermore, the limit of 100 % of the activation of muscles is active. All these custom and other important solver options are listed in Table 4.12.

Outcome parameters

The effects of a varying ligament stiffness are identified by evaluating the following parameters: joint and ligament forces, resulting moments generated by the ligament forces with the respective distance to the joint as moment arm and lumbar kinematics.

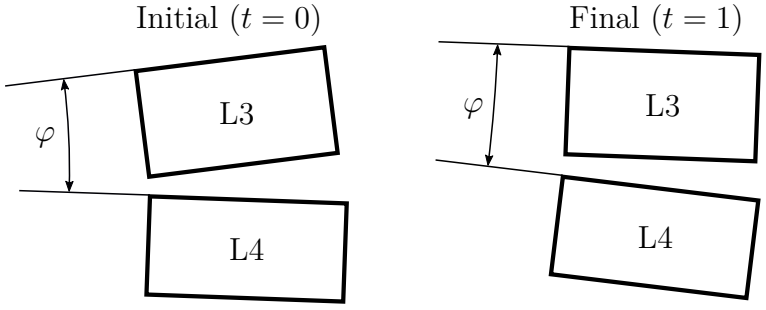

Figure 4.12: This measurement of the angles between adjacent vertebrae to calculate the ROM uses the L3/L4 motion segment as an example.

The latter is investigated by evaluation of each motion segment's ROM. The ROM is defined by

$$\Delta\varphi = \varphi(t = 1) - \varphi(t = 0) \tag{4.32}$$

with φ representing the angle between upper endplates of adjacent vertebrae at the initial ($t = 0$) and final ($t = 1$) time step. Figure 4.12 illustrates the measurement of the angle at an example.

4.3.2 Influence of lumbar geometrical parameters on loading

This study is conducted to investigate the influence of ten anatomical parameters on lumbar loading. Figure 4.13 depicts an overview. In course of this study, simulations

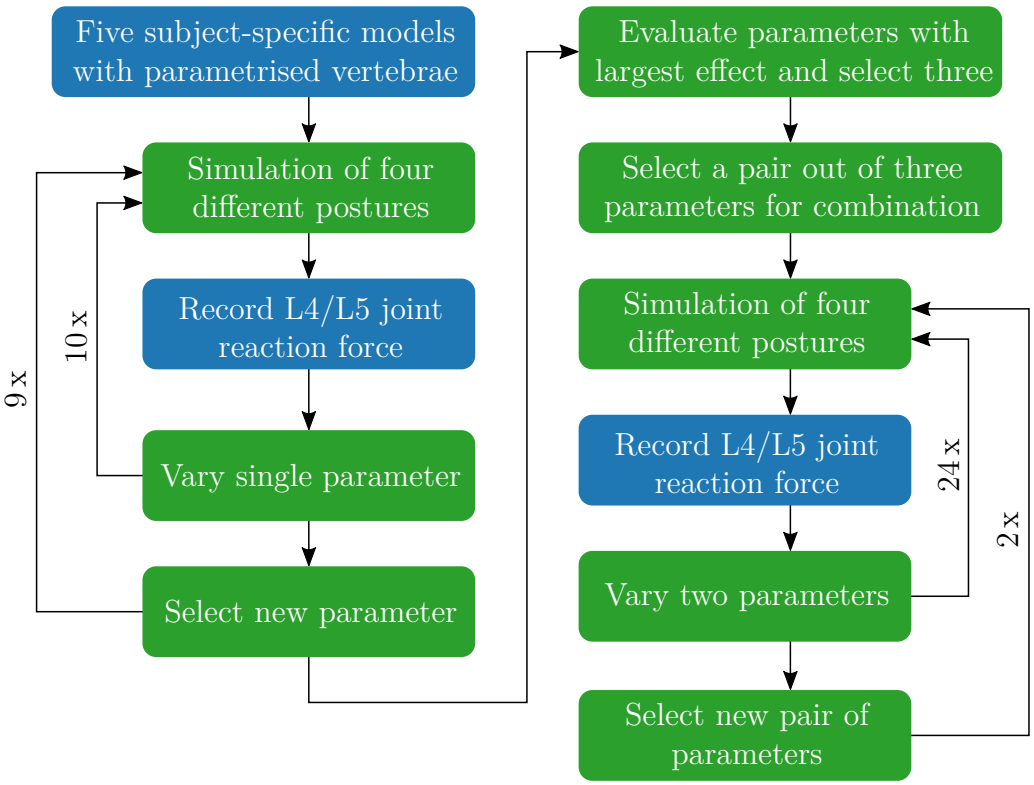

Figure 4.13: Flow chart of the study regarding influences of lumbar anatomical parameters on lumbar loading. Blue boxes represent input or result data and green boxes are actions.

with five subject-specific models are performed. Each model's lumbar geometry is parametrised and the models are configured to adopt four different postures. The study is divided into two main sections: the first part evaluates the effects of single parameter variation on lumbar loading while the second one analyses influences of combined parameter changes. Therefore, each parameter value is set in individual simulations with all model-posture combinations and the reaction forces at the L4/L5 level is recorded and evaluated. Subsequently, three parameters, that show a large influence, are selected and the effects of all possible pairs are analysed in simulations with all model-posture combinations. Again, these analyses are focused on the reaction forces of the L4/L5 level.

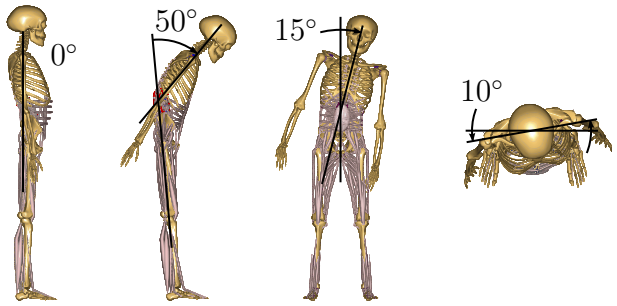

Figure 4.14: The four static postures which are simulated in the study (from left to right): upright standing, flexed, lateral bended and axial rotated. The stated values are used as input for the posture driver.

Body models

All five subject-specific full body models, as described in Section 4.1 in combination with version 1.4.1 of the AMMR and version 6.0.3 of the AMS, are utilised in this study. They are configured with the following options: a linear disc stiffness, ligaments calibrated in groups, no facet capsular ligament and an active contact between facet surfaces. Each model is scaled with the appropriate data (Table 4.1) and the analysed postures are set with the posture driver.

Parameter study

Every parameter-model combination is analysed in each of the four static postures (Figure 4.14) upright standing (0°), flexed (50°), lateral bended (15°) and axial rotated (10°). The used parameters are depicted in Figure 4.8 and listed in Table 4.13 in conjunction with their step sizes, abbreviations and intervals. Simulations with the set numbers one to ten are used to examine the influence of a single parameter on lumbar loading while the remaining three are utilised to evaluate the effects of combined changes. Variables for the latter sets are selected based on their influence on lumbar loading. All in all, 3700 simulations are conducted: 2200 with single parameter changes and 1500 concerning combined variations.

The interval size of every anatomical parameter is derived from standard deviations published in literature [61, 62, 85]. Only the one for the lumbar lordosis is set to ±5° because larger values cause problems in the models. The intervals are centred around the according dimension of each model's vertebra and the changes affect the muscle and ligament attachment points of the lumbar vertebrae L1 to L5.

Every simulation is run with gravity and an activated FDK solver. The solver settings are configured similar to the set-up used for the validation simulations. Changes are limited to an increased number of iterations to receive as much successful simulation runs as possible. A downside of an increased value is a higher computation time. All settings, differentiating from the default values, are listed in Table 4.14.

Table 4.13: A detailed listing of all simulations for the parameter study. Specified are the varied parameters and abbreviations, sizes of the intervals and numbers of steps for each model-posture combination.

Set no.	Parameter	Abbreviation	No. of steps	Interval
1	Vertebral body width	VBW	11	±5 mm
2	Vertebral body height	VBH	11	±4 mm
3	Vertebral body depth	VBD	11	±5 mm
4	Transverse process width	TPW	11	±13 mm
5	Spinous process length	SPL	11	±6 mm
6	Pedicle length	PDL	11	±2 mm
7	Disc height	DiH	11	±3 mm
8	Interfacet width	IFW	11	±7.5 mm
9	Interfacet height	IFH	11	±6.5 mm
10	Lumbar lordosis	LOR	11	±5°
11	Disc height	DiH	5	±3 mm
	Vertebral body depth	VBD	5	±5 mm
12	Vertebral body height	VBH	5	±4 mm
	Disc height	DiH	5	±3 mm
13	Vertebral body height	VBH	5	±4 mm
	Vertebral body depth	VBD	5	±5 mm

Table 4.14: Solver settings of the parameter study.

Option	Value
Type of muscle recruitment	Polynomial
Power of polynomial criterion	3.0
Limit activation of muscles	Off
Force dependent kinematic solver	On
Limit of FDK iterations	2000
FDK force tolerance	0.5

Outcome parameter

The evaluation of the results is based on the joint force of the L4/L5 lumbar level. It is computed as a three-dimensional reaction force in the joint and the resultant vector represents the outcome variable.

4.3.3 Case study: disc herniation and loading of multifidus muscle group

This case study is divided into two parts and utilises all five validated subject-specific models. The first part (Figure 4.15 left) investigates the influence of a progressing disc

herniation on the lumbar multifidus muscle with this muscle in a healthy state. Throughout the simulations the models perform four basic motions and the force of the multifidus muscle as well as the disc forces are recorded and analysed. Additionally to four basic motions, two parameters are varied. These simulate the progressing disc herniation. In

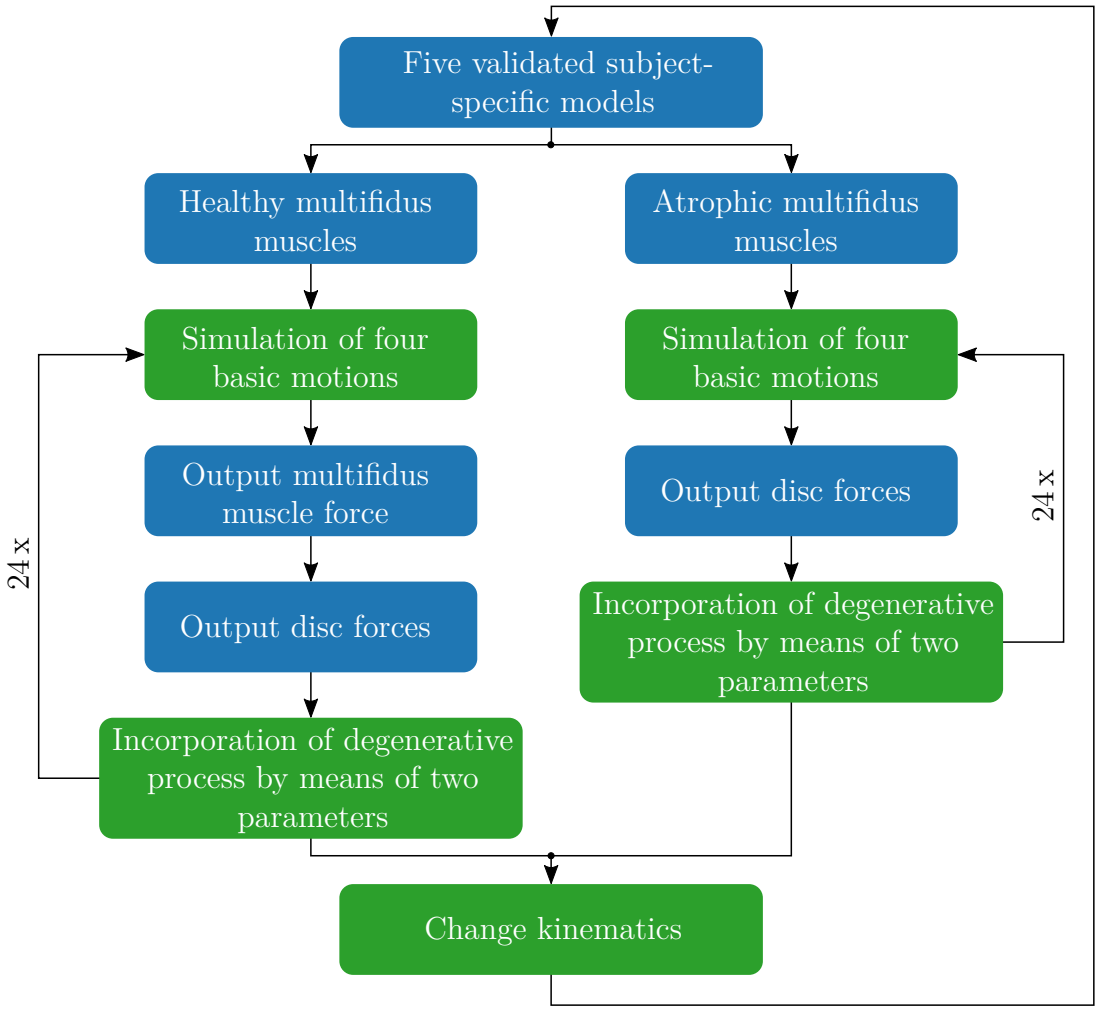

Figure 4.15: The design of the case study regarding atrophy of multifidus muscles after disc herniation with actions in green boxes and results or data in blue boxes.

the second part (Figure 4.15 right) the effects on lumbar loading in case of atrophic lumbar multifidus muscles combined with different levels of disc herniation are analysed. The same basic motions and parameters are examined, but this time only the disc forces are recorded and evaluated. Each part is then repeated with different kinematics for the lumbar spine.

Models and motions

All five subject-specific models are configured with the following options. Each element representing a ligament is calibrated individually. A non-linear disc stiffness with active scaling in dependence of the subject's disc size is applied. The surface contact between

facets is used and the FCL is activated. Furthermore, the models are scaled to their body weight and height.

Beside standing in an upright posture the analysed motions are comprised of flexion from 0° to 40°, lateral bending from −15° to 15° and axial rotation from −10° to 10°.

Configuration of simulations

In course of this case study the previously described model-posture configurations are simulated with a progressing disc degeneration at the L4/L5 level. This process is modelled by means of a stepwise reduction of the corresponding disc stiffness and disc height. The interval of the stiffness ranges from 100 % to 10 % of the model's disc stiffness and is reduces by a step size of 22.5 %. The relative reduction of the disc height ranges between 0 mm (original disc height) and −4 mm (reduced disc height). The according step size is 1 mm. This results in five steps for each parameter.

The first part is simulated with an intact multifidus muscle group, hence, the concerning option to enable or disable these muscles is set to one and set to zero (inactive multifidus muscles) in the second part. Additionally, everything is repeated with different kinematics in the lumbar spine meaning an activated spine rhythm. Every simulation consists of seven time steps which are evenly distributed over the analysed motion.

This time both kinematic options, FDK and spine rhythm, are used. Again, gravity is applied. The solver is configured as previously but with a reduced number of iterations (400) for the FDK calculation. This shortens the computation time but still yields a sufficient number of successful simulations. The settings of the solver are summarised in Table 4.15.

Table 4.15: The configuration of the solver for the case study. Simulations which are conducted with the spine rhythm are configured similarly but all FDK options are disabled.

Option	Value
Type of muscle recruitment	Polynomial
Power of polynomial criterion	3.0
Limit activation of muscles	Off
Force dependent kinematic solver	On
Limit of FDK iterations	400
FDK force tolerance	0.5

Outcome parameters

In case of an intact lumbar multifidus musculature with a progressing disc herniation, the outcome parameters are the forces generated by the lumbar multifidus fascicles.

Their changes are tracked individually and in a total force for the musculature of the left and right side. Afterwards, the resultant lumbar joint forces are evaluated for and in combination of healthy and atrophic multifidus muscle fascicles. The differences between FDK and spine rhythm kinematics are analysed in both sub parts of the case study.

5 Results

The results section reports the outcome of the validation simulations and of the three conducted studies. In most instances, only typical results, that represent the specific characteristics, are shown in the figures. In a few occasions, additional graphs can be found in the appendix.

5.1 Validation of the model

Three different groups of validation simulations are conducted in this thesis: absolute intradiscal pressure (IDP) values in an upright standing posture, the progression of the IDP over basic motions and the relative differences between an upright standing pose and various other stances. The following sections describe the validation results of each of these simulation groups.

5.1.1 Absolute values

The validation of absolute values compares the computed and processed joint reaction forces with various literature data of experimental IDP measurements of different subjects and mean values with standard deviations of a group of subjects. Therefore, each resulting joint reaction force is converted to an IDP by using the approach described in Section 4.2.1. This method utilises different correction factors, ranging from 0.55 to 0.77 with a mean value of 0.66, because all individual correction factors are unknown. Hence, the computed joint reaction forces are converted to a range of IDP values.

Figure 5.1 depicts the resulting comparison between published data and simulations of all models in all utilised model configurations. The abscissa values of the diagram give the model numbers while the ordinate indicates the IDP in MPa. The different configurations of each model are grouped together and the previously described range of IDP values per simulation is shown as a value with error bars. Reported experimental IDP values are plotted as solid horizontal lines and dashed horizontal lines correspond to the related standard deviation. The entire corridor of published IDP values, used for this comparison, is highlighted with a grey background.

The resulting IDPs at the L4/L5 level of all models and configurations are within or partly within the corridor created by published data. All configurations of the models of subjects one and two return results within the corridor. The IDPs of simulations with a model of subject three are in good agreement with the published data, but are slightly outside the corridor for the third configuration that uses the spine rhythm and a correction factor close to the upper end of the range. Models of subjects four and five show higher values than ones of the other three. This leads to minor deviations from

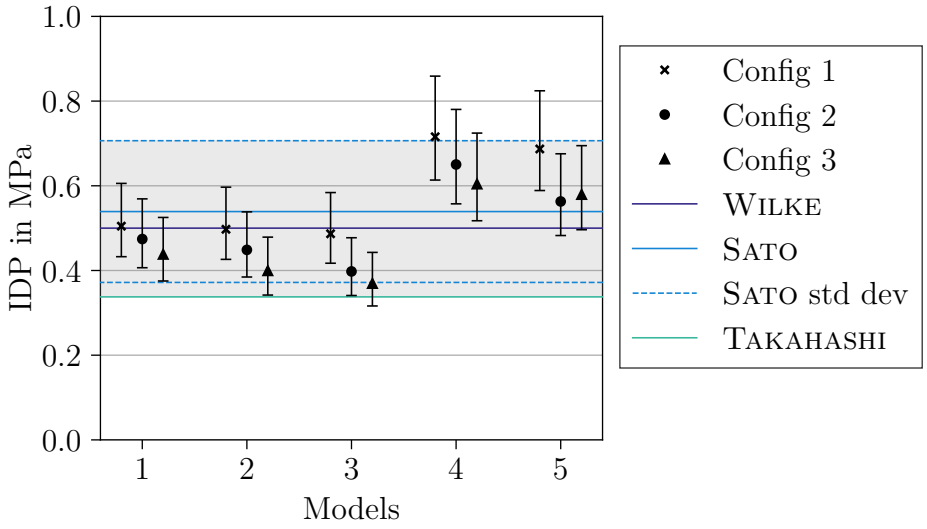

Figure 5.1: Comparison of the IDP of literature data [80, 92, 103] with the results from simulations in all three utilised configurations. The error bars result from the conversion of the compressive force to a pressure value (Equation 4.28) in combination with the different correction factors in a range of 0.55 to 0.77 with a mean value of 0.66.

the literature data in dependency of the correction factor. If a mean correction factor or a value larger than the mean is used to convert the resulting joint reaction forces of the models of subject four and five in combination with the first configuration, the calculated IDPs are close to or above the upper boundary of the corridor. The other configurations improve the results, but larger correction factors still lead to IDPs above the corridor for a model of subject four. Whereas, simulations with the model of subject five and these configurations return IDPs completely within the range of the published data. Furthermore, all simulations with models that are configured to use a non-linear disc stiffness lead to a decreased IDP in comparison with results of the same models but with a linear stiffness. An application of the spine rhythm (SR) instead of FDK further reduces the IDP except for the model of subject five. In this case, the IDPs are minimally higher than the ones with FDK. Overall, the IDPs of all models and all configurations correspond well to the reported data and most deviations are only of a minor form.

5.1.2 Progression of intradiscal pressure

This part of model validation concentrates on the progression of the IDP over three basic motions. Each model is examined in each of the three configurations and, as before, the resulting joint reaction forces at the L4/L5 lumbar level are converted to IDPs. Only a single correction factor, the mean value, is considered. Afterwards, these calculated IDPs are compared to data of a single subject reported by Wilke et al. [103].

The according diagrams show the IDP at the L4/L5 lumbar level in dependency of the

motion. As described in Section 4.1.4, the motion is expressed as the angle between the reference systems of the pelvis and the thorax. An angle of zero degree corresponds to an upright standing posture, where the reference systems of both segments are equally aligned. In addition to the angles, each diagram denotes the direction of rotation. Literature data is shown as a black dashed line and simulated data is displayed as a solid line with each discrete step marked. Figure 5.2 depicts the results of the configuration using FDK and a non-linear disc stiffness as an example. The diagrams of the remaining configurations can be found in the Appendix A.6.1.

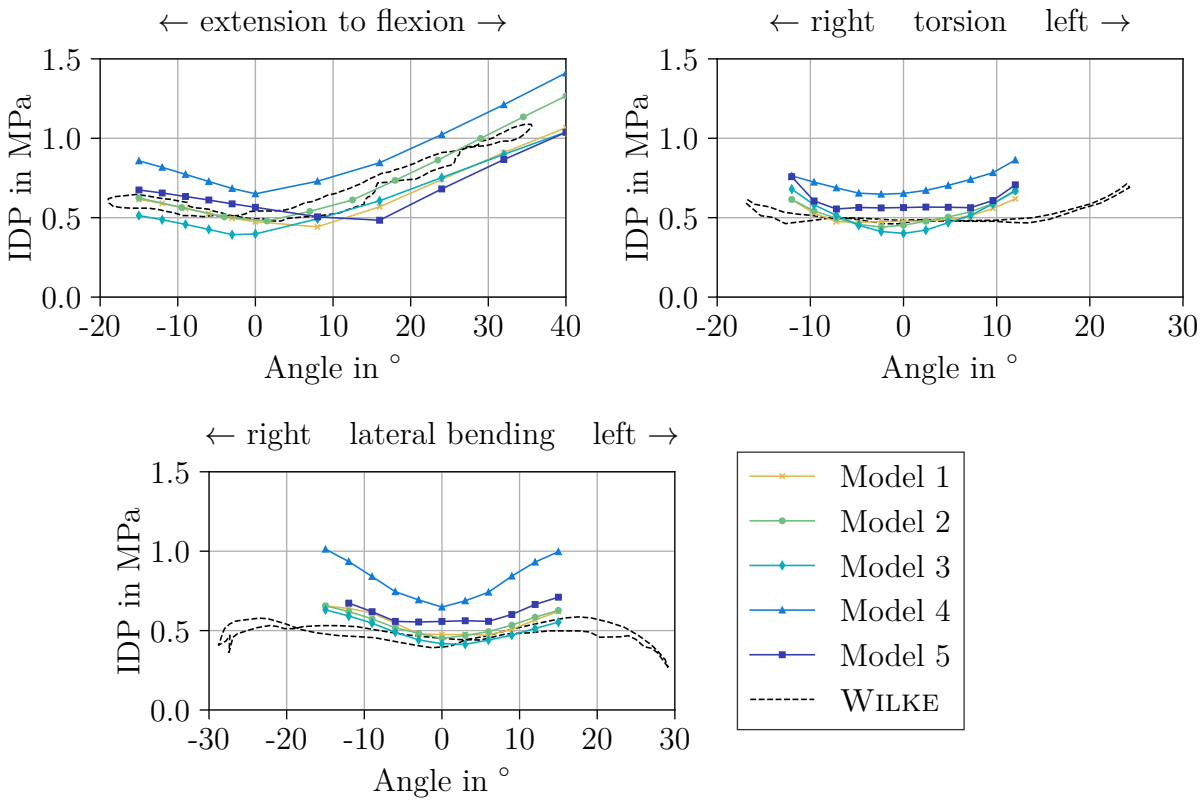

Figure 5.2: The three diagrams show a comparison of the L4/L5 IDP between the five simulated models and data reported by Wilke et al. [103] during extension to flexion (top left), a torsional motion around the vertical axis (top right) and a bending motion from right to left (bottom). The results represent the configurations with FDK and a non-linear disc stiffness.

All simulations regarding this part of validation finish successfully. However, a few time steps in simulation runs with flexion and lateral bending complete only by exceeding the specified FDK force tolerance, despite an adaption of the step size. Simulations with models of subject four and five are mainly affected. In rare cases, a time step of a computation with the model of subject one returns results with a force residue above the tolerance. The results of those time steps are excluded from the evaluation.

Wilke et al. [103] report a rising IDP shortly after the subject starts a flexion or extension motion. The rate of increase during flexion is slightly larger than the one

during extension. In addition, the IDP grows over the complete range of the flexion movement, while it flattens at the end of the extension motion. The first configuration (Figure A.1 top left) shows a good agreement for models of subject one to three, even though the rate of increase of the IDP during the flexion part is a bit too small. The simulation steps, covering the extension motion of model four, return errors and are excluded but the ones for the flexion part result in a growth of IDP corresponding to the published data. The computed progression of the disc pressure for subject five is nearly symmetrical for extension and flexion, with the lowest value at around 12° flexion. Configuration two provides similar results (Figure 5.2 top left). Both rates of increase, the extension and flexion rate, are comparable to the reported data. However, the lowest value of IDP for model five is computed around 16° flexion. Simulations with the third configuration also result in appropriate trends (Figure A.2 top left). Only model two and three show an increase in disc pressure above the data of Wilke et al. [103].

The IDP of a torsional movement in the published data starts to increase after exceeding 10°. Furthermore, this increase is only of a minor form, comparable to the one during the extensional motion. However, the simulation results of configuration one (Figure A.1 top right) show a growth of the IDP as soon as the rotational motion starts. In addition, it reaches values far above the literature data. Whereas the IDPs of all models configured with the second set-up increase after a certain deflection and with a much flatter growth rate (Figure 5.2 top right). The usage of the spine rhythm (configuration three) instead of FDK leads to a further decreased rate of growth for all models (Figure A.2 top right). These curves correspond very good to the curve reported by Wilke et al. [103].

The shape of the curve of the published IDP data during lateral bending resembles two consecutive cosines with a very small amplitude and the range of motion (ROM) is as twice as large as the simulated ROM. The resulting IDPs of simulations configured according to the first set-up (Figure A.1 bottom) and with models of the subjects one to three are comparable with each other. Lateral bending to the left corresponds good to the reported data for the investigated ROM, however, the other half, the deflection to the right, shows a higher growth rate than specified in literature. Simulations with model four lead to a further increased rate of growth in both directions and there are errors in the simulations with large deflections to the right. The results of model five resemble the ones from the first three models but with a flat central part. Configuration two returns curves which are very similar to the previous ones (Figure 5.2 bottom). However, the third configuration influences the rate of increase in IDP heavily (Figure A.2 bottom). Here, the disc pressure rises very fast for all models after half of the deflection per side is reached.

Overall, the progression of lumbar IDP at the L4/L5 level is comparable to the one reported in literature. Especially, results of a flexion motion show good agreement with the data of Wilke et al. [103] for all configurations and models. There are several differences for the remaining motions which are dependent on the individual configuration of the simulation. The usage of a disc stiffness with a linear material model leads to a large rise of IDP with increasing axial torsion (configuration one), while configurations

with a non-linear material model of the disc stiffness result in a much flatter ascent, one comparable to literature (configurations two and three). The progression of the IDP, resulting from simulations with the other two motions, does not change a lot by switching the characteristics of the disc stiffness. However, the applied spine rhythm does influence those loading conditions. While simulations with FDK show a good overall agreement for nearly all investigated motions, the IDP turns out to ascend much too fast with lateral bending and an active spine rhythm. Exceptions for FDK simulations are the torsional motion in combination with a linear disc stiffness and model four with lateral bending.

5.1.3 Changes of intradiscal pressure between postures

This third part of validation examines the relative differences in IDP at the L4/L5 level between seven static postures and the standing position. The chosen stances are derived from frequent activities. Simulations with all models positioned in every posture are conducted and the resulting eight IDP values per model are normalised to the corresponding IDP of the standing position. This normalisation, given as a percentage, allows a comparison between subjects and it is repeated for the reported experimental IDPs of various subjects [56, 80, 92, 103]. Subsequently, a bar diagram is created to compare the normalised data of simulation and literature. This procedure is performed for all three model configurations.

A diagram shows eight groups of up to nine bars. Each group is labelled on the abscissa and it represents the results of a single posture. It is divided into bars for the published experimental data on the left side and bars for the simulated data on the right side. The four published studies do not include data for all postures, hence, there are some bars missing. In addition, a terminated simulation also leads to a missing bar. An 'x' on top of a bar indicates simulations which exceed the specified FDK force tolerance.

The normalised results of the standing position are always at 100 % because this posture is the reference. All results of the first model configuration are depicted in Figure A.3 in the appendix. The according results of models one to four in the forward flexed posture are close together (ranging between 219 % and 256 %) and are in the range of the literature data (171 % to 357 %). Model five returns a value of 161 % which is far below the results of the other models, but close to the lowest published value. A relaxed as well as an unsupported straight sitting position in this configuration show similar characteristics. The results of the first four models in the former posture range between 57 % and 66 %, while model five leads to a value of 41 %. Only one study provides information about this posture and the normalised value is 60 %. The results of simulations with model one to four in the latter posture (ranging between 104 % and 118 %) are in the range of the experimental values (90 % to 143 %). Again, the relative difference of model five (76 %) is slightly below. A standing model with a weight close to the body results in values between 353 % and 486 % which are much higher than the largest normalised value of literature (300 %). This posture in combination with model two exceeds the FDK force tolerance and leads to an even higher value of 628 %. A stretching of the arms leads

to remaining force residues above the tolerance for all models, but still, the normalised IDP values of the simulations (between 251 % and 413 %) are close to the normalised value of the published data (360 %). Simulations regarding weight lifting show similar computational problems. Only the computation with the first model is without errors, but the resulting change of IDP is far below the published data (276 % versus a range between 430 % and 486 %). The results of the faulty simulations with the remaining four models are even lower. The lying posture, by contrast, leads to simulated results between 19 % and 28 % which nearly is in the range of the experimental data (20 % to 43 %).

Figure 5.3 shows the bar graph with the models configured according to configuration two. This set-up returns results comparable to the ones with configuration one for all postures without a weight. All normalised values of the simulations with a flexed forward standing posture (225 % to 306 %) are within the range of the literature data (171 % to 357 %). The results of the sitting relaxed posture, ranging from 52 % to 67 %, are also close to the experimental data point at 60 %. The normalised values from simulations with the unsupported straight sitting posture (87 % to 114 %) are also comparable to the ranges of literature (90 % to 143 %). In contrast to the previous configuration, simulations with this second configuration lead to a relative change in IDP within the range of the experimental data for the posture with the weight close to the body. Even though computations with model one (244 %), two (197 %) and four (161 %) only finish by exceeding the FDK tolerance, the resulting values are within the reported range between 123 % and 300 %. They are also close to the values of the successful simulations (120 % and 191 %). Again, extending the arms shows computational problems for all models, but the final values range from 231 % to 369 % and are partly around the normalised value of the published data (360 %). Even weight lifting returns an improved normalised IDP. Simulations of three models finish error-free. The results of model one (542 %) and three (566 %) are somewhat higher than the normalised values of literature data between 430 % and 486 %. The result of model four (459 %) is within the range of published data. Both faulty simulations show values (589 %, 462 %) close to the other ones. The lying posture returns results between 22 % and 26 % which is completely within the experimental range of data (20 % to 43 %).

Configuration three influences the results heavily (Figure A.4). In a flexed forward standing posture and in a straight sitting position, the simulations of the first three models show results considerably above the reported values. The results of the former posture are at least 76 % and the ones of the latter position are at least 32 % above the highest value of the experimental data. The other two models lead to a relative change in IDP in the range of the published data and noticeably below the ones of the other models. The according values are 304 % (model four) and 285 % (model five) as well as 101 % (model four) and 145 % (model five) for standing flexed forward as well as sitting straight without support, respectively. This difference between the first three and the last two models continues through nearly all postures. Only the relaxed sitting position shows a similar relative difference of IDP for all models. The interval starts at 59 % and ends at 99 % while the data point of the experiments is at 60 %. The simulations with a weight in the model's hands and configured with the third set-up perform very well in this part of

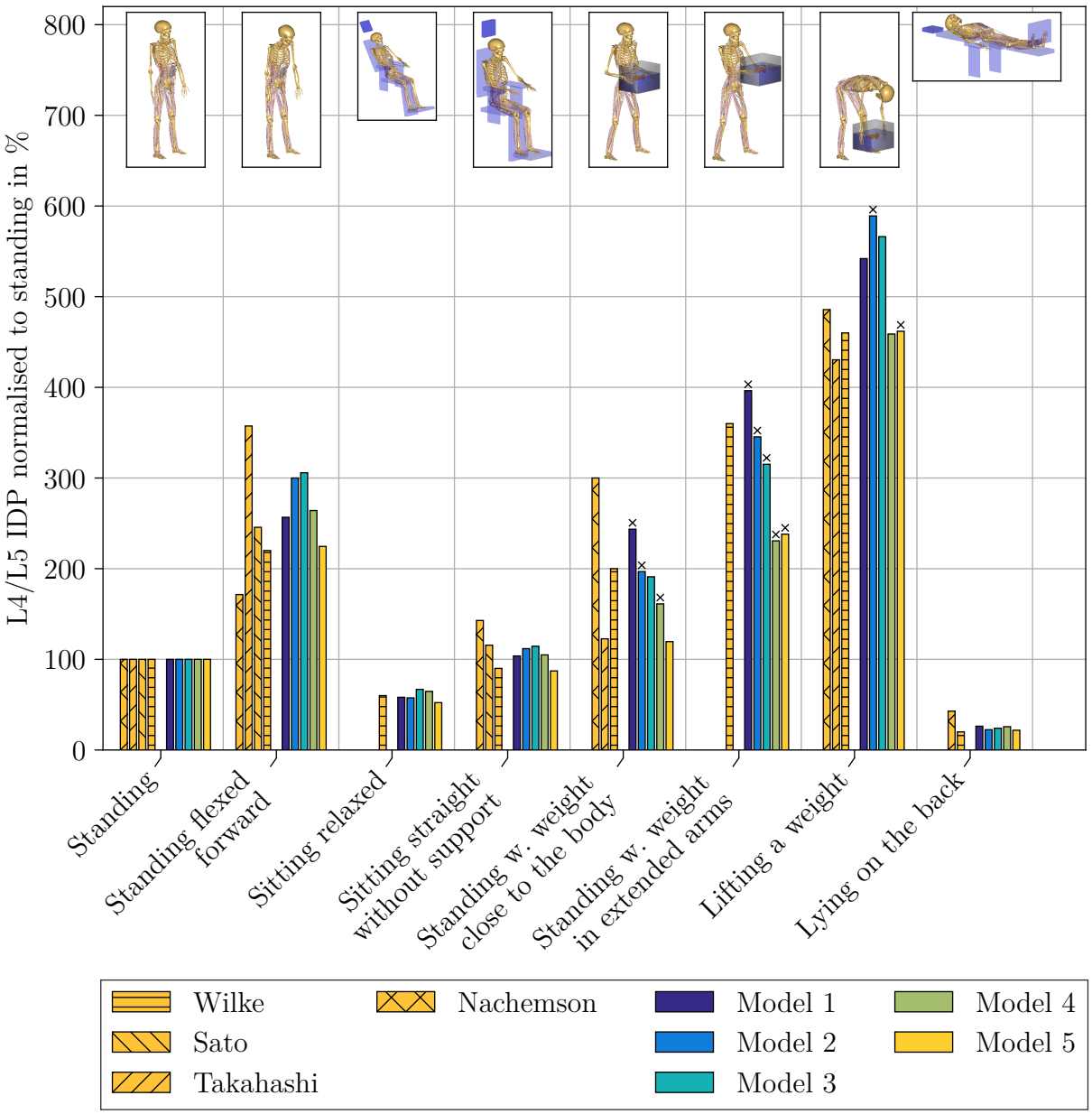

Figure 5.3: Relative changes of the IDP between various postures for every model in configuration two and for reported experimental data [56, 80, 92, 103]. All values are normalised to the standing posture. Simulations marked with an 'x' finish with a residue above the specified FDK force tolerance.

validation. The case with the weight close to the body leads to simulation results comparable to the published data over all models. The range of literature data from 123 % to 300 % includes all computed results. The according interval starts at 127 % and ends at 206 %. A distance between the weight and the body impairs the validation results only for model four and five. Here, the relative change in IDP is 141 % and 122 % below the single literature value of 360 %. The other three models return comparable results which are in a range between 329 % and 367 %. The validation results of the lifting task are reasonable except for model two. This result deviates considerably with a value 104 % above the largest value of experimental data. The interval of the other models starts at 404 % and ends at 543 %. This range is somewhat larger than the one of literature data (430 % and 486 %). The outcomes of the lying posture are fine for model one (13 %), two (13 %) and five (14 %) but are slightly too low for model three (6 %) and four (3 %). Both reported values (20 % and 43 %) are above the simulated data.

Overall, most simulations result in a reasonable range for relative differences of IDP between postures. Changes between model configurations using the FDK solver only show a minor variation. The lifting tasks deviate the most, and they more often lead to simulation residues above the specified tolerance. Usually, computations with an activated spine rhythm show higher values than the ones with FDK, although they stay in a reasonable range, too. Though, the flexed and upright seated posture for model one, two and three show much higher normalised values.

5.2 Influence of ligament stiffness on kinematics

Fluoroscopic recordings of three subjects, that perform a guided flexion motion, are used to create models. These models differentiate from another in their body height, body weight, joint position of the L3/L4 and L4/L5 level as well as in the simulated ROM. The foundation for all three models is the first one of the five subject-specific models. This sensitivity study investigates the effect of lumbar ligament stiffness on the loading of the lumbar spine. After the calculation and verification of positions of the CORs and subsequent simulations with a varying ligament stiffness, the computed forces in joints and ligaments as well as moments generated by ligaments are evaluated and visualised. Additionally, the influence on the spinal ROM is analysed.

5.2.1 Verification of centres of rotation

The first step in this study is the calculation of CORs from the fluoroscopic recordings. Therefore, the method described in Section 4.3.1 is used and the results are verified with data of a flexion motion reported by Pearcy and Bogduk [65].

This published data includes the mean values of each COR for ten subjects and three different deviations. The mean positions of all CORs can be described as close to the superior endplate of the inferior vertebra of a motion segment with a minor displacement in anterior-posterior direction. The first deviation described in the publication indicates two standard deviations from the mean value. The other two represent the 96 % confidence limits for two observer errors. These errors are important because the

gathered data in this study was evaluated by hand. The within-observer error indicates the deviation that an analyst introduces to the results during the evaluation process, whereas the between-observer error quantifies the error made by different analysts.

Each diagram in Figure 5.4 depicts the results for one model along with the published data. The coordinate system of a diagram represents a lateral view on the lumbar spine of each model in an upright standing posture. Its origin is located at the posterior corner of the superior endplate of the sacrum. This position roughly corresponds to landmark five in Figure 4.2. The lower three lumbar vertebrae L3 to L5 are illustrated as boxes in the diagram and a line indicates the superior endplate of the sacrum (S1). Each calculated position of a COR is drawn as a coloured dot, while the locations of the CORs from literature are marked with a coloured x. Ellipses represent the previously described deviations and errors. As mentioned above, the smallest ellipse indicates two standard deviations from the mean value. The other two ellipses are the within-observer and between-observer errors.

The calculations of the superior two CORs for subject one return a location close to the upper endplate of the inferior vertebra with a minor displacement to the posterior side. Furthermore, they are placed near the ellipse representing the standard deviation that is specified in literature. The position of the COR of the L5/S1 level also is close to the superior endplate of the inferior vertebra but it is considerably shifted to the posterior side. Nevertheless, it is within the ellipses that indicate the observer errors.

Calculations for subject two result in similar locations for the L3/L4 and L4/L5 CORs. Again, both are close to the superior endplate and they are slightly shifted in anterior-posterior direction. In addition, they are near the boundary that specifies the standard deviation. The position of the L5/S1 COR however, is about 35 mm in anterior-posterior direction and 12 mm in caudal-cranial direction which is far off the location and the boundaries of errors reported in literature.

The calculated CORs of the third subject show a different characteristic. Both CORs (L3/L4 and L4/L5) are positioned considerably outside the observer errors. However, the location of the L5/S1 COR is inside the ellipse of the standard deviation and it is positioned at the superior endplate of the sacrum with a small displacement in anterior-posterior direction.

Overall, the L3/L4 and L4/L5 CORs of the first two subjects correspond good to the positions reported in literature. The according CORs of subject three are far off these boundaries. CORs of L5/S1 show the largest deviations from literature values throughout most subjects and are completely off a reasonable position for subject two. However, this COR of subject three is located at a position that corresponds to the reported data.

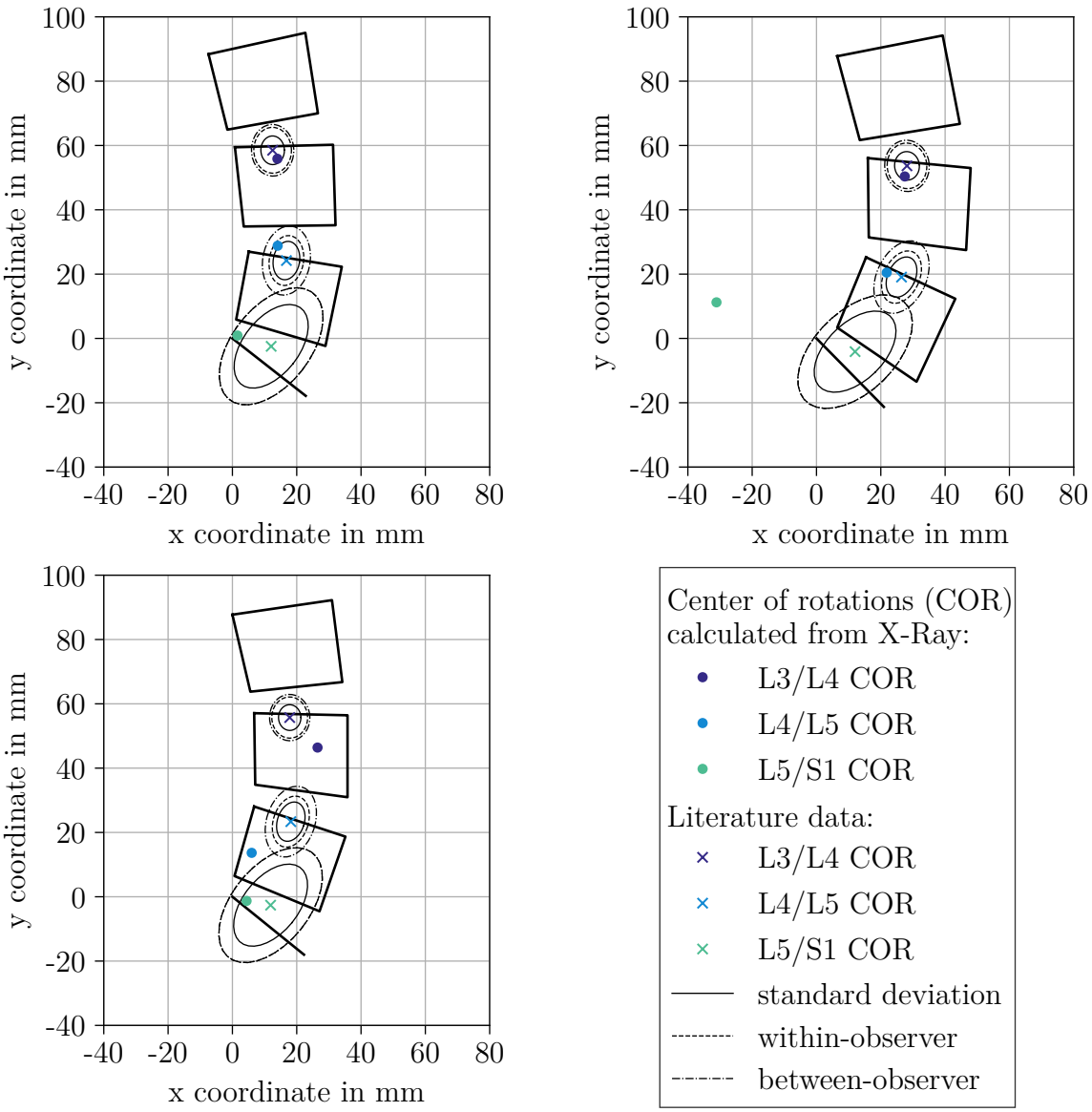

Figure 5.4: Verification of calculated locations of COR (coloured dots) for subject one (top left), two (top right) and three (bottom). The crosses represent the mean positions reported in literature and the ellipses are corresponding deviations [65].

5.2.2 Forces and moments

The tracked forces and moments of the simulations with all three models are described and evaluated. Their progression over the flexion motion is analysed and, additionally, the trends of the joint forces and moments are investigated in view of the influence of the ligament stiffness.

At first the resulting forces are examined. The according figures depict the progression of the forces at two lumbar levels in dependence of the flexion angle. The left diagram shows results for the L3/L4 level and the right one does this for the L4/L5 level. Each graph contains four curves: two of them represent progressions of joint forces (dashed line) and the other two indicate trends of total ligament forces (solid line). The curves of each pair differ in the applied ligament stiffness. One shows simulation results with the minimal ligament stiffness and the other one depicts the outcome with the maximal ligament stiffness. The total ligament forces are always negative because ligaments can only exert tensile forces which always act contrary to the displacement. Additionally, the relative increase of the forces at maximal flexion is marked. This value is of main interest.

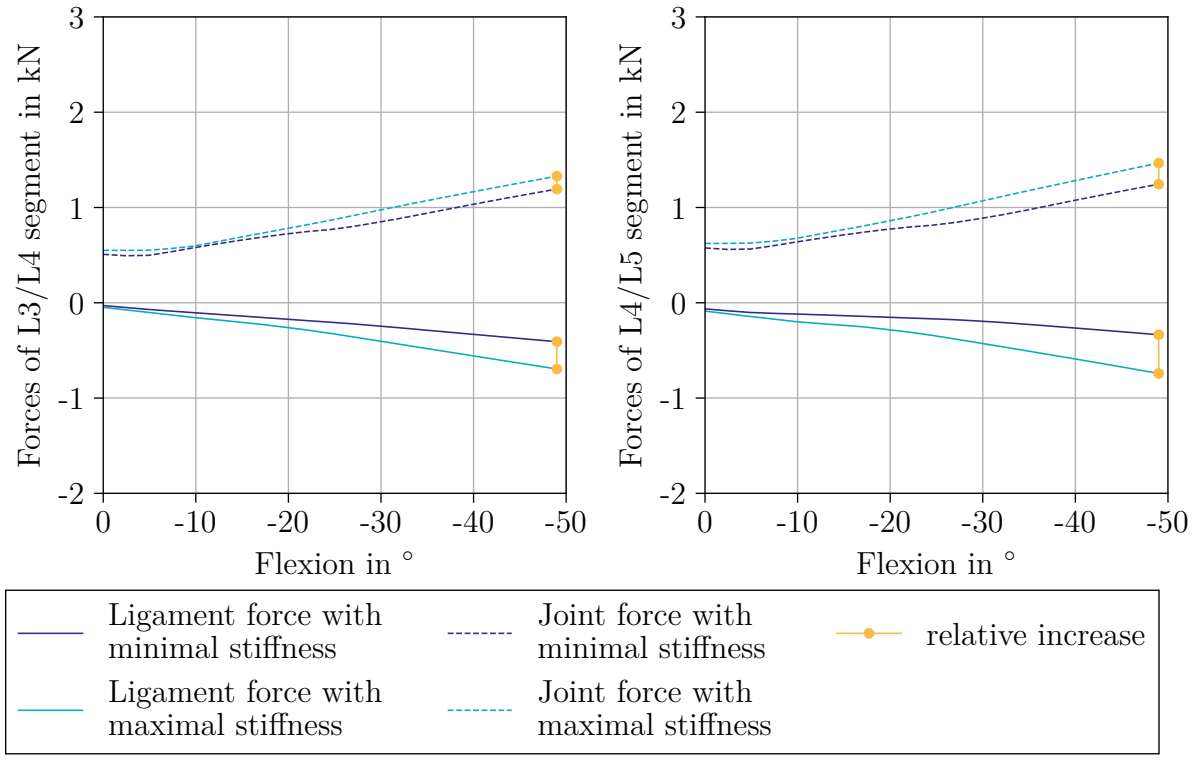

Figure 5.5: Results of joint and ligament forces at the L3/L4 (left) and L4/L5 level (right) at maximal and minimal ligament stiffness for subject one. The relative increase between the lowest and highest stiffness at maximal flexion is marked.

Figure 5.5 shows the results for the simulations with the first subject as an example. The absolute values of all tracked forces grow with an increasing flexion angle. The forces in

the initial upright position (0° flexion) are nearly the same for maximal and minimal stiffness values, however, their gain with the flexion motion is different and leads to different values at the final flexion angle. As mentioned above, this gap at the end of the motion is of main interest. At the L3/L4 level, it results in values of 288 N and 136 N for the total ligament force and the resultant joint force, respectively. The according base values are 409 N and 1193 N. At the L4/L5 level, the gaps measure 409 N (total ligament force) and 222 N (resultant joint force) with the initial values at 341 N and 1244 N. That are gains of 70 % (L3/L4) and 120 % (L4/L5) in the total ligament force as well as 11 % (L3/L4) and 18 % (L4/L5) in the resultant joint force due to a higher stiffness of the ligaments. Even though the superior level exhibits a larger initial value of total ligament force, all relative increases in both forces and the corresponding final values are higher at the inferior level. Simulations with the other two subjects result in similar characteristics for the investigated forces. The relative growth in total ligament force for the second subject is 87 % at the L3/L4 level and 131 % at the L4/L5 level. The according percentage increases for the resultant joint forces are 16 % and 24 %. Simulations with the third subject yield a growth of total ligament force of 93 % and 121 % at the L3/L4 level and L4/L5 level, respectively. The resultant joint forces increase by 8 % (L3/L4) and 15 % (L4/L5).

The figures that depict the results of the joint moments are analogous to the figures of the forces. They depict the resulting moments in dependency of the flexion angle for two lumbar levels. Again, only moments simulated with minimal and maximal ligament stiffness are shown and the difference at the final flexion angle is marked.

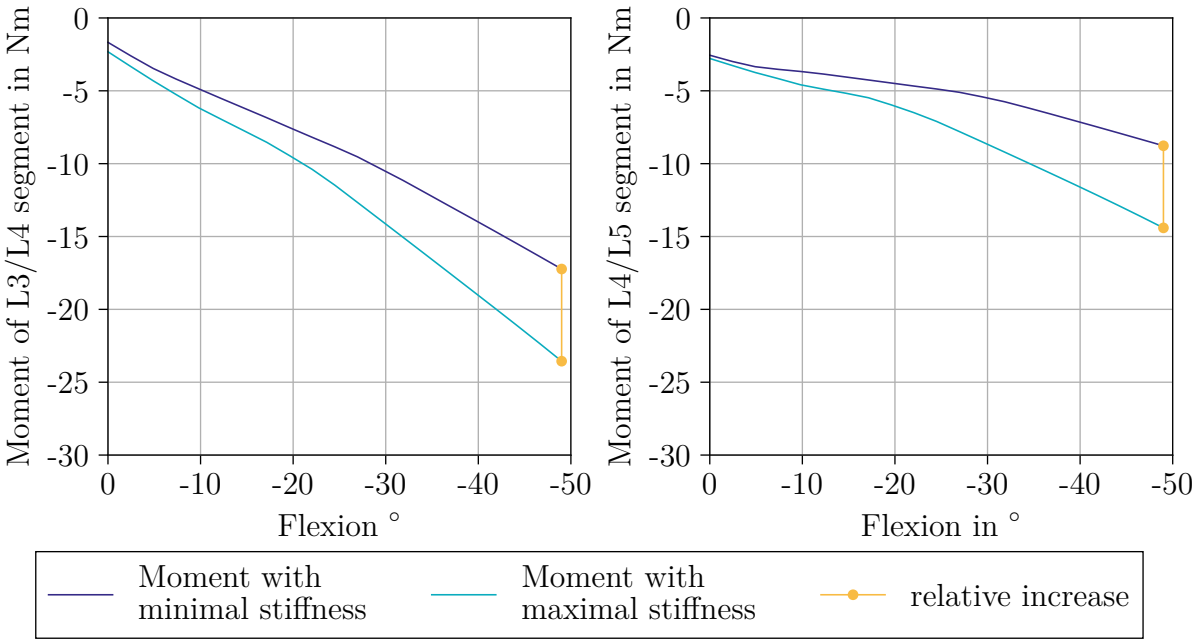

Figure 5.6: Computed moments around the medio-lateral axis at minimum and maximum ligament stiffness. Both investigated lumbar levels, L3/L4 (left) and L4/L5 (right), are shown for subject one. The relative increase between the lowest and highest stiffness at maximal flexion is marked.

As previously, Figure 5.6 illustrates these results for the first subject as an example. Again, the initial values at each lumbar level are nearly the same. All analysed joint moments grow with an increasing flexion angle, but the curves that represent the moments of simulations with the maximal ligament stiffness rise at a higher rate. While the final absolute value with the lowest ligament stiffness and at the L3/L4 level is 17 Nm, the value with a maximal ligament stiffness results at 24 Nm. For the L4/L5 level, the according results are 9 Nm and 15 Nm. This yields relative increases of 37 % and 66 % for the respective levels. The absolute value of the joint moments of the lower lumbar level is smaller than the one from the upper level, however, the relative increase is higher. This relative growth of joint moments results in 50 % (L3/L4) and 67 % (L4/L5) for simulations with the second subject. The third subject provides values of 50 % and 69 %.

In total, the analysed forces and moments increase with a rising stiffness of the ligaments and during a flexion motion. Furthermore, the joint forces and total ligament forces of the subjacent lumbar level are always higher than the ones from the upper level when the maximal stiffness is applied. In addition, the relative rate of growth of all evaluated properties between minimal and maximal stiffness is larger at the L4/L5 level, even though the absolute values of the joint moments, that are generated by the ligament forces, are higher at the L3/L4 level. These characteristics continue through the results of all three subjects. Therefore, the mean increases and corresponding standard deviations of all tracked properties are calculated and listed in Table 5.1. They show the exact same relationship.

Table 5.1: Mean values and standard deviations of the relative increase of lumbar forces and moments in percent.

Level	Joint force	Ligament force	Moment
L3/L4	12 ± 4	83 ± 12	45 ± 8
L4/L5	19 ± 4	124 ± 6	67 ± 2

5.2.3 Range of motion

The effects of different ligament stiffness values on lumbar ROM are analysed. Therefore, each motion segment's movement range is calculated by the angular differences between the upper endplates. Furthermore, the ROMs, that result from simulating a flexion motion with the three subjects, are compared to the ones calculated from the experiments. This leads to a total of eight curves per plot and each of these graphs represents the results of one subject. These diagrams indicate the current stiffness on the abscissa and the ROM on the ordinate. The minimal stiffness used in the simulations corresponds to 0 % on the abscissa and maximal stiffness is at 100 %. The five dark coloured curves plotted in every diagram show the simulation results, while the light ones represent the data of the experiments. Obviously, there is no influence of ligament stiffness on the experimental results, hence, these values are plotted as horizontal lines.

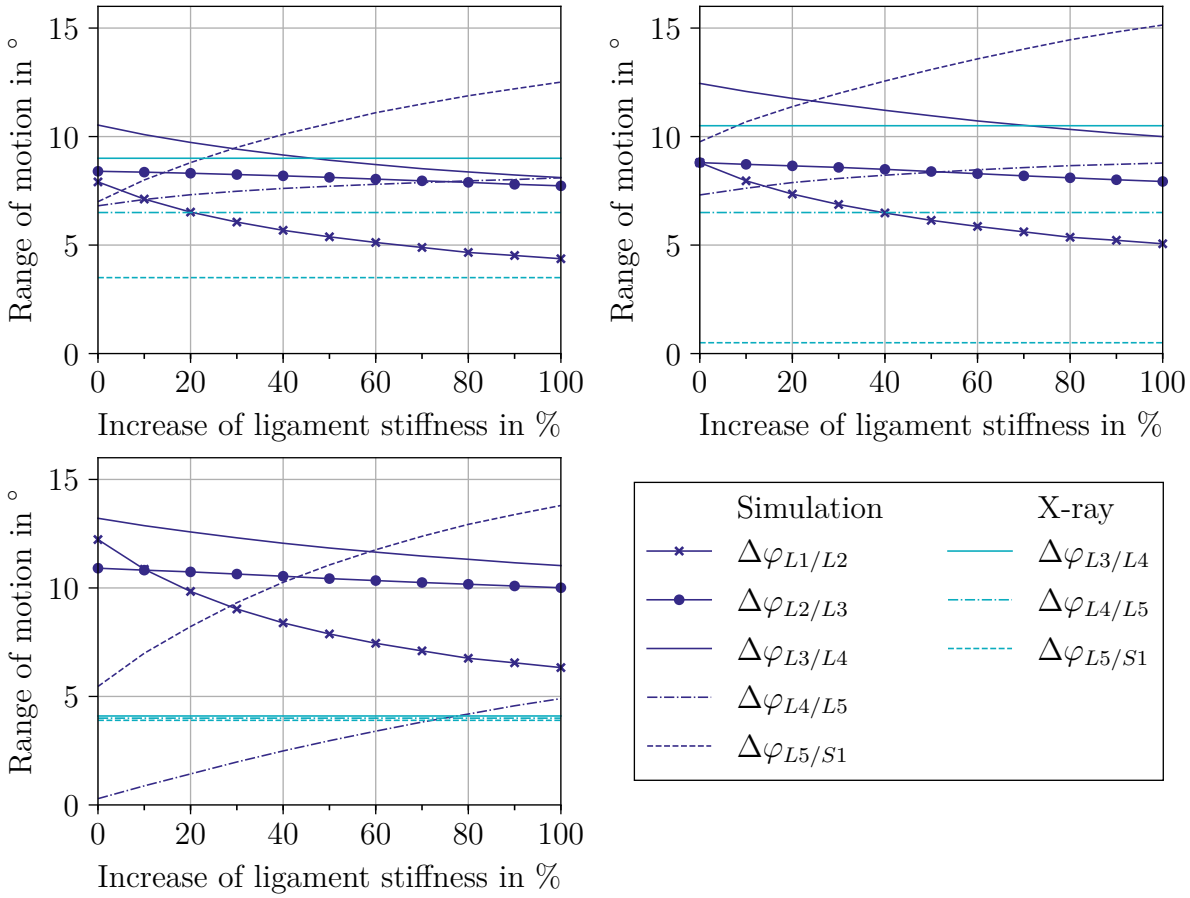

Figure 5.7: Range of motion of every lumbar level as a function of the ligament stiffness. Each diagram shows the simulated (dark color) and experimental (light color) results of a single subject with subject one at the top left. Subject two is at the top right and subject three is at the bottom.

The top left graph of Figure 5.7 depicts the results for the first subject. The simulation results of the upper three lumbar segments (L1/L2, L2/L3 and L3/L4) show a decrease in ROM of up to 3.5° over an increase of the ligament stiffness. The ROM of the L4/L5 segment increases by 1.3° and the one for the L5/S1 segment by 5.5°. A comparison of the experimental data to the simulation data reveals a good match for the L3/L4 segment. The simulated results of the L4/L5 segment is close to the experimental data but the ones for the L5/S1 segment show a larger gap of at least 3.5°.

The results of the second subject are illustrated in the graph at the top right of Figure 5.7. Basically, the characteristics of the ROMs of this subject are similar to ones from the first subject when subjected to a variation of the ligament stiffness. They only differ in absolute height of the starting value but not in change of the ROMs. Even the comparison with the experimental data is similar for the L3/L4 and L4/L5 motion segments. The former corresponds good and the latter is close to the experimental data. Only the difference for the L5/S1 segment increases and results in a value of 9°.

The lower diagram shows the ROMs for the third subject. These results deviate more from the others. Still, the top three motion segments show a decrease in ROM and the lower two an increase, but with different values. As before, the greatest decline exist at the L1/L2 segment, but this time with a value of 6°. The changes of the L2/L3 and L3/L4 segments are comparable to the changes from the other subjects. However, the increase in ROM of the L4/L5 segment is considerably higher than previously (4.6°) and the results of the L5/S1 segment are also larger with a value of 8.3°. Furthermore, this subject shows deviations between the simulated and experimental ROMs. The differences of the L3/L4 segment are the largest with at least 7° and the ones for the L5/S1 segment show a great range of 5° to about 13°. Only the ROM of the L4/L5 segment corresponds good to the experimental data. Interestingly, this subject shows nearly the same ROM in the experiments for all evaluated segments.

Altogether, the subjects show an increase of ROM in the L4/L5 and L5/S1 segments and a decrease in the other three segments when subjected to a rising ligament stiffness. Moreover, the comparison of simulated and experimental ROMs reveal a good agreement at the L3/L4 segment for the first and second subject at an average ligament stiffness. The L4/L5 results show good comparability at a low ligament stiffness for these two subjects and at a median stiffness for the third subject. However, the simulation's outcome of the L5/S1 level has a larger distance to the results of the experiments for all subjects.

5.3 Parameter study of the lumbar geometry

This study is split into two parts: the first part analyses the influence of a single parameter on lumbar loading at the L4/L5 level and the second part evaluates the effects of parameter combinations. 71 % of all simulations finish successfully (49 % single parameter, 22 % combinations) and the others aborted due to numerical problems. Computations with model number four sustain the most terminations. The flexed pose shows the highest number of successful simulations.

5.3.1 Variation of a single parameter

All simulation data, that result from investigations with single parameter variation, are plotted in diagrams like the ones in Figure 5.8. Each graph includes the simulation output of a single model-motion combination that is subjected to an individual variation of nine different parameters (all except the lordosis). The abscissa of every diagram indicates the range of parameter modification and the ordinate shows the L4/L5 resultant joint force in percent. The corresponding reference value is the joint force that is computed with the original dimension of the current studied parameter.

The above selection of model-motion combinations are typical examples of all occurred particularities, hence, the important findings are explained based on these results. The top left diagram depicts the simulation output of model five in an upright standing posture. Here, the alterations of the vertebral body height (VBH) and the disc height (DiH) result in a larger relative change of load of about 22 % and 19 %, respectively. Apart

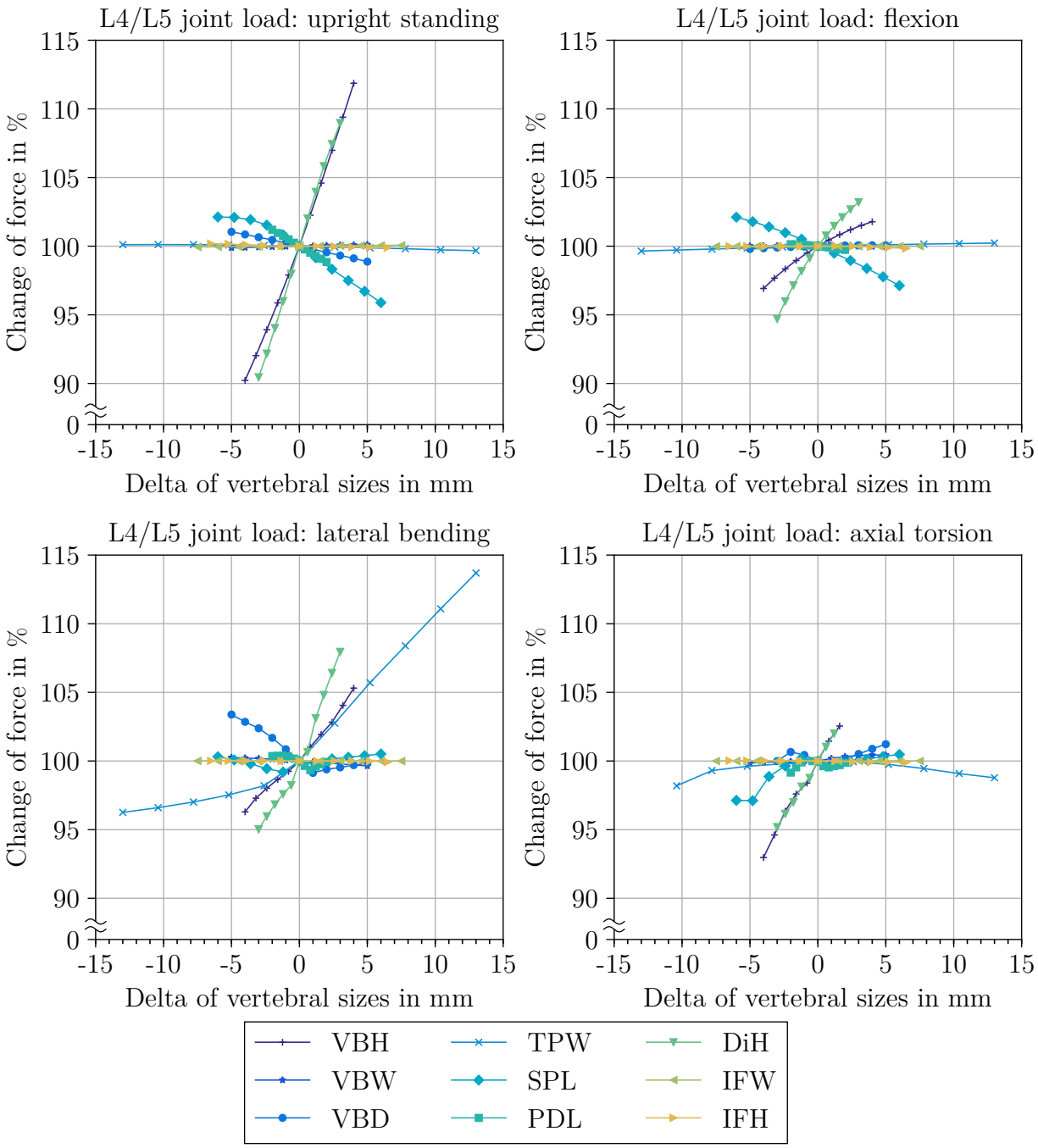

Figure 5.8: Each diagram depicts the percentage change of the L4/L5 joint force as a function of the varying parameters. The unchanged vertebral dimensions are used to compute the according base values. This representative selection shows the results of the following model-posture configuration: model five with upright standing (top left) and flexion (top right), model one with lateral bending (bottom left) and model one with axial torsion (bottom right).

from the spinous process length (SPL) which affects the targeted joint force around 6 %, the remaining parameters only show a negligible influence. The change in progression of that dimension is another interesting detail. The diagram next to the previously described graph illustrates the results of simulations with model five in a flexed posture (top right). This time, the DiH is the parameter with the greatest influence on loading, but the modification range of 9 % is considerably smaller than before. The influences of the SPL and VBH result in values of around 6 % and 5 %. All other parameters show no effect on the joint force in this case. The plot in the bottom left location of Figure 5.8 depicts the simulation output of the combination of model one and lateral bending. This set-up strongly affects the target value by altering the transverse process width (TPW). The corresponding load change results at a value of 16 % and its progression shows a kink. Other parameters that considerably influence the joint force are the DiH and the VBH. The former modifies the target value by 13 % while the latter alters it by approximately 9 %. In addition, the curves of the pedicle length (PDL) and the SPL exhibit an unstable trend of the relative change in joint force. The bottom right plot illustrates the outcome of the simulations with a model-motion combination of model one and axial torsion. As before, the parameter with the greatest effect is the VBH. It changes the load by nearly 10 %. This parameter is solely followed by the DiH, which influences the joint force with about 7 %. Additional unusual details in the simulations with this model-motion combination are the unstable progressions due to the SPL, the vertebral body depth (VBD) and the PDL.

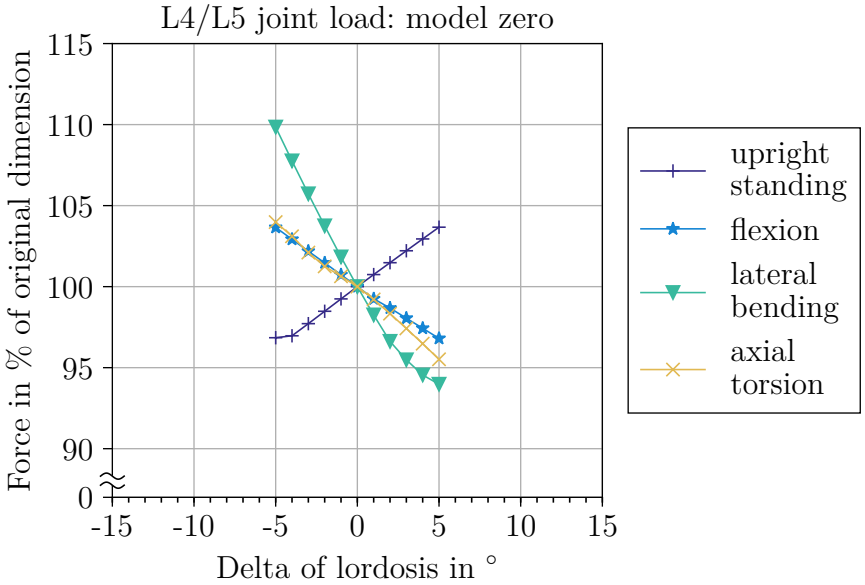

Figure 5.9: Relative changes of L4/L5 loading as a function of the lordosis angle for model one.

The results of simulations with changes to the lordosis angle (LOR) are depicted in a separate diagram. An example is given with Figure 5.9. The general structure of this plot is the same as above. It merely differs in the content. In this case, the graph illustrates the relative changes of the L4/L5 joint force of the simulations with model one in each

of the four studied postures. The parameter of the LOR affects the target value in all cases. Here, the alteration ranges between 7 % and 16 %.

Overall, the parameters of the VBH and the DiH constantly lead to the greatest effects on lumbar loading. Especially, if they are combined with models in a flexed or upright standing pose. The corresponding load changes vary between 5 % and 22 %. Another vertebral dimension with a larger influence on the L4/L5 joint load is the parameter of the TPW. However, it mainly affects the target in a lateral bended posture. There it changes the load by up to 16 %. It also affects the joint forces when combined with axial rotation but only marginally (in a range of 4 % to 6 %). Changing values of the SPL alter the L4/L5 loads by about 7 % when the model is position in upright and it has a minor effect under torsion. The sensitivity to this parameter is especially noticeable in simulations with model five which results in load variations of 5 % to 10 %. Beside the previously mentioned parameters, only the VBD changes the joint force by about 5 %. Most other parameters have an effect that is negligible. Furthermore, the angular parameter for the LOR influences the loading with values between 2 % and 16 %. The greatest effects are seen in a lateral bended pose for model one. Axial rotated and flexed postures follow with descending influences but even an upright standing stance shows some sensitivity to this parameter.

5.3.2 Combined changes of two parameters

Similar to the evaluation of single parameter changes, the subsequent graphs show a selection of typical results of the computations with combined parameter variations. Each three-dimensional surface plot in Figure 5.10 depicts the influence of a simultaneous change of two parameters on the joint load. As previously the ordinate, the z-axis of each graph indicates the relative alteration of this load. The reference value is the load that results from computations with the parameters at their default values (original dimensions of the lumbar spine). Additionally, all surfaces are coloured according to the result value at each data point and the corresponding mapping of colours to values is also depicted in the figure. The x- and y-axis indicate the change of the specified parameter. All graphs of Figure 5.10 illustrate the results of computations with model five in a flexed posture.

The plot at the top left location shows the influence of a variation of the VBD and VBH. There is hardly an effect of changes to the VBD on the target value, the VBH, on the contrary, influences the results in a range of 4 % to 6 %. The diagram on the top right depicts the effects of a combined alteration of the VBH and DiH. In this case, both parameters affect the loading. The VBH changes the simulation output by up to 8 %, while the DiH modifies it in an interval from 6 % to 12 %. The third graph (bottom) contains the outcome when adjusting the VBD and the DiH. Again, the former dimension only shows a negligible effect, whereas the latter factor has a considerable influence on the loading. This parameter changes the joint force in a range of 7 % to 10 %.

In summary, the investigated parameter combinations considerable change the result, only if the VBH, the DiH or a combination of both is altered. The third parameter, the

VBD, does hardly influence the joint force in all simulated cases.

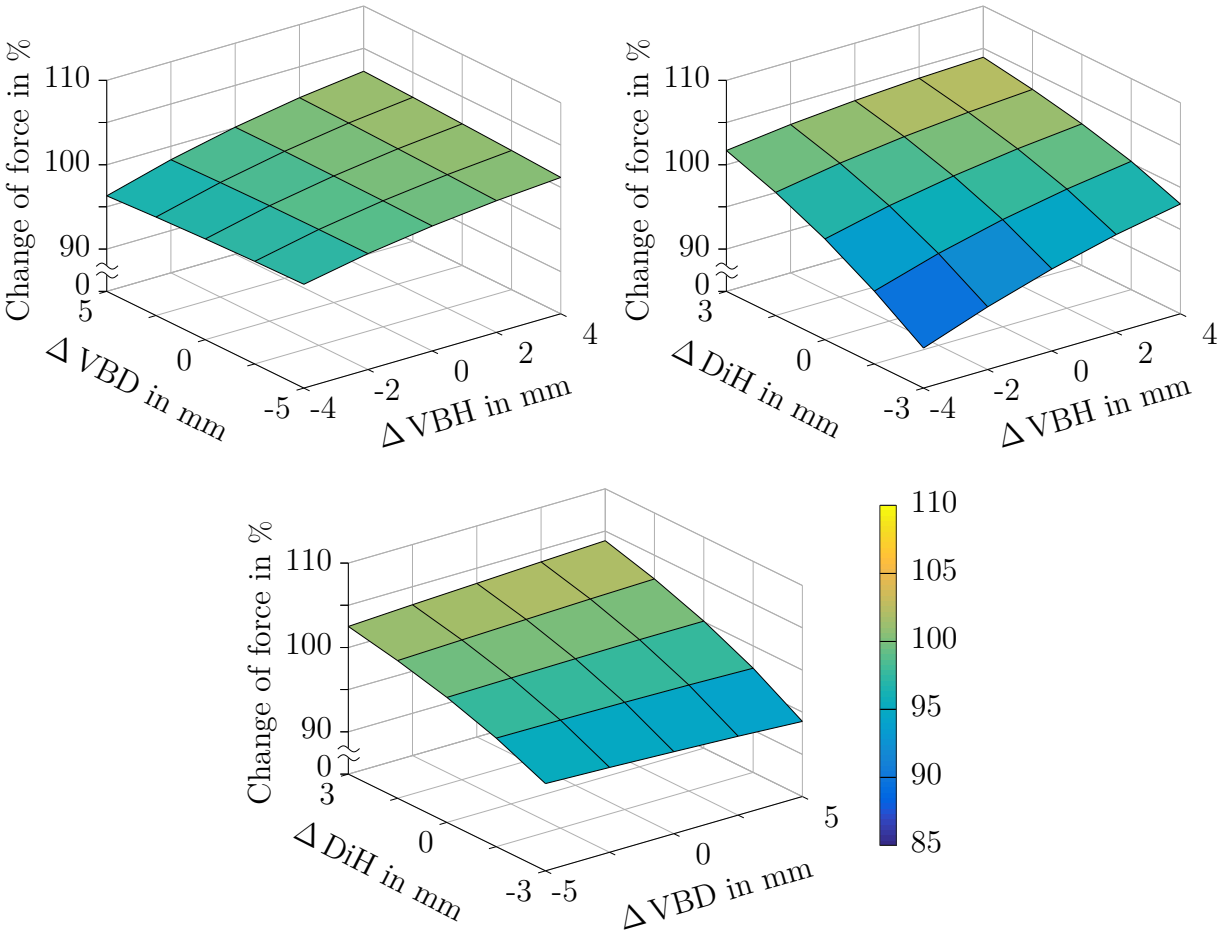

Figure 5.10: Effect of simultaneous changes to two parameters on the L4/L5 joint load. All graphs illustrate results of simulations with model five in a flexed posture.

5.4 Disc herniation and multifidus muscle atrophy

In this case study, the consequences of a disc herniation on multifidus muscle forces are investigated. Subsequently, the effects of an atrophic multifidus muscle group in combination with the disc herniation on lumbar loading are analysed. At first, the forces in all fascicles of the multifidus muscle are evaluated. The second part concentrates on the analysis of the disc force in the lumbar levels from T12/L1 to L4/L5. Furthermore, all results are examined with respect to the applied kinematic option (force dependent kinematics (FDK) or spine rhythm (SR)).

In course of this study, a total of 2000 simulations are conducted and 91 % finish successfully. Another 8 % of the simulations with an activated FDK solver complete with

Table 5.2: Number of terminations per model and motion during simulations of the case study.

Model no.	Motions				per model
	standing	flexion	lateral bending	axial rotation	
1	1	2	0	0	3
2	2	3	0	0	5
3	0	0	40	12	52
4	18	24	0	20	62
5	4	5	50	2	61
per motion	25	34	90	34	183

residues above the error tolerance in one or more simulation steps. The remaining simulations terminate while computing, where half of them are configured with a spine rhythm. These terminations occur in simulations with all models and motions, but agglomerate with model four and five. Especially, lateral bending motions prove to be sensitive. Table 5.2 shows the termination numbers in dependence of model and motion.

5.4.1 Multifidus muscle forces with disc herniation

As stated initially, all forces in multifidus fascicles are evaluated. This task is split into two parts. At first, the forces in individual fascicles per side of the body are analysed and afterwards the total forces of all fascicles per side are examined. The results of both approaches are shown as surface graphs. Only data in the final position of a motion is analysed, because this time step returns the greatest forces. Each set of force values of a muscle fascicle is plotted as a separate surface. Consequently, there are 19 surfaces in such a graph. In case of the total forces only a single surface is depicted in the diagram. Nevertheless, the structure of both types of graphs is similar. The independent variables, the disc stiffness and the disc height, are plotted on the x- and y-axis, while the axis of the affected parameter indicates the force exerted by the muscle. The healthy condition of the model is always located at the data point in the back corner of each view. Whereas the data point, that is positioned at the opposite corner in the front, describes a completely degenerated disc. In addition, each figure compares the output of computations with FDK and the SR. Results of FDK simulations are always in the top row and the ones with the SR in the bottom row. FDK and SR graphs have a diverging scale because their ranges of result values differ considerably. The colouring of the surfaces corresponds to the respective result value.

Figure 5.11 depicts the individual fascicle forces of a selection of simulations. These samples contain all characteristics that occur throughout the study. They originate from computations with model two in combination with a torsional movement (left column) and a flexion motion (right column). In the top left diagram are the fascicle forces of a torsional motion computed with FDK. Most fascicles exert a virtually constant force with

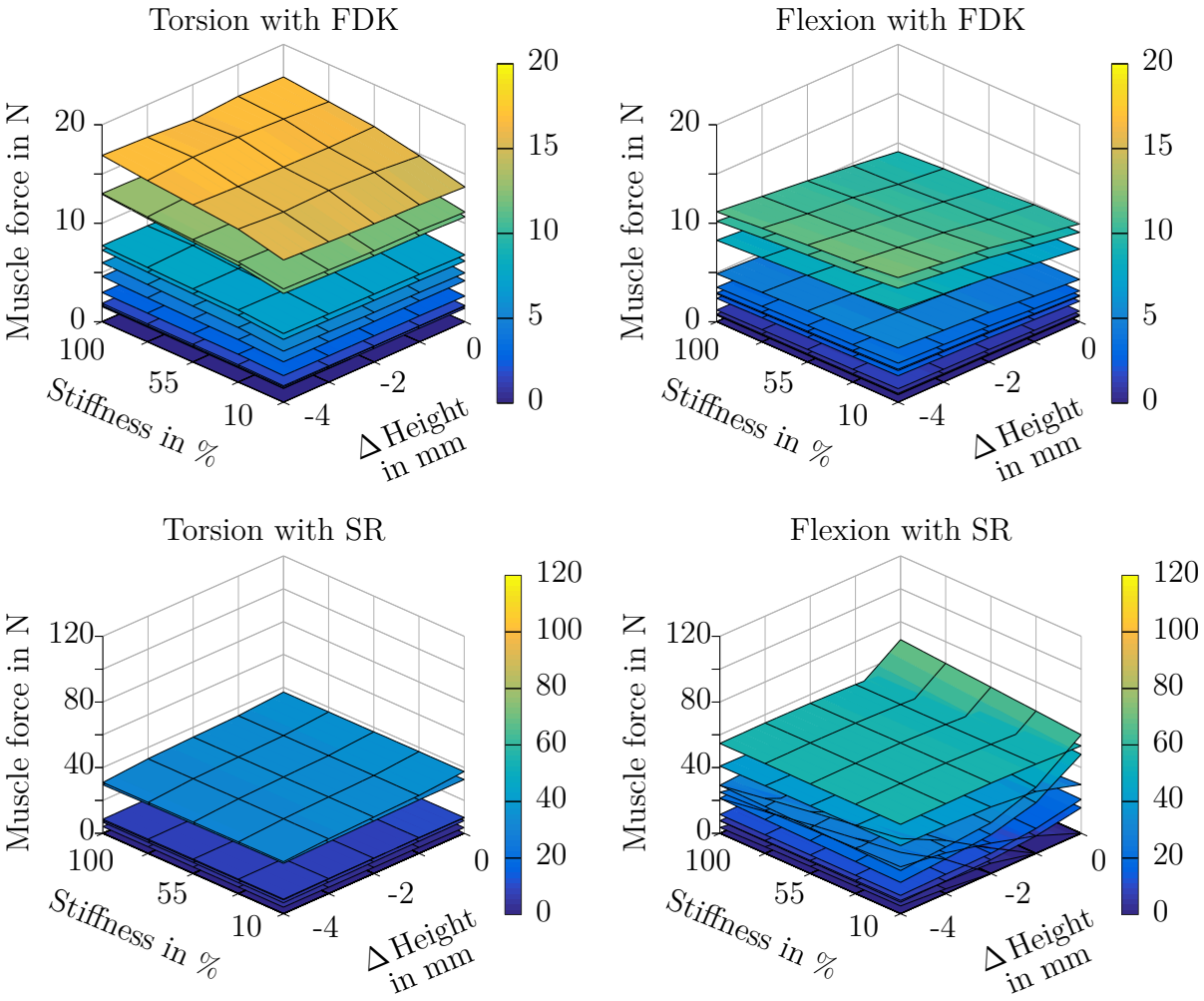

Figure 5.11: Typical results for the individual fascicle forces of the multifidus muscle in dependence of a progressing disc herniation. The torsional (left column) motion shows results of fascicles from the right side of the body, while the flexion (right column) motion depicts results of the left side. Simulations for graphs in the top row are configured to use the FDK solver and the ones in the bottom row used the spine rhythm (SR). The corner in the background represents a healthy condition while the one in the foreground stands for a herniated disc.

a value below 10 N. Merely three fascicles are activated in such a way that the muscle force results between 10 N and 20 N. Furthermore, these bunches of muscle fibres react to a change of the disc stiffness, but with an irrelevant height and a decrease in muscle force with a progressive degeneration of the disc. The graph located at the top right illustrates results for a flexion motion that are computed with the FDK option. Here, the greatest force exerted by a fascicle is 13 N, even below the values with a torsional motion. A minor influence of the degeneration is apparent, but again, in a very weak form. The forces exerted by fascicles are much higher, if the simulations are configured to use the SR. An example is present in the bottom left plot which shows simulations of axial rotation. In this case, the maximal force results in the healthy condition at a value of 37 N. As previously, the forces decrease with disc degeneration. The fourth plot at the bottom left depicts the individual multifidus fascicle forces for a flexion motion combined with the SR. This configuration leads to the greatest forces exerted by individual fascicles. However, this maximal value of 69 N occurs with the model in a healthy state and decreases over a progressive disc degeneration. In comparison to the other drops in force values, this decrease is much more pronounced. Additionally, this configuration shows rising forces in some fascicles if the disc deteriorates, however, their maximal value still is below the forces of other fascicles with a healthy disc.

These findings for individual fascicle forces can be summarised as follows. The greatest forces are simulated with flexion (up to 20 N) and axial rotation (up to 21 N) if the FDK option is active. A usage of the SR returns force values up to 102 N with a flexion motion. Furthermore, models that perform lateral bending or axial rotation or are positioned in an upright standing posture show a decrease in force of multifidus fascicles with progressive disc degeneration. Rising forces are merely present in flexion motions, however, the increase is of only a few newton if FDK is used. An application of the SR results in a much larger growth in force with a deteriorating disc, but the resulting maximal force values either are in a range that is exerted by fascicles with a healthy disc or are even lower. Moreover, simulations with the SR constantly result in higher forces than those with FDK.

As a next step, the total multifidus muscle forces are analysed. Figure 5.12 shows the results of simulations for the same model-motion combinations as previously, but this time the total multifidus muscle forces are plotted as a function of a progressive disc degeneration. The forces, shown in the graph in the top left corner which illustrates axial rotation in combination with an activated FDK option, decrease if the degeneration evolves. As a result, the healthy condition returns the greatest force value of 80 N. By contrast, the total muscle force increases if a flexion motion is performed and the FDK option is activated. This growth is of about 16 N. Axial torsion simulated with the SR leads to a similar output as with FDK. There is a decrease in force of 11 N and the healthy state returns the maximal value of 100 N. In contrast to the evaluation of individual fascicle forces, the flexion motion in combination with the SR results in the greatest force value as soon as the disc herniation reaches the worst condition. The total force in a healthy state is 239 N and the maximal value is 283 N.

Altogether, most of the investigated motions lead to a decrease in total multifidus muscle force, they merely show a negligible increase or the maximal value is below values with

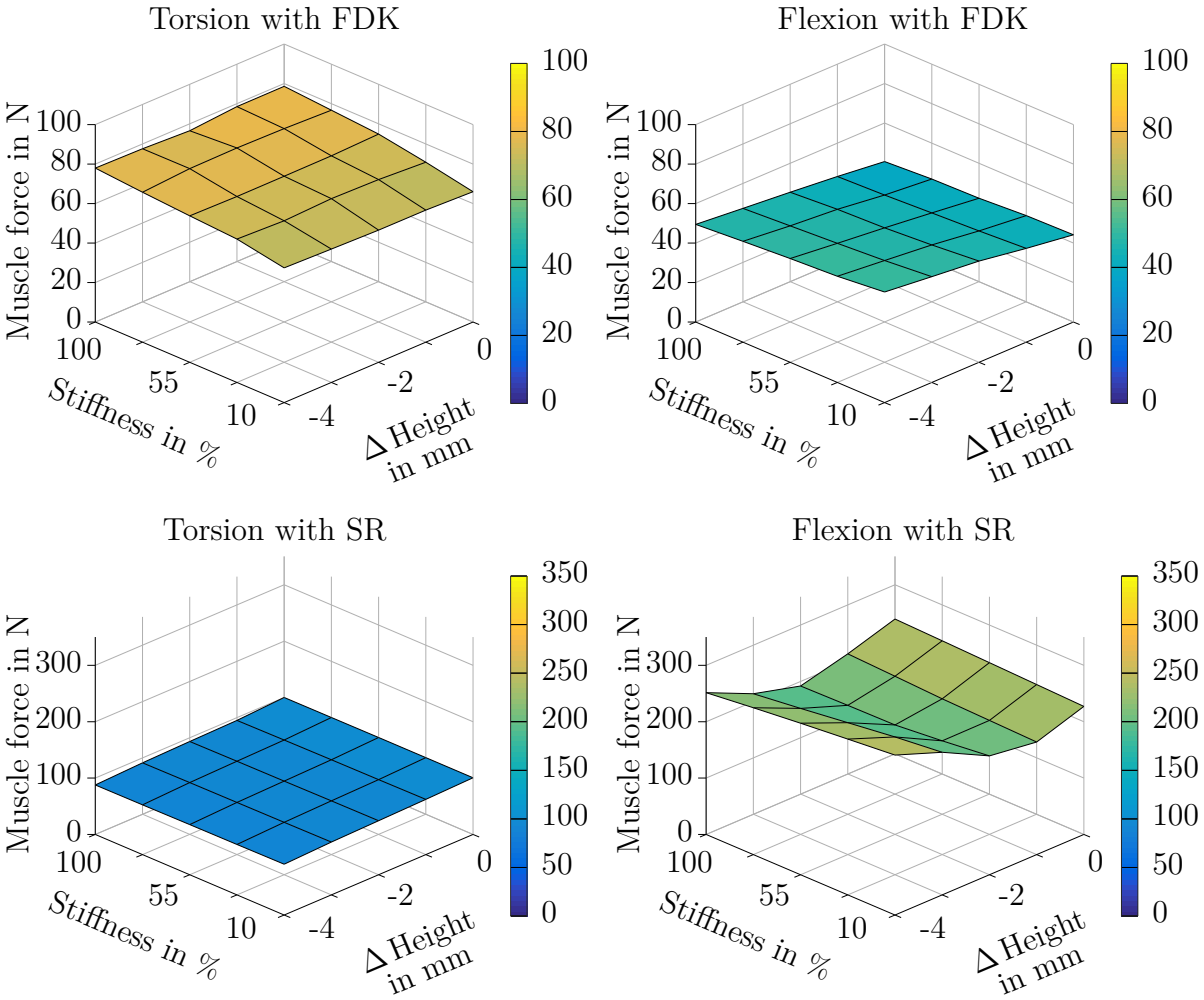

Figure 5.12: A selection of typical results for the total forces of the multifidus muscle. The forces of the muscles on the right side of the body are used in the graphs showing a torsional motion and the ones on the left side for the flexion movement. These diagrams depict the results of a single model (the second one) that are either simulated with the spine rhythm (SR) (bottom) or with FDK (top).

a healthy disc. Of course, there are a few exceptions. Especially if the model performs a flexion motion, the results show a contrary characteristic. Table 5.3 lists changes of total muscle force of all model, motion and rhythm combinations. In each case, this table shows the greatest total multifidus muscle force without determining a specific body side. As mentioned before and with the values of this table, it is obvious that flexion results in an increase of the force with an advancing disc herniation in all simulated cases. The amount of the gain is dependent on the kinematics, e.g. FDK leads to a maximal increase of 58 %, while simulations with the spine rhythm give 120 % as largest gain. In addition, there is a large difference in the maximal forces between the two kinematics with much higher forces in the multifidus muscle when using the spine rhythm. Usage of the FDK solver leads to the highest total forces with flexion or axial rotation depending on the model. The SR only produces the greatest total forces with flexion.

Table 5.3: Gain of total forces of the multifidus muscles with a progressive disc herniation. Additionally, the absolute values of the forces that are used to calculate the gain are listed. The values of the degenerated state are the maximal forces of simulations representing any diseased state and not necessarily the ones with the worst case.

Model no.	Motion	Gain (%)		Healthy (N)		Degenerated (N)	
		FDK	SR	FDK	SR	FDK	SR
1	upright standing	0	0	0	41	0	41
	flexion	57	74	25	183	39	317
	lateral bending	0	52	2	65	2	99
	axial rotation	4	7	35	69	36	74
2	upright standing	–	4	0	40	–	41
	flexion	38	9	40	321	56	349
	lateral bending	9	24	8	77	9	95
	axial rotation	0	0	79	100	68	90
3	upright standing	100	0	4	27	8	27
	flexion	27	9	56	412	71	448
	lateral bending	163	6	8	68	21	72
	axial rotation	1	0	77	135	77	135
4	upright standing	0	0	0	77	–	77
	flexion	–	72	79	165	–	284
	lateral bending	5	19	7	165	8	197
	axial rotation	2	5	67	107	69	113
5	upright standing	–	0	0	51	–	51
	flexion	58	120	36	139	57	305
	lateral bending	–	–	7	88	–	–
	axial rotation	4	0	14	73	15	73

– simulation terminated, a gain of 0 % corresponds to decrease or no change

5.4.2 Disc forces with an atrophic multifidus muscle

In this second step of the study, the consequences of a disc herniation combined with an atrophic multifidus muscle are investigated. As in the above evaluation, differences between the two kinematic approaches (FDK/SR) are analysed, too. The resultant disc force at each lumbar level is used as target parameter in all cases.

This evaluation is conducted by means of surface graphs, which show the reaction of the disc force. Each graph contains five surfaces and each of the surfaces corresponds to the target parameter of a lumbar level from T12/L1 to L4/L5. As previously described, the disc forces are computed in dependency of the disc degeneration, hence, each lumbar level contains 25 data points. These values are distributed over the different states of the disc herniation in accordance with the x- and y-axis. Both axes indicate the specific condition that is used in the according simulation run. The z-axis shows the disc force in percent and the computed force with the disc of the model in a healthy condition is used as reference value. Such a force equates to the resultant joint forces of the simulation model. Only the final position of every motion is used in the analysis. The diagrams of all investigated configurations are evaluated, but only a selection of typical results is shown subsequently.

In order to cover all characteristics of and difference between the simulation outputs, four different plots, each with a distinct configuration of the simulations, are depicted in Figure 5.13. Both graphs in the top row illustrate results of computations with the FDK option activated. While the left one shows disc forces with a healthy multifidus muscles, the right diagram does this for an atrophic musculature. The plots in the bottom row distinguish themselves from the top ones merely by usage of the SR. All results in these graphs originate from computations with model two performing a flexion motion. The diagrams are orientated in such a way, that the disc's healthy condition is located on the left side and the final degeneration state on the right side.

The outcome of simulations with a healthy musculature and FDK (top left graph) hardly indicates an influence of the herniation on the disc force except for the affected level. At this location, a sole decrease of stiffness increases the joint force, but the concurrent reduction of disc height reverses it. A single parameter change would alter the joint force by approximately 10 % in both directions. Atrophic multifidus fascicles do not change this behaviour as shown in the top right diagram. Still, all lumbar levels only result in a minimal decrease of disc force, while the herniated level is only influenced if the model is subjected to either a stiffness decrease or a reduction of the disc height. The missing data point in this configuration indicates a terminated simulation run. If any model performs a flexion or torsional movement combined with FDK, the joint forces decrease with a fully herniated disc. The largest reductions can be solely observed at the affected level and with a value of up to 25 %. Load changes at the remaining levels for these two motions do not exceed 5 %, in most instances. This characteristic is reversed for standing and lateral bending, but as before, the maximal changes do not surpass the 5 % mark in computations with models one to three. Model four shows a slightly higher growth with up to 8 % and the joint forces even decline for simulations with the last model.

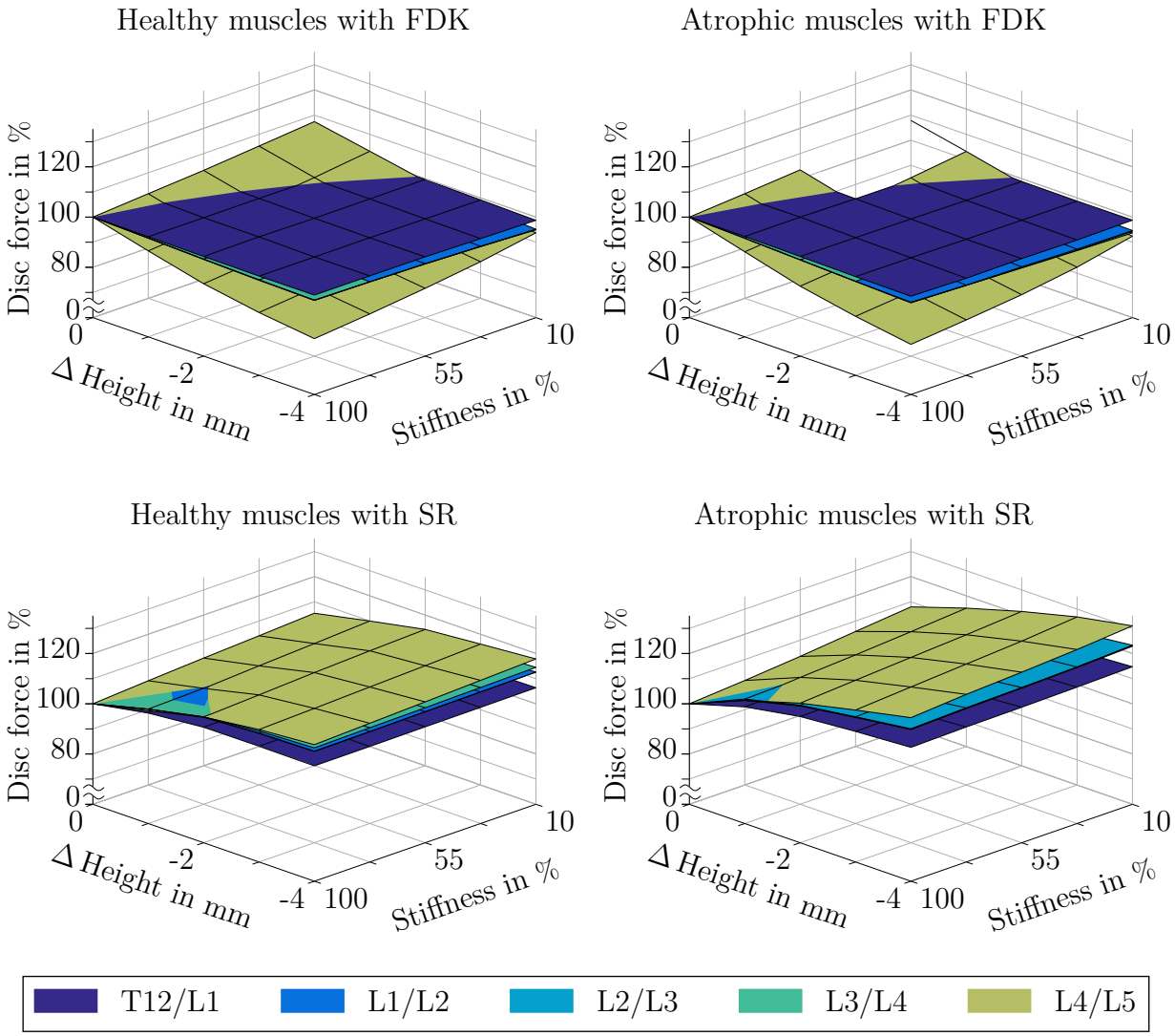

Figure 5.13: The graphs show the relative disc force of each lumbar level as a function of progressing disc herniation. The predicted disc force in a healthy condition is used as base value. The diagrams on the left represent results with healthy multifidus muscles while the ones on the right depict the outcome with atrophic fascicles of multifidus muscle. All pictures illustrate simulations with model two and a flexion motion.

Table 5.4: Lumbar disc forces in percent when referencing a fully degenerated disc to its healthy condition. All values originate from simulations of model two that performs a flexion motion with an activated SR.

	T12/L1		L1/L2		L2/L3		L3/L4		L4/L5	
	H	A	H	A	H	A	H	A	H	A
Standing	106	111	105	108	105	107	103	105	102	104
Flexion	106	115	113	123	113	123	114	123	118	131
Lateral bending	120	120	118	120	120	121	121	120	118	119
Axial rotation	100	101	100	100	99	99	98	98	95	96

However, the application of the SR alters this behaviour, especially for a flexion motion as depicted in the diagrams in the bottom row of Figure 5.13. In the above example of flexion, all lumbar discs show an increase in force for an aggravating injury. The simulations with healthy multifidus fascicles return a growth of the disc force of up to 18 %, whereby the T12/L1 level is affected at least (6 %) and the L4/L5 level at most. The intermediate discs receive a change in around 14 %. Degenerated muscles intensify this effect. Then, the joint force of the topmost level increases by 15 %, the intermediate levels grow by around 23 % and the L4/L5 disc force is raised by 31 %. The other motions also show a growth in disc forces, except axial rotation. The increase, while the model is postured in upright standing, does not go beyond 11 % and lateral bending leads to a maximal rise of 21 %. A more detailed breakdown, that includes the distribution over the lumbar levels of model two, is listed in Table 5.4. The other models show similar gains for the flexion motion, e.g. approximately 24 % from computations of model one for the intermediate lumbar levels. Nearly all motions, that are simulated with the SR, result in an increase of the lumbar loading. However, the amount of additional loading is very small in the upright standing pose and with axial rotation. The lateral bended posture, by contrast, leads to a considerable increase with values of up to 26 %. Table A.4 in the appendix summarises the resulting disc forces with healthy and atrophic multifidus fascicles for all model-motion combinations.

Overall, the application of the FDK solver mostly leads to a decrease in disc forces. Only, lateral bending and axial rotation show minimal increases in most instances and a maximal growth of 8 % on rare occasions. A flexion motion only raises the forces if the herniation is solely modelled as a stiffness reduction. Even then, the highest growth is about 10 %. However, usage of the SR results in elevated values for lumbar loading in almost all cases. The greatest increments occur with flexion and lateral bending, while the other two motions rarely exceed 10 %.

6 Discussion

The focus of this study is to create a validated, scalable model with an interchangeable subject-specific lumbar spine and assessable characteristics. The subject-specific part includes the vertebral geometry and lordosis of the lumbar spine and additionally, the model is scaled to the subject's body height and body weight. The model is tested with data of five different subjects. Therefore, a basic musculoskeletal full body model is heavily modified. The modifications are implemented in an iterative process, hence, the basic model is improved in three main steps. Each step is completed with a study. The findings of the first and second study have already been published [68, 69].

6.1 Model

The generic model is configured without muscles at the upper body part (chest, neck, shoulders and arms) to save computation time. Furthermore, no short segmental muscles are implemented because there is no literature data available regarding PCSA, even though HAN et al. [35] added those muscles. In another study, HAN et al. [33] included these muscles in a three-dimensional model, but only with an assumed PCSA of $0.1\,\mathrm{cm}^2$.

Modelling of two lumbar ligaments, the ITL and LF, is achieved with more than a single element per vertebral level because those ligaments cover a larger area. Originally, a single ligament characteristic/model is defined for each group of elements per motion segment. The generic model has a symmetrical design, therefore this style of implementation does not cause any problems or inaccuracies. Whereas, subject-specific vertebral geometry is not symmetrical at all, hence, each element is accompanied by its own ligament model. This is necessary, due to the definition of a ligament model (Section 3.1.3) which includes the slack length. This length is the same for all elements of a group in the symmetrical design of the generic model. But each subject-specific lumbar geometry is asymmetrical, with a differently inclined transverse process, slightly rotated spinous processes and so on. The initial implementation uses the slack length of the element calibrated last for all other elements in the group. Thus, the ligament could generate a force with the spine in a neutral position or there would be no force at all or far too late.

Published information indicates that the position of the lumbar joints has an influence on lumbar loading [31]. Additionally, findings of experimental studies suggest that a realistic location is shifted posteriorly and close to the upper endplate of the inferior vertebra [65]. Therefore, the initial position of the joints at the centre between two vertebrae is modified according to the reported data. The new method of joint positioning ensures that only CORs are relocated without changing the orientation and position

of the subject's lumbar vertebrae. Aside from the L5/S1 motion segment, all lumbar CORs are altered. The necessary vertebral body height can only be determined manually at this level and such an approach prevents an automatic positioning of the lumbar vertebrae.

As aforementioned, the human body model which is created includes a semi-automatic process to generate a full body model with a subject-specific geometry of the lumbar spine. This process is designed to minimise manual intervention, hence, non-automatic steps consist of only the following: segmentation of clinical images to create a surface geometry of the bony part of the lumbar spine, picking of landmarks, building of a file tree of the model and entering of body height and body weight for model scaling. These steps can be performed prior to loading the model and the time-consuming positioning process of the individual lumbar vertebrae is done automatically.

The subject-specific geometry of the lumbar spine is implemented via morphing of the generic vertebral geometry and not by individual modelling of each vertebra and its connections. This procedure keeps all nodes defined for each segment and all connections of the vertebrae like attachment points of muscles and ligaments, joints, and so on. In this way, it is possible to generate models based on different subjects and even new ones in the future. Furthermore, it facilitates the semi-automatic process of the model generation. An important feature is to keep the subject's lordosis. Therefore, the programmed positioning method uses the location of the generic L5 vertebra to position the subject's lumbar spine in the model, maintaining the relative orientation and distances between all vertebrae of the subject. Certainly, this technique changes the sagittal balance which has to be further investigated.

The surface geometry of the facets is integrated similarly. The only difference is the reference point. This time, an additional node at the centre of the corresponding vertebral body is used. This enables a rotation of the facet's contact surface for future studies. Usage of the complete surface geometry of a vertebra for a surface contact would extend the computational time dramatically.

All FCLs are created as a single element between two nodes with a distance of 2 mm. This length might be to small but otherwise, there would be no force in the ligament because of a large slack length conditioned by the distance between adjacent facets. Even full flexion would not show a force in the ligament.

Utilisation of the FDK solver activates an order of rotation of the form z-y-x for the lumbar joints, but the linear disc stiffness is based on the spine rhythm with a reversed order. Therefore, incorporated parameters are misused. More precisely, the parameter intended for the calculation of the stiffness value for the flexion-extension motion is applied for lateral bending and vice versa. This problem is addressed by the implemented fix.

The sole use of the novel non-linear disc stiffness model results in instabilities and eventually to terminations of a lot of simulations. This may be caused by the difference between the subjects. The public available non-linear model is developed using data of a male subject with a body height of 160 cm [99], hence, this subject is far smaller than

the ones in this study. Their body height ranges between 168 cm and 185 cm. Therefore, scaling of the disc stiffness is added. The according published study identified the two parameters endplate depth and endplate width as the ones with the largest influence on lumbar loading [51]. Unfortunately, only mean values of the L4 and L5 vertebral body depth and width are available for the non-linear disc stiffness. As a consequence, the scaling method is implemented based on this information.

For calibration purposes, the model is set in an upright standing posture. Literature reported that the lordosis in this position is comparable to lying on the back [7, 49] which is usually applied while acquiring a CT scan.

The approach chosen to identify the actual orientation of a vertebra during parametrisation does not consider the rotation around the anterior-posterior axis. However, this approach is sufficient because deviations around this axis are diminutive. Parametrisation of the disc height is solely achieved by modifying the inferior joint node of the superior vertebra of each motion segment. Otherwise, the altered position would not match specifications reported in literature which characterises the CORs depending on vertebral body height and width of the inferior vertebra [65].

Moreover, the maximum iterations of FDK solver are restricted to a certain number in all simulations. This is a compromise between a reasonable computation time and the number of successful simulations.

6.2 Model validation

Model validation is split into three parts and all of them are based on measurements of IDPs. At first, the absolute values in an upright standing posture are validated. Secondly, the progression of IDP over basic motions is compared to published data. At last, relative differences between various postures are analysed.

The absolute IDP values resulting from simulations with the models in an upright standing posture correspond well to the ones reported in literature [80, 92, 103]. In dependence of the correction factor used to convert a computed joint reaction force to an IDP, every configuration of subject and model shows values within the range of the published data. Moreover, the values match even better to the corridor as the model is improved. Nevertheless, there are deviations for model four and five. The increased IDP of model four can either be related to the severe degeneration at the L4/L5 lumbar disc of this subject or to a much higher body weight. Even though subject five has a lordosis angle in the range of the other subjects and in a normal range between 30° and 80° as reported in literature [7], the actual lumbar curvature is much more pronounced. This could explain the elevated level of IDP of this model and the inverted behaviour when changing from FDK to the spine rhythm.

Simulations of basic motions return results with comparable characteristics to the aforementioned absolute IDP. Overall, the computed curves show a similar appearance as the ones from literature, particularly, the curves produced with the second model configuration and the FDK solver. In this set-up, only model four shows slightly higher

results, but with similar trends. Possibly, the applied correction factor is not correct. However, only the progression is of interest in this part of validation, hence, a shift in vertical direction of the whole curve is unproblematic. The horizontal displacement of the minimal pressure value for model five is probably connected to the extreme lordosis. Usage of a linear disc stiffness influences the behaviour of the torsional motion. There, the IDP is rising excessively, indicating an overvalued torsional stiffness. The fact, that this movement only shows minor deflections in axial rotation of the lumbar vertebrae and is mostly performed via coupled motions of lateral bending and flexion/extension, supports this assumption. Coupled motions shall be present but not too dominant for axial rotation [26, 46, 88]. In contrast, an application of the spine rhythm leads to a quickly increasing slope of the IDP for a lateral bending motion. This may be caused by the spine rhythm which forces this motion to act exclusively around the anterior-posterior axis. A physiological approach would include some coupled motions [1, 45]. In general the simulated progressions of IDPs compare very satisfactory to the literature data, especially, in view of the fact that the published data is of a single subject and, therefore, can only give an indication of the growth rates.

The validation of relative changes of IDP is performed to facilitate a comparability of pressure measurements between different subjects. Upright standing is used as reference position, therefore, all according values are 100 %. This validation shows good agreement in the majority of cases. However, simulations of tasks combining flexion and lifting of a weight return results with larger deviations. Missing information about the exact stance, meaning specific flexion angle and distance between L4/L5 joint and weight, is a reason. The flexion angle already shows an influence in the validation analysis of the IDP's progression. Besides, the position of the weight has a notable effect, too, because it changes the lever arm between the load and the L4/L5 joint and the exact location is unknown. This seems very important for the case combining flexion and weight lifting. Furthermore, these lifting tasks prove to be very challenging as most of them finish with a residue above the specified FDK error tolerance. Especially the two weighted cases in an upright standing posture are prone to errors. Hence, the according results are just an indication with unknown deviations but still they result in a reasonable range. It is also noticeable that model number five shows the lowest IDP most of the time. This could be connected to the extreme curvature of the lumbar spine. Interestingly, usage of the spine rhythm produces similar results for the weighted cases but a much higher change in lumbar loading for pure flexion and unsupported seating. These levels of lumbar loading are elevated, particularly for model one to three. The forced motion caused by the spine rhythm could increase the IDP in those cases, because a larger rotation induces a stronger reaction of the disc stiffness. Eventually, this effect could increase the whole loading of the lumbar spine. In addition, the anatomical differences between individuals may also cause some deviations and published experimental data show a larger distribution of IDP values in various postures.

Overall, the simulated loads of all models correspond good to the experimental data. Only model four shows larger differences and model five minor ones in a few tested configurations. The published experimental data is often collected from experiments with only a single subject, hence, it seems obvious that there is a wider range of val-

ues.

6.3 Influence of ligament stiffness on kinematics

This study is conducted only with a single lumbar geometry because other clinical images and, therefore, other models are not available at that time. The three simulated models only differ in lumbar joint positions and are scaled to body height and weight for three subjects.

After calculation of the subject's COR from the fluoroscopic recordings, the results are verified with literature data. This verification is good for the L3/L4 and L4/L5 levels for subject one and two with rotational centres close to the superior endplate at the inferior vertebra with a slight displacement to the posterior vertebral part. However, results of subject three yielded CORs far off the literature data. Unfortunately, it is not known if there are experimental inconsistencies. Therefore, it is supposed that this subject has completely different rotational centres than documented in the literature. In addition, the COR at the L5/S1 level is always close to the boundary of published data or completely off. It is already reported in the publication of Panjabi [60] that the error of calculation could be rather large with small amplitudes of motion, which is especially present at this lumbar level.

The main goal of this study is to investigate the effects of different ligament stiffnesses on lumbar kinematics. Therefore, a flexion motion is simulated and forces of ligaments and intervertebral joints are recorded. This data is accompanied by joint moments that are produced by ligament forces referenced to the COR of the according lumbar level. Furthermore, evaluation of the simulations draw upon the ROM of each lumbar vertebra. It is calculated from the measurements of the angles between the superior endplates of two adjacent vertebrae. Moreover, relative differences of forces and moments between minimal and maximal ligament stiffness are determined at full flexion.

Simulations of the first two subjects reveal similar results for the ROM, but the outcome of subject three shows an alternative characteristic. The ROM at the L4/L5 lumbar level $\Delta\varphi_{L4/L5}$ of subject three is close to zero with a minimal ligament stiffness. This issue may be induced by the deviations of the COR when compared to literature data and the remaining subjects. Furthermore, differences between the simulated L5/S1 ROM $\Delta\varphi_{L5/S1}$ and the fluoroscopic recordings of all subjects are rather large. The missing modifications to the centres of rotation of this level may be the main reason for this behaviour. However, the calculations do not return reasonable results as aforementioned.

Though, the results of all simulations indicate that an increase in ligament stiffness could transfer loads and motions to the lower part of the lumbar spine, the rate of growth of both outcome parameters is higher in the lower motion segments. The change of ROM is clearly visible with a decreasing deflection at the upper lumbar levels and a simultaneous increase at the lower levels. Although, the L3/L4 level yields higher absolute values for the moments than the L4/L5 level, the intervertebral joint forces,

ligament forces and moments gain more with an increased ligament stiffness at the lower motion segment.

This knowledge may be helpful for future subject-specific simulations regarding the lumbar spine. It strongly suggests that a reasonable range of values for ligament stiffness has to be adopted in order to predict realistic loadings and kinematics of the lumbar spine. Else, kinematics and kinetics of the lumbar part may be overestimated by the simulation.

Furthermore, these findings could be interesting in case of a lumbar degeneration if it is connected to an increase in lumbar stiffness. This context could lead to an increase of motion at the lower lumbar segments and may even load those parts at a higher rate, hence, lower lumbar discs could potentially degenerate faster.

This study has some limitations. The lumbar ligament stiffness is changed uniformly over all levels and does not incorporate an individual distribution. Additionally, all stiffness values of the ligaments are derived from a single publication [67], but to current knowledge, there is no other report available covering the biomechanical properties of the lumbar intertransverse ligament. Thus, the available data is used, even though, the properties were acquired by experiments with ligaments of the T7/T8 and T9/T10 spinal level. Furthermore, mean values are utilised in the lumbar segments of the simulation models, because there are no subject-specific values available. Moreover, the nominal strain is assumed to be 75 % of the failure strain and a linear force-strain characteristic is assumed for the ligaments. There is no facet capsular ligament present in the models as well as there are no customisations regarding the locations of the CORs at the upper lumbar levels T12 to L3 because of missing data.

The results of this study show that an increase of lumbar ligament stiffness could shift lumbar loading to the lower levels. Additionally, lumbar flexion seems to amass at the lower levels, too. Both effects indicate a higher risk to the lower lumbar levels in case of a high stiffness of lumbar ligaments.

6.4 Parameter study of the lumbar geometry

The main intention of this study is to find the geometrical lumbar parameters with the greatest influence on lumbar loading. Therefore, various parameters of the lumbar spine of five different models are altered in a specified range and their effect on lumbar loading is evaluated. Afterwards, a combination of selected parameters is analysed in regard to the same background.

An evaluation of the results indicate that the vertebral body height and disc height are the parameters with the greatest effect on lumbar loading. Each of them shows changes between 5 % and 22 % throughout the study. Literature reports similar facts [35, 58]. Furthermore, simulations of a lateral bended posture result in an increased IDP range for changes to the transverse process width. The same applies to computations with axial rotation but with a lower intensity. Another, parameter of interest is the lordosis which affects lumbar loading with up to 15 %.

A change in the moment arms of muscles and ligaments can mainly be accounted for the variations in lumbar loading. For example, the mass of the upper thorax is displaced along the vertical axis of the body in case of modifications to the vertebral body height and disc height, while the lordosis parameter affects the distance along the anterior-posterior axis. Both displacements increase or decrease the moment arms and, therefore, affect muscle activity or ligament forces, which alter IDP. The modification of the parameter of the transverse process width does the same thing along the mediolateral axis: it changes the largest moment arm and shows its main effect on lumbar loading in a lateral bended posture. Additionally, influences can be seen under torsion because of coupled motions.

Some results exhibit a non-linear characteristic, for example dimensional alterations to the spinous process length in an upright standing posture. Such a sudden change in curvature is always connected to the development of a force in a ligament when it is stretched beyond its slack length. This extra force affects the IDP and changes its current trend.

Simulations with combined parameter changes respond with results that show a relationship to the ones from single parameter changes. If the influence of a parameter on IDP is large in the stand-alone variations, it shows similar effects in simulations with simultaneous changes to two variables and vice versa. Actually, the results of single alterations are summed in combined parameter modifications with a slight increase close to the edges of the studied intervals.

Sometimes, simulations terminate at a very early stage and most of the time, the current configuration of the lumbar spine does not correspond to a natural characteristic. For example, an extremely large or small disc height or an exaggerated lordosis causes such terminations. Possibly, an adapted stiffness of ligaments and the disc could compensate the occurring problems.

However, this study has several limitations. There are no signs of an influence caused by the interfacet width and height. This can be connected to two reasons and one of them are the studied postures. A main function of the facets is to limit extension as well as large axial rotation and both are not included in the study. Secondly, the utilised model lacks facet capsular ligaments, which oppose flexion motions [3]. Moreover, the subject-specific geometry is only implemented for L1 to L5 vertebrae leaving the adjacent geometry unchanged. This causes abnormal positions of the ligaments at the transitions. Besides, there are no working facet joints at the T12/L1 and L5/S1 level. Furthermore, neither the stiffness values of the disc and ligaments nor the properties of muscles and intra-abdominal pressure are adapted. Ligament characteristics are implemented with a linear elastic model and the slack length is determined in an upright standing posture, but it is unclear if this assumption is correct for every subject. While degenerations are modelled from the geometric side, the effects on other parameters like the disc or ligament stiffness is neglected. Additionally, the subject-specific modifications do not include an accumulation of mass at a specific region, e.g. abdominal mass, because this distribution is realised according to Winter [104]. Influences of the sagittal profile on various parameters are disregarded, too.

Overall, the findings indicate that a subject-specific lumbar model requires at least a correct vertebral body height, disc height, transverse process width and lumbar lordosis. These measurements can easily be taken from radiographs. Furthermore, modifications to the lumbar stiffness should be considered because of the sensitivity to unusual configurations.

6.5 Disc herniation and multifidus muscle atrophy

This study is based on a hypothesis of Robie et al. [73]. They suggested that an overload of the multifidus muscle group after a disc herniation induces multifidus muscle atrophy. This degeneration of muscles leads to high levels of shear forces in the adjacent discs and causes further degenerations. Therefore, simulations with five different models performing four basic motions and including a progressing disc herniation are conducted and evaluated in consideration of an overloaded multifidus muscle group. Afterwards, the multifidus muscles fascicles passing the degenerated level are deactivated and the same configurations are simulated, but are evaluated with regard to the loading of the adjacent levels. In all simulations, the herniation is modelled as a stepwise stiffness reduction and height loss at the L4/L5 level. All configurations are simulated with FDK and a second time with an active spine rhythm to consider different lumbar motion patterns.

The utilised full body model is further improved to reduce the error rate of the simulations. All measures taken prove successful, because the percentage of errors during simulations decreases from 29 % in the second study to 9 %. While the individual models for each element of the ligaments surely have a minor effect on stability, the main improvement to error-proneness involves the non-linear disc stiffness in combination with its scaling procedure. As before, most errors occur in simulations with model four followed by model five and three. Again, this is probably connected to the subjects, given the fact that subject three and four have very high BMI values (30 and 41) and subject five has an exaggerated lordosis.

Individual fascicles of multifidus muscles are loaded in all simulated motions because they play a major role in spinal stabilisation [63]. But contrary to published results of Robie et al. [73], individual fascicles in this group are not overloaded after introducing a disc herniation to the model. Instead, most fascicles experience smaller loads as disc degeneration aggravates. A few fascicles show an increased loading, but have their maximum below values of fascicles in a healthy condition. Only a flexion motion with the FDK solver results in a minor integral increase, but the highest values are lower than the ones in a healthy condition, e.g. around 12 N for flexion and maximal degeneration of the disc versus 17 N for rotation and a healthy condition. The total force in the multifidus muscle group shows a similar characteristic as the force in the individual fascicles, but with slight changes to a few combinations of models and motions. Even though, a FDK simulation with model three performing a lateral bending or upright standing motion leads to an increase in muscle force by 163 % or 100 %, respectively, the obtained absolute values are very low. Again, the generated total forces are below the levels of another motion for the model in a healthy condition. This fact even applies to

the results of a flexion motion with the FDK solver. However, an application of the spine rhythm changes the picture in case of flexion. There, the muscle force increases by up to 120 % and shows higher absolute values compared to the other motions. This increase could be the result of the stiffness reduction and, hence, a loss of lumbar stability due to the herniated disc. The changed lumbar motion pattern could cause higher forces in the muscle to compensate this. These results lead to the assumption, that an overload of the multifidus muscle group could be possible, but it seems to be highly dependent on the individual subject.

Lumbar loading does not change a lot in most simulated cases, if FDK is activated. There are only slight changes to the joint force at the herniated lumbar level. The observed decrease of lumbar loading could be connected to the way FDK works. Less resistance in the joint, due to the loss of disc stiffness, allows for an increased range of motion and/or could produce less joint force. The results indicate that the FDK solver affects both possibilities, hence, there is a slight increase in the ROM of the L4/L5 joint and the observed decrease in joint force. However, a change to the utilised rhythm leads to a different outcome. Simulations with an activated spine rhythm lead to a nearly constant joint force for standing and axial rotation and increase the lumbar loading for flexion and lateral bending. An atrophic multifidus muscle intensifies the latter effect.

These results indicate that the loss of stability caused by a disc herniation is at first counteracted by a raised force in the multifidus muscle, thus, the higher total forces in this muscle. As a consequence, the disc forces increase too. An atrophy of the multifidus muscle forces other muscles to adopt the stabilising role, which further increase the lumbar loading over all levels. This puts adjacent discs to a higher risk of degeneration. A similar hypothesis is reported by Meng et al. [52]. Though, as stated in the results section, a lateral bending motion does not show an influence on multifidus muscle force with FDK and, therefore, this result may be connected to the motion pattern of the spine rhythm.

There are some limitations to this study: regardless of the utilisation of FDK, all simulations with the spine rhythm are based on a single motion pattern, yet results indicate its important effect. Furthermore, each model is based upon data of a subject, which shows signs of additional lumbar degenerations. All individualisations of the models are confined to the lumbar geometry only, meaning, there is no adaption of the properties of lumbar ligaments. Additionally, there are no modifications to the body weight distribution which means no local accumulation of fat is considered.

Overall, the results indicate that the hypothesis of Robie et al. [73] could be realistic. A disc herniation could lead to an increased loading of the multifidus muscle which as a consequence causes atrophies. Therefore, other muscles seem to adapt its stabilising role and the lumbar loading increases as a whole. This in turn, could endanger adjacent lumbar levels to degeneration. However, it has to be noted, that those effects are highly dependent on the subject and its individual motion pattern.

7 Summary and outlook

One major task of this thesis is to create a novel musculoskeletal model of the lumbar spine by heavily modifying a full body model from the AMMR. The new model incorporates a subject-specific approach for the whole lumbar section, including the position and orientation of the vertebrae besides their shape, as a main feature. This morphing of the geometry is intended to work automatically and in a short amount of time after supplying all necessary information to the software. Starting with CT scans used as input data, the bony structure of the subject's lumbar spine is segmented as a surface geometry which facilitates a morphing process in the AMS. Additionally, this method requires landmark coordinates of each lumbar vertebrae and a scaling routine alters the model with an individual body height and body weight. Various optional features are added to the model: a non-linear disc stiffness with scaling according to lumbar dimensions, altered calibration of the lumbar ligaments and application of the force dependent kinematics solver. Overall, five distinct subjects are modelled in different configurations. Furthermore, each model could perform basic motions like flexion/extension, lateral bending and axial rotation in a certain range. All implemented options and the half-automatic way of model generation work well, hence, an easy creation of the subject-specific models is possible.

Three major configurations are validated in terms of lumbar loading and on the following levels: absolute loading in an upright standing posture, progression of the loading over basic motions and relative differences of lumbar loading between a set of predefined postures. All simulated configurations return good results with frequent deviations for two models. Both show divergent anatomical or anthropometrical deviations to the other subjects.

The created subject-specific models are used to carry out different parameter and case studies to check model quality, model sensitivity and analyse degenerations. At first, a parameter study about the influence of ligament stiffness on lumbar loading and lumbar range of motion during a flexion movement is conducted. Therefore, one subject-specific model's lumbar joint positions at the L3/L4 and L4/L5 level are modified according to calculated instantaneous centres of rotation. These calculations are performed based on fluoroscopic recordings of three different subjects, resulting in three models for this study. They only differentiate in lumbar joint position, body weight and height. The new joint locations are verified with literature data and subject three shows some abnormalities. Afterwards, the influence of the lumbar ligaments is determined by changing their stiffness property in eleven steps in a certain interval. Results indicate that a higher ligament stiffness could deflect loading and motion to the lower lumbar levels. This could lead to either an overestimation of the risk of degeneration or to an increased deterioration of lumbar segments due to a condition with rising ligament stiffness.

The second study analyses the sensitivity of lumbar loading to spinal dimensions. Five

models each one with a differently shaped lumbar spine, body height and body weight are set up in the four basic postures: upright standing, flexion, lateral bending and axial rotation. Ten different parameters are varied in eleven steps between given intervals. Additionally, three of them are selected for simulations with simultaneously changing a pair of two parameters. Results indicate that the disc height, vertebral body height and lumbar lordosis are parameters with a large influence on lumbar loading throughout all analysed postures. Furthermore, the transverse process width shows an increased effect in a lateral bended and axial rotated pose. Combined changes of two parameters result in an influence on lumbar loading, comparable to a summation of the effects in the according single parameter variation. Therefore, subject-specific models require at least a correct disc height, vertebral body height and lumbar lordosis. Ideally, the transverse process width is also adapted to the subjects dimension. All recommended measurements can be acquired from radiographs. Furthermore, the simulations reveal that the model is very sensitive to the lumbar stiffness, hence, this parameter needs special attention throughout modelling.

Lastly, a study is conducted to analyse the development of multifidus muscle atrophy after disc herniation and subsequent load transfer to adjacent discs. Again, five models are used throughout the simulations, but with a non-linear disc stiffness model that is scaled according to the subject. At first, the effect of disc herniation on multifidus muscle force is analysed. Therefore, a disc herniation is introduced to the models by a stepwise reduction of the disc stiffness and disc height at the L4/L5 level. Secondly, simulations with an atrophic multifidus muscle are carried out, hence, the concerning fascicles are deactivated. Here, the lumbar loading is evaluated. Additionally, both parts of the study are simulated with two different lumbar kinematics: force dependent kinematics and a predefined spine rhythm. Increasing stress of the multifidus muscle with progressing disc herniation is only measurable in a flexion motion but with absolute values far below relevant levels with the FDK solver. An application of the spine rhythm raises the absolute values to concerning levels, therefore, the multifidus muscle could be overloaded and endangered to atrophy. Similarly, there are only slight changes in disc force at the herniated level if FDK is active. Once more, usage of the spine rhythm alters the behaviour and an increase of lumbar loading over all levels is observable for flexion and lateral bending over a progressing disc herniation. An atrophic or deactivated multifidus muscle intensifies this effect. Finally, the conducted simulations indicate that a disc herniation could be followed by multifidus muscle atrophy due to an elevated level of muscle loading. Furthermore, a ruptured disc and an atrophic multifidus muscle could endanger adjacent lumbar levels to degeneration due to higher stresses. Both implications are highly individual. Furthermore, the non-linear disc stiffness model with concurrent stiffness scaling according to the subject improves model stability.

Overall, the created workflow to generate a partly subject-specific model works well and results in models which can be utilised to simulate certain subject-specific problems. Relevant parameters regarding individual models can be identified and their effect on the model can be rated on the basis of the information of the conducted studies. Subject-specific models should be individualised at least with the correct body height, body weight, vertebral body height, disc height, transverse process width and lumbar

lordosis. Furthermore, a proper lumbar stiffness should be modelled and other subject-specific properties should be taken into consideration, especially the spinal kinematics.

Therefore, future studies should include at least one additional spinal rhythm and the results of the parameter studies should be checked with a different spine rhythm. Furthermore, the option of full FDK at the lumbar joints has to be tested and validated. The remaining translational degrees of freedom are already implemented as an FDK version in the model and are described in the Appendix A.4. Besides, simulations with a healthy subject could clarify the effect of present degenerations and an increased number of subjects could further support the current conclusions.

Bibliography

[1] Abouhossein, A.; Weisse, B.; Ferguson, S. J.: *A multibody modelling approach to determine load sharing between passive elements of the lumbar spine.* Computer Methods in Biomechanics and Biomedical Engineering, Vol. 14, No. 6, pp. 527–537, 2011

[2] Abumi, K.; Panjabi, M. M.; Kramer, K. M.; Duranceau, J.; Oxland, T.; Crisco, J. J.: *Biomechanical evaluation of lumbar spinal stability after graded facetectomies.* Spine, Vol. 15, No. 11, pp. 1142–1147, 1990

[3] Adams, M. A.; Hutton, W. C.: *The mechanical function of the lumbar apophyseal joints.* Spine, Vol. 8, No. 3, pp. 327–330, 1983

[4] Aiyangar, A. K.; Zheng, L.; Tashman, S.; Anderst, W. J.; Zhang, X.: *Capturing three-dimensional in vivo lumbar intervertebral joint kinematics using dynamic stereo-X-ray imaging.* Journal of Biomechanical Engineering, Vol. 136, No. 1, p. 011004, 2014

[5] Andersen, M. S.; Damsgaard, M.; Rasmussen, J.: *Force-dependent kinematics: a new analysis method for non-conforming joints.* In: *Proceedings of the XIII International Symposium on Computer Simulation in Biomechanics.* Leuven, Belgium, 2011

[6] Arjmand, N.; Plamondon, A.; Shirazi-Adl, A.; Larivière, C.; Parnianpour, M.: *Predictive equations to estimate spinal loads in symmetric lifting tasks.* Journal of Biomechanics, Vol. 44, No. 1, pp. 84–91, 2011

[7] Been, E.; Kalichman, L.: *Lumbar lordosis.* The Spine Journal, Vol. 14, No. 1, pp. 87–97, 2014

[8] Belavỳ, D. L.; Armbrecht, G.; Richardson, C. A.; Felsenberg, D.; Hides, J. A.: *Muscle atrophy and changes in spinal morphology: is the lumbar spine vulnerable after prolonged bed-rest.* Spine, Vol. 36, No. 2, pp. 137–145, 2011

[9] Bergmark, A.: *Stability of the lumbar spine.* Acta Orthopaedica Scandinavica, Vol. 60, No. sup230, pp. 1–54, 1989

[10] Berry, J. L.; Moran, J. M.; Berg, W. S.; Steffee, A. D.: *A morphometric study of human lumbar and selected thoracic vertebrae.* Spine, Vol. 12, No. 4, pp. 362–367, 1987

[11] Bitzer, E. M.; Lehmann, B.; Bohm, S.; Priess, H.-W.: *BARMER GEK Report Krankenhaus 2015.* Asgard Verlagsservice GmbH, Siegburg, 2015

[12] Bogduk, N.; Macintosh, J. E.; Pearcy, M. J.: *A universal model of the lumbar back muscles in the upright position.* Spine, Vol. 17, No. 8, pp. 897–913, 1992

[13] Boocock, M.-G.; Mawston, G.-A.; Taylor, S.: *Age-related differences do affect postural kinematics and joint kinetics during repetitive lifting.* Clinical Biomechanics, Vol. 30, No. 2, pp. 136–143, 2014

[14] Chapman, A.-R.; Vicenzino, B.; Blanch, P.; Hodges, P.-W.: *Patterns of leg muscle recruitment vary between novice and highly trained cyclists.* Journal of Electromyography and Kinesiology, Vol. 18, No. 3, pp. 359–371, 2008

[15] Chazal, J.; Tanguy, A.; Bourges, M.; Gaurel, G.; Escande, G.; Guillot, M.; Vanneuville, G.: *Biomechanical properties of spinal ligaments and a histological study of the supraspinal ligament in traction.* Journal of Biomechanics, Vol. 18, No. 3, pp. 167–176, 1985

[16] Cholewicki, J.; McGill, S. M.: *Lumbar posterior ligament involvement during extremely heavy lifts estimated from fluoroscopic measurements.* Journal of Biomechanics, Vol. 25, No. 1, pp. 17–28, 1992

[17] Christophy, M.; Faruk Senan, N. A.; Lotz, J. C.; O'Reilly, O. M.: *A musculoskeletal model for the lumbar spine.* Biomechanics and Modeling in Mechanobiology, Vol. 11, No. 1-2, pp. 19–34, 2011

[18] Comerford, M.; Mottram, S.: *Movement and stability dysfunction – contemporary developments.* Manual Therapy, Vol. 6, No. 1, pp. 15–26, 2001

[19] D'hooge, R.; Hodges, P.; Tsao, H.; Hall, L.; Macdonald, D.; Danneels, L.: *Altered trunk muscle coordination during rapid trunk flexion in people in remission of recurrent low back pain.* Journal of Electromyography and Kinesiology, Vol. 23, No. 1, pp. 173–181, 2013

[20] Damsgaard, M.; Christensen, S. T.; Rasmussen, J.: *An efficient numerical algorithm for solving the muscle recruitment problem in inverse dynamics simulations.* In: *Proceedings of International Society of Biomechanics XVIIIth Congress.* Zurich, Switzerland, 2001

[21] De Zee, M.; Hansen, L.; Wong, C.; Rasmussen, J.; Simonsen, E. B.: *A generic detailed rigid-body lumbar spine model.* Journal of Biomechanics, Vol. 40, No. 6, pp. 1219–1227, 2007

[22] Dreischarf, M.; Rohlmann, A.; Zhu, R.; Schmidt, H.; Zander, T.: *Is it possible to estimate the compressive force in the lumbar spine from intradiscal pressure measurements? A finite element evaluation.* Medical Engineering & Physics, Vol. 35, No. 9, pp. 1385–1390, 2013

[23] Ekin, E. E.; Yildiz, H. K.; Mutlu, H.: *Age and sex-based distribution of lumbar multifidus muscle atrophy and coexistence of disc hernia: an MRI study of 2028 patients.* Diagnostic and Interventional Radiology, Vol. 22, No. 3, pp. 273–276, 2016

[24] Essendrop, M.: *Significance of intra-abdominal pressure in work related trunk-loading.* Ph.D. Thesis. Denmark: National Institute of Occupational Health, 2003

[25] Frankenfield, D. C.; Rowe, W. A.; Cooney, R. N.; Smith, J. S.; Becker, D.: *Limits of body mass index to detect obesity and predict body composition.* Nutrition (Burbank, Los Angeles County, Calif.), Vol. 17, pp. 26–30, 2001

[26] Fujii, R.; Sakaura, H.; Mukai, Y.; Hosono, N.; Ishii, T.; Iwasaki, M.; Yoshi-kawa, H.; Sugamoto, K.: *Kinematics of the lumbar spine in trunk rotation: in vivo three-dimensional analysis using magnetic resonance imaging.* European Spine Journal, Vol. 16, No. 11, pp. 1867–1874, 2007

[27] Gadomski, B. C.; Rasmussen, J.; Galibarov, P.; Puttlitz, C. M.: *The effect of coupled motions and lifting tasks on human lumbar nucleus pressures and annulus fibrosus stresses in a muscle-loaded finite element model.* In: *Proceedings of International Society of Biomechanics XXIIIth Congress.* Brussels, Belgium, 2011

[28] Galibarov, P. E.; Dendorfer, S.; Christensen, S. T.: *On modelling spine curvature dependent on muscular and external forces in multibody dynamics system.* In: *Proceedings of International Society of Biomechanics XIIIth Congress.* Brussels, Belgium, 2011

[29] Gatton, M. L.; Pearcy, M. J.: *Kinematics and movement sequencing during flexion of the lumbar spine.* Clinical Biomechanics, Vol. 14, No. 6, pp. 376–383, 1999

[30] Hallett, M.; Shahani, B.-T.; Young, R.-R.: *EMG analysis of stereotyped voluntary movements in man.* Journal of Neurology, Neurosurgery and Psychiatry, Vol. 38, No. 12, pp. 1154–1162, 1975

[31] Han, K.-S.; Kim, K.; Park, W. M.; Lim, D. S.; Kim, Y. H.: *Effect of centers of rotation on spinal loads and muscle forces in total disk replacement of lumbar spine.* Proceedings of the Institution of Mechanical Engineers, Part H: Journal of Engineering in Medicine, Vol. 227, No. 5, pp. 543–550, 2013

[32] Han, K.-S.; Rohlmann, A.; Kim, K.; Cho, K. W.; Kim, Y. H.: *Effect of Ligament Stiffness on Spinal Loads and Muscle Forces in Flexed Positions.* International Journal of Precision Engineering and Manufacturing, Vol. 13, No. 12, pp. 2233–2238, 2012

[33] Han, K.-S.; Rohlmann, A.; Yang, S.-J.; Kim, B. S.; Lim, T.-H.: *Spinal muscles can create compressive follower loads in the lumbar spine in a neutral standing posture.* Medical Engineering & Physics, Vol. 33, No. 4, pp. 472–478, 2011

[34] Han, K.-S.; Rohlmann, A.; Zander, T.; Taylor, W. R.: *Lumbar spinal loads vary with body height and weight.* Medical Engineering & Physics, Vol. 35, No. 7, pp. 969–977, 2013

[35] Han, K.-S.; Zander, T.; Taylor, W. R.; Rohlmann, A.: *An enhanced and validated generic thoraco-lumbar spine model for prediction of muscle forces.* Medical Engineering & Physics, Vol. 34, No. 6, pp. 709–716, 2012

[36] Heuer, F.; Schmidt, H.; Klezl, Z.; Claes, L.; Wilke, H.-J.: *Stepwise reduction of functional spinal structures increase range of motion and change lordosis angle.* Journal of Biomechanics, Vol. 40, No. 2, pp. 271–280, 2007

[37] Hodges, P.; Holm, A.-K.; Hansson, T.; Holm, S.: *Rapid atrophy of the lumbar multifidus follows experimental disc or nerve root injury.* Spine, Vol. 31, No. 25, pp. 2926–2933, 2006

[38] Hyun, J.-K.; Lee, J.-Y.; Lee, S.-J.; Jeon, J.-Y.: *Asymmetric Atrophy of Multifidus Muscle in Patients With Unilateral Lumbosacral Radiculopathy.* Spine, Vol. 32, No. 21, pp. 598–602, 2007

[39] Ivicsics, M.; Bishop, N.; Püschel, K.; Morlock, M.; Huber, G.: *Increase in facet joint loading after nucleotomy in the human lumbar spine.* Journal of Biomechanics, Vol. 47, No. 7, pp. 1712–1717, 2014

[40] Jemmett, R.; Macdonald, D.; Agur, A.: *Anatomical relationships between selected segmental muscles of the lumbar spine in the context of multi-planar segmental motion: a preliminary investigation.* Manual Therapy, Vol. 9, No. 4, pp. 203–210, 2004

[41] Kim, H.-J.; Chun, H.-J.; Lee, H.-M.; Kang, K.-T.; Lee, C.-K.; Chang, B.-S.; Yeom, J. S.: *The biomechanical influence of the facet joint orientation and the facet tropism in the lumbar spine.* The Spine Journal, Vol. 13, No. 10, pp. 1301–1308, 2013

[42] Kim, W. H.; Lee, S.-H.; Lee, D. Y.: *Changes in the cross-sectional area of multifidus and psoas in unilateral sciatica caused by lumbar disc herniation.* Journal of Korean Neurosurgical Society, Vol. 50, No. 3, pp. 201–204, 2011

[43] Kim, Y. E.; Choi, H. W.: *Effect of disc degeneration on the muscle recruitment pattern in upright posture: a computational analysis.* Computer Methods in Biomechanics and Biomedical Engineering, Vol. 18, No. 15, pp. 1622–1631, 2015

[44] Kjaer, P.; Bendix, T.; Sorensen, J. S.; Korsholm, L.; Leboeuf-Yde, C.: *Are MRI-defined fat infiltrations in the multifidus muscles associated with low back pain.* BMC Medicine, Vol. 5, No. 1, 2007

[45] Lee, B. W.; Lee, J.-E.; Lee, S.-H.; Kwon, H.-K.: *Kinematic analysis of the lumbar spine by digital videofluoroscopy in 18 asymptomatic subjects and 9 patients with herniated nucleus pulposus.* Journal of Manipulative and Physiological Therapeutics, Vol. 34, No. 4, pp. 221–230, 2011

[46] Li, G.; Wang, S.; Passias, P.; Xia, Q.; Li, G.; Wood, K.: *Segmental in vivo vertebral motion during functional human lumbar spine activities.* European Spine Journal, Vol. 18, No. 7, pp. 1013–1021, 2009

[47] Lombard, W.-P.: *The action of two-joint muscles.* American Physical Education Review, Vol. 8, No. 3, pp. 141–145, 1903

[48] MacDonald, D. A.; Moseley, G. L.; Hodges, P. W.: *The lumbar multifidus: does the evidence support clinical beliefs.* Manual Therapy, Vol. 11, No. 4, pp. 254–263, 2006

[49] Madsen, R.; Jensen, T. S.; Pope, M.; Sørensen, J. S.; Bendix, T.: *The effect of body position and axial load on spinal canal morphology: an MRI study of central spinal stenosis.* Spine, Vol. 33, pp. 61–67, 2008

[50] McMillan, D.-W.; Garbutt, G.; Adams, M.-A.: *Effect of sustained loading on the water content of intervertebral discs: implications for disc metabolism.* Annals of the Rheumatic Diseases, Vol. 55, No. 12, pp. 880–887, 1996

[51] Meijer, G. J. M.; Homminga, J.; Hekman, E. E. G.; Veldhuizen, A. G.; Verkerke, G. J.: *The effect of three-dimensional geometrical changes during adolescent growth on the biomechanics of a spinal motion segment*. Journal of Biomechanics, Vol. 43, No. 8, pp. 1590–1597, 2010

[52] Meng, X.; Bruno, A. G.; Cheng, B.; Wang, W.; Bouxsein, M. L.; Anderson, D. E.: *Incorporating six degree-of-freedom intervertebral joint stiffness in a lumbar spine musculoskeletal model–method and performance in flexed postures*. Journal of Biomechanical Engineering, Vol. 137, No. 10, pp. 1010081–1010089, 2015

[53] Miller, J. A.; Schmatz, C.; Schultz, A. B.: *Lumbar disc degeneration: correlation with age, sex, and spine level in 600 autopsy specimens*. Spine, Vol. 13, No. 2, pp. 173–178, 1988

[54] Moseley, G. L.; Hodges, P. W.; Gandevia, S. C.: *Deep and superficial fibers of the lumbar multifidus muscle are differentially active during voluntary arm movements*. Spine, Vol. 27, No. 2, E29–E36, 2002

[55] Myklebust, J. B.; Pintar, F.; Yoganandan, N.; Cusick, J. F.; Maiman, D.; Myers, T. J.; Sances, A.: *Tensile strength of spinal ligaments*. Spine, Vol. 13, No. 5, pp. 526–531, 1988

[56] Nachemson, A.: *Towards a better understanding of low-back pain: a review of the mechanics of the lumbar disc*. Rheumatology, Vol. 14, No. 3, pp. 129–143, 1975

[57] Nachemson, A.: *Lumbar Intradiscal Pressure: Experimental Studies on Post-Mortem Material*. Acta Orthopaedica Scandinavica, Vol. 31, No. sup43, pp. 1–104, 1960

[58] Niemeyer, F.; Wilke, H.-J.; Schmidt, H.: *Geometry strongly influences the response of numerical models of the lumbar spine – a probabilistic finite element analysis*. Journal of Biomechanics, Vol. 45, No. 8, pp. 1414–1423, 2012

[59] Noailly, J.: *Model developments for in silico studies of the lumbar spine biomechanics*. PhD thesis. Technical University of Catalonia, 2009

[60] Panjabi, M.-M.: *Centers and angles of rotation of body joints: a study of errors and optimization*. Journal of Biomechanics, Vol. 12, No. 12, pp. 911–920, 1979

[61] Panjabi, M.-M.; Goel, V.; Oxland, T.; Takata, K.; Duranceau, J.; Krag, M.; Price, M.: *Human lumbar vertebrae. Quantitative three-dimensional anatomy*. Spine, Vol. 17, No. 3, pp. 299–306, 1992

[62] Panjabi, M.-M.; Oxland, T.; Takata, K.; Goel, V.; Duranceau, J.; Krag, M.: *Articular facets of the human spine. Quantitative three-dimensional anatomy*. Spine, Vol. 18, No. 10, pp. 1298–1310, 1993

[63] Panjabi, M. M.: *The Stabilizing System of the Spine. Part I. Function, Dysfunction, Adaptation, and Enhancement*. Journal of Spinal Disorders, Vol. 5, No. 4, pp. 383–389, 1992

[64] Passias, P. G.; Wang, S.; Kozanek, M.; Xia, Q.; Li, W.; Grottkau, B.; Wood, K. B.; Li, G.: *Segmental lumbar rotation in patients with discogenic low back pain during functional weight-bearing activities*. The Journal of Bone and Joint Surgery - American Volume, Vol. 93, No. 1, pp. 29–37, 2011

[65] Pearcy, M. J.; Bogduk, N.: *Instantaneous axes of rotation of the lumbar intervertebral joints*. Spine, Vol. 13, No. 9, pp. 1033–1041, 1988

[66] Pearcy, M.; Portek, I.; Shepherd, J.: *Three-dimensional x-ray analysis of normal movement in the lumbar spine*. Spine, Vol. 9, No. 3, pp. 294–297, 1984

[67] Pintar, F.-A.; Yoganandan, N.; Myers, T.; Elhagediab, A.; Sances, A.: *Biomechanical properties of human lumbar spine ligaments*. Journal of Biomechanics, Vol. 25, No. 11, pp. 1351–1356, 1992

[68] Putzer, M.; Auer, S.; Malpica, W.; Suess, F.; Dendorfer, S.: *A numerical study to determine the effect of ligament stiffness on kinematics of the lumbar spine during flexion*. BMC Musculoskeletal Disorders, Vol. 17, No. 1, 2016

[69] Putzer, M.; Ehrlich, I.; Rasmussen, J.; Gebbeken, N.; Dendorfer, S.: *Sensitivity of lumbar spine loading to anatomical parameters*. Journal of Biomechanics, Vol. 49, No. 6, pp. 953–958, 2016

[70] Quint, U.; Wilke, H.-J.; Shirazi-Adl, A.; Pamianpour, M.; Löer, F.; Claes, L. E.: *Importance of the intersegmental trunk muscles for the stability of the lumbar spine: a biomechanical study in vitro*. Spine, Vol. 23, No. 18, pp. 1937–1945, 1998

[71] Rasmussen, J.; Damsgaard, M.; Voigt, M.: *Muscle recruitment by the min/max criterion – a comparative numerical study*. Journal of Biomechanics, Vol. 34, No. 3, pp. 409–415, 2001

[72] Rasmussen, J.; de Zee, M.; Damsgaard, M.; Christensen, S.-T.; Marek, C.; Siebertz, K.: *A general method for scaling musculo-skeletal models*. In: *International Symposium on Computer Simulation in Biomechanics*. Cleveland, Ohio, USA, 2005

[73] Robie, B.; Dendorfer, S.; Rasmussen, J.; Christensen, S. T.: *Axial Rotation Requires Greatest Load in Multifidus Muscle*. In: *2011 Annual Meeting of the AANS/CNS Section on Disorders of the Spine and Peripheral Nerves*. 2011

[74] Rohlmann, A.; Graichen, F.; Bender, A.; Kayser, R.; Bergmann, G.: *Loads on a telemeterized vertebral body replacement measured in three patients within the first postoperative month*. Clinical Biomechanics, Vol. 23, No. 2, pp. 147–158, 2008

[75] Rohlmann, A.; Petersen, R.; Schwachmeyer, V.; Graichen, F.; Bergmann, G.: *Spinal loads during position changes*. Clinical Biomechanics, Vol. 27, No. 8, pp. 754–758, 2012

[76] Rohlmann, A.; Zander, T.; Graichen, F.; Bergmann, G.: *Effect of an orthosis on the loads acting on a vertebral body replacement*. Clinical Biomechanics, Vol. 28, No. 5, pp. 490–494, 2013

[77] Rohlmann, A.; Zander, T.; Graichen, F.; Bergmann, G.: *Lifting up and laying down a weight causes high spinal loads.* Journal of Biomechanics, Vol. 46, No. 3, pp. 511–514, 2012

[78] Rohlmann, A.; Zander, T.; Graichen, F.; Dreischarf, M.; Bergmann, G.: *Measured loads on a vertebral body replacement during sitting.* The Spine Journal, Vol. 11, No. 9, pp. 870–875, 2011

[79] Röhrle, H.; Scholten, R.; Sigolotto, C.; Sollbach, W.; Kellner, H.: *Joint forces in the human pelvis-leg skeleton during walking.* Journal of Biomechanics, Vol. 17, No. 6, pp. 409–424, 1984

[80] Sato, K.; Kikuchi, S.; Yonezawa, T.: *In vivo intradiscal pressure measurement in healthy individuals and in patients with ongoing back problems.* Spine, Vol. 24, No. 23, pp. 2468–2474, 1999

[81] Schendel, M. J.; Wood, K. B.; Buttermann, G. R.; Lewis, J. L.; Ogilvie, J. W.: *Experimental measurement of ligament force, facet force, and segment motion in the human lumbar spine.* Journal of Biomechanics, Vol. 26, No. 4-5, pp. 427–438, 1993

[82] Schiebler, T.-H.: *Anatomie. Histologie, Entwicklungsgeschichte, makroskopische und mikroskopische Anatomie, Topographie.* 9. vollständig überarbeitete Auflage, Springer, Berlin/Heidelberg/New York, 2006

[83] Schmidt, T.-A.; An, H.-S.; Lim, T.-H.; Nowicki, B.-H.; Haughton, V.-M.: *The stiffness of lumbar spinal motion segments with a high-intensity zone in the anulus fibrosus.* Spine, Vol. 23, No. 20, pp. 2167–2173, 1998

[84] Schünke, M.; Schulte, E.; Schumacher, U.: *Prometheus. Allgemeine Anatomie und Bewegungssystem.* 2. überarbeitete und erweiterte Auflage, Thieme, Stuttgart, 2007

[85] Scoles, P. V.; Linton, A. E.; Latimer, B.; Levy, M. E.; Digiovanni, B. F.: *Vertebral body and posterior element morphology: the normal spine in middle life.* Spine, Vol. 13, No. 10, pp. 1082–1086, 1988

[86] Sebro, R.; O'Brien, L.; Torriani, M.; Bredella, M. A.: *Assessment of trunk muscle density using CT and its association with degenerative disc and facet joint disease of the lumbar spine.* Skeletal Radiology, Vol. 45, No. 9, pp. 1221–1226, 2016

[87] Shin, D. S.; Lee, K.; Kim, D.: *Biomechanical study of lumbar spine with dynamic stabilization device using finite element method.* Computer-Aided Design, Vol. 39, No. 7, pp. 559–567, 2007

[88] Shin, J.-H.; Wang, S.; Yao, Q.; Wood, K. B.; Li, G.: *Investigation of coupled bending of the lumbar spine during dynamic axial rotation of the body.* European Spine Journal, Vol. 22, No. 12, pp. 2671–2677, 2013

[89] Shirazi-Adl, A.: *Nonlinear stress analysis of the whole lumbar spine in torsion–mechanics of facet articulation.* Journal of Biomechanics, Vol. 27, No. 3, pp. 289–299, 1994

[90] Srbinoska, H.; Dreischarf, M.; Consmüller, T.; Bergmann, G.; Rohlmann, A.: *Correlation between back shape and spinal loads.* Journal of Biomechanics, Vol. 46, No. 11, pp. 1972–1975, 2013

[91] Stokes, I. A.: *Mechanical function of facet joints in the lumbar spine.* Clinical Biomechanics, Vol. 3, No. 2, pp. 101–105, 1988

[92] Takahashi, I.; Kikuchi, S.-i.; Sato, K.; Sato, N.: *Mechanical load of the lumbar spine during forward bending motion of the trunk-a biomechanical study.* Spine, Vol. 31, No. 1, pp. 18–23, 2006

[93] Teichtahl, A. J.; Urquhart, D. M.; Wang, Y.; Wluka, A. E.; O'Sullivan, R.; Jones, G.; Cicuttini, F. M.: *Physical inactivity is associated with narrower lumbar intervertebral discs, high fat content of paraspinal muscles and low back pain and disability.* Arthritis Research & Therapy, Vol. 17, No. 1, 2015

[94] van Bolhuis, B.-M.; Gielen, C.-C.: *A comparison of models explaining muscle activation patterns for isometric contractions.* Biological Cybernetics, Vol. 81, No. 3, pp. 249–261, 1999

[95] Wagner, H.; Anders, C.; Puta, C.; Petrovitch, A.; Mörl, F.; Schilling, N.; Witte, H.; Blickhan, R.: *Musculoskeletal support of lumbar spine stability.* Pathophysiology, Vol. 12, No. 4, pp. 257–265, 2005

[96] Wang, S.; Park, W.-M.; Kim, Y.-H.; Cha, T.; Wood, K.; Li, G.: *In vivo loads in the lumbar L3-L4 disc during a weight lifting extension.* Clinical Biomechanics, Vol. 29, No. 2, pp. 155–160, 2014

[97] Ward, S. R.; Kim, C. W.; Eng, C. M.; Gottschalk 4th, L. J.; Tomiya, A.; Garfin, S. R.; Lieber, R. L.: *Architectural analysis and intraoperative measurements demonstrate the unique design of the multifidus muscle for lumbar spine stability.* Journal of Bone & Joint Surgery. American Volume, Vol. 91, No. 1, pp. 176–185, 2009

[98] Ward, S. R.; Tomiya, A.; Regev, G. J.; Thacker, B. E.; Benzl, R. C.; Kim, C. W.; Lieber, R. L.: *Passive mechanical properties of the lumbar multifidus muscle support its role as a stabilizer.* Journal of Biomechanics, Vol. 42, No. 10, pp. 1384–1389, 2009

[99] Weisse, B.; Aiyangar, A. K.; Affolter, C.; Gander, R.; Terrasi, G. P.; Ploeg, H.: *Determination of the translational and rotational stiffnesses of an L4-L5 functional spinal unit using a specimen-specific finite element model.* Journal of the Mechanical Behavior of Biomedical Materials, Vol. 13, pp. 45–61, 2012

[100] Whatley, B. R.; Wen, X.: *Intervertebral disc (IVD): Structure, degeneration, repair and regeneration.* Materials Science and Engineering: C, Vol. 32, No. 2, pp. 61–77, 2012

[101] Wilke, H.-J.; Claes, L.; Schmitt, H.; Wolf, S.: *A universal spine tester for in vitro experiments with muscle force simulation.* European Spine Journal, Vol. 3, No. 2, pp. 91–97, 1994

[102] Wilke, H.-J.; Neef, P.; Caimi, M.; Hoogland, T.; Claes, L.-E.: *New in vivo measurements of pressures in the intervertebral disc in daily life.* Spine, Vol. 24, No. 8, pp. 755–762, 1999

[103] Wilke, H.; Neef, P.; Hinz, B.; Seidel, H.; Claes, L.: *Intradiscal pressure together with anthropometric data–a data set for the validation of models.* Clinical Biomechanics, Vol. 16 Suppl 1, pp. 111–126, 2001

[104] Winter, D.-A.: *Biomechanics and Motor Control of Human Movement.* 3. Edition, John Wiley & Sons, New York, 2005

[105] Winter, D.-A.: *Biomechanics and Motor Control of Human Movement.* 4. Edition, John Wiley & Sons, New York, 2009

[106] Yoshihara, K.; Shirai, Y.; Nakayama, Y.; Uesaka, S.: *Histochemical changes in the multifidus muscle in patients with lumbar intervertebral disc herniation.* Spine, Vol. 26, No. 6, pp. 622–626, 2001

[107] Zander, T.; Rohlmann, A.; Calisse, J.; Bergmann, G.: *Estimation of muscle forces in the lumbar spine during upper-body inclination.* Clinical Biomechanics, Vol. 16 Suppl 1, pp. 73–80, 2001

[108] Zirbel, S. A.; Stolworthy, D. K.; Howell, L. L.; Bowden, A. E.: *Intervertebral disc degeneration alters lumbar spine segmental stiffness in all modes of loading under a compressive follower load.* The Spine Journal, Vol. 13, No. 9, pp. 1134–1147, 2013

A Appendix

A.1 Source code for hinge joint example

```
//Definition of global reference frame.
AnyFixedRefFrame GlobalRef = {};

//Definition of the segment.
AnySeg Segment = {
  Mass = 1;
  Jii = {0.001, 0.1, 0.1};
};

//Linear measurement.
AnyKinLinear LinearMeasurement = {
  AnyRefFrame &firstRef = .GlobalRef;
  AnySeg &secondRef = .Segment;
};

//Rotational measurement.
AnyKinRotational RotationalMeasurement = {
  AnyRefFrame &firstRef = .GlobalRef;
  AnySeg &secondRef = .Segment;
  Type = RotVector;   //definition of rotation sequence x, y, z
};

//Selecting five variables from both measurements.
AnyKinMeasureOrg MeasureOrganizer = {
  AnyKinLinear &firstMeasure = .LinearMeasurement;
  AnyKinRotational &secondMeasure = .RotationalMeasurement;
  MeasureOrganizer = {0,1,2, 3,4};
};

//Driver for creation of hinge joint only.
AnyKinEqSimpleDriver SimpleDriver = {
  AnyKinMeasureOrg &Input = .MeasureOrganizer;
  DriverPos = {0,0,0, 0,0};
  DriverVel = {0,0,0, 0,0};
  DriverAcc = {0,0,0, 0,0};
};

//Alternative driver to create a hinge joint and control motion
//around the z-axis. Use this driver to get a kinematically
```

```
//determined model and comment all other drivers and measure
//organizers.
//AnyKinEqSimpleDriver SimpleDriver = {
//AnyKinLinear &Input1 = .LinearMeasure;
//AnyKinLinear &Input2 = .RotationalMeasure;
//DriverPos = {0,0,0, 0,0,0};
//DriverVel = {0,0,0, 0,0,0.1};  //rotational velocity of 0.1 rad/s
                                 //around the z-axis
//DriverAcc = {0,0,0, 0,0,0};
//};
```

A.2 Importing data of bony landmarks

Below is the source code of the utilised Python script and its AMS hook to import landmark data generated by MeshLab. Each section is accompanied by a short description of the method.

A.2.1 The script

The following Python script reads positional data from an XML file and returns it in a matrix. After opening the file stated in its arguments, it reads its content line by line. Each line is parsed for the three coordinates and a final check ensures that the current landmark is active. Finally, the accumulated data is formatted in proper form and after closing the file the data is returned to its calling function.

```
  import optparse
  import re
  import os

  def ReadMLFile(context,filename, path = None):
    filelocation = os.path.join(path, filename)
    fin = open(filelocation, 'r')
    output =[]
    cnt = 0
    for line in fin:
      m = re.search('<point x="', line)
      if m == None:
        continue
      line = line[:m.start()] + line[m.end():]
      m = re.search('" y="', line)
      line = line[:m.start()] + ' ' + line[m.end():]
      m = re.search('" z="', line)
      line = line[:m.start()] + ' ' + line[m.end():]
      m = re.search('" active="1" name="', line)
      line = line[:m.start()] + ' ' + line[m.end():]
      m = re.search('"/>', line)
      res = line[:m.start()].split()
```

```
23      vec = [float(res[0]), float(res[1]), float(res[2])]
24      output.append(tuple(vec))
25      fin.close()
26      return tuple(output)
```

A.2.2 Example for usage of the hook

Below is an example for the usage of the PYTHON hook in the AMS. It demonstrates the import procedure of landmark data for the L5 vertebra. The first ten lines declare the wrapper function which can be used in the subsequent ANYBODY code. Line #1 states the functions name and line #2 the design of its return values. Next is the type of the function (`AnyFunExMonoPy` equates a PYTHON function) and its name (`ReadMLFile`) in the PYTHON script. The `ModuleFile` argument defines the file which includes the PYTHON function while the `ArgList` statement declares the according arguments without assigning a value. Line #11 and #12 assign necessary file names and paths to variables. Finally, the PYTHON function is called with the according arguments (Line #13).

```
1   AnyFunEx FunCEx = { //Wrapper function for external applications
2     AnyMatrix Return = {iarr(1,.Size)*0,iarr(1,.Size)*0,iarr(1,.Size
     )*0}';
3     AnyFunExMonoPy ReadMLFile = { //\gls{API} for Python functions
4       ModuleFile = "ReadMeshlabIn.py"; //Python script
5       ArgList = { //Argument list
6         AnyStringVar filename = "";
7         AnyStringVar path = "";
8       };
9     };
10  };
11  AnyFileVar thisfile = namestr+"ScalingSTLRBF.any"; //Get the
     current filename
12  AnyStringVar thisfile_path = FilePathReferenceOf(thisfile); //Get
     the current filepath
13  AnyMatrix P1 =  FunCEx("L5_processed_picked_points.pp",
     thisfile_path+"\PickedPoints\"); //Start the import
```

A.3 Leg muscles

All leg muscles in the model are listed in Table A.1. There is no specific order of appearance.

Table A.1: Leg muscles implemented and activated in the generic full body model from the AMMR.

No.	Name	No.	Name
1	soleus	18	gracilis
2	gastrocnemius	19	iliopsoas
3	flexor digitorum longus	20	gluteus minimus
4	flexor hallucis longus	21	gluteus medius
5	tibialis posterior	22	gluteus maximus
6	peroneus brevis	23	tensor fasciae latae
7	tibialis anterior	24	piriformis
8	extensor digitorum longus	25	adductor longus
9	extensor hallucis longus	26	adductor magnus
10	vasuts lateralis	27	quadratus femoris
11	vastus medialis	28	abductor brevis
12	vastus intermedius	29	obturatorius internus
13	rectus femoris	30	obturatorius externus
14	semitendinosus	31	pictineus
15	biceps femoris caput longum	32	gemmelus inferior
16	biceps femoris caput breve	33	gemmelus superior
17	sartorius		

A.4 Translational lumbar disc stiffness

An optional non-linear translational stiffness at the lumbar discs is incorporated in the model for application with the FDK solver. The publication providing information about the rotational disc stiffness also gives detail about this translational stiffness [99]. Table A.2 lists necessary parameters P_1 and P_2 for the translational stiffness of the form

$$k = P_1 \cdot P_2 \cdot e^{P_2 \cdot \Delta l} \tag{A.1}$$

which is the foundation for the programmed stiffness. Δl represents the corresponding translation displacement. This translational stiffness can be activated in the model with a switch and it requires the non-linear rotational stiffness and the FDK solver.

The structure of implementation is similar to the one for the non-linear rotational disc stiffness, described in Section 4.1.7. At first, the current direction of translation has to be determined for compression/tension and anterior/posterior shear by simple value comparison of the current position. The results are saved in parameters A and B for compression and tension and C and D for posterior and anterior shear. Each parameter has either

Table A.2: Parameters P_1 and P_2 required in Equation A.1 for different configurations to model the translational lumbar disc stiffness. This data is provided by Weisse et al. [99].

Direction	P_1 (N)	P_2 (mm^{-1})	Ligaments & facets
Lateral shear	222	0.738	stiffness included in disc stiffness
Anterior shear	726	0.450	
Posterior Shear	145	0.649	
Compression	221	1.810	
Tension	415	0.993	
Lateral shear	200	0.696	present as individual elements with a stiffness value
Anterior shear	160	0.578	
Posterior Shear	161	0.600	
Compression	368	1.260	
Tension	865	0.449	

a value of one or zero which depends on the current translation. Therefore, the parameters of a single pair (A, B) or (C, D) have always different values. Afterwards, the force acting against a motion in cranial-caudal direction is calculated by

$$F = -1 \cdot (A \cdot k_c \cdot \Delta l + B \cdot k_t \cdot \Delta l) \cdot s \tag{A.2}$$

where k_c and k_t are the stiffness coefficients for compression and tension according to Equation A.1, Δl is the corresponding translational displacement and s is the scaling factor described in Section 4.1.7. Similarly, the force in anterior-posterior direction is calculated by

$$F = -1 \cdot (C \cdot k_p \cdot \Delta l + D \cdot k_a \cdot \Delta l) \cdot s. \tag{A.3}$$

Again, the stiffness coefficients for posterior shear k_p as well as anterior shear k_a are calculated according to Equation A.1. The force in the third direction, the medio-lateral direction, is calculated by

$$F = -1 \cdot k_{lat} \cdot \Delta l \cdot s \tag{A.4}$$

where k_{lat} is the corresponding stiffness coefficient for lateral shear.

A.5 Validation: description of postures

The following Table A.3 lists the most important joint angles used throughout validation simulations.

Table A.3: Important driver and mannequin settings for various joints to set up the models in the postures for validation.

Joint	Value	Joint	Value
Standing		*Standing flexed forward*	
Thorax flexion-extension	0°	Thorax flexion-extension	−50°
Thorax lateral bending	0°	Thorax lateral bending	0°
Thorax axial rotation	0°	Thorax axial rotation	0°
Seating relaxed		*Seating straight with no support*	
Backrest inclination	30°	Backrest inclination	0°
Legrest inclination	10°	Legrest inclination	0°
Thorax lateral bending	0°	Thorax lateral bending	0°
Thorax axial rotation	0°	Thorax axial rotation	0°
Glenohumeral Flexion	30°	Glenohumeral Flexion	10°
Glenohumeral External Rotation	−14°	Glenohumeral External Rotation	−14°
Elbow Flexion	77°	Elbow Flexion	97°
Elbow Pronation	90°	Elbow Pronation	90°
Hip Flexion	85°	Hip Flexion	85°
Hip Abduction	0.5°	Hip Abduction	0.5°
Hip External Rotation	0.05°	Hip External Rotation	0.05°
Knee flexion	75°	Knee flexion	75°
Ankle Plantar Flexion	−10°	Ankle Plantar Flexion	−10°
Standing lift close		*Standing lift flexed*	
Thorax flexion-extension	0°	Thorax flexion-extension	−45°
Thorax lateral bending	0°	Thorax lateral bending	0°
Thorax axial rotation	0°	Thorax axial rotation	0°
Glenohumeral Flexion	−15°	Glenohumeral Flexion	89°
Glenohumeral Abduction	10°	Glenohumeral Abduction	10°
Glenohumeral External Rotation	0°	Glenohumeral External Rotation	−5°
Elbow Flexion	89.5°	Elbow Flexion	10°
Elbow Pronation	0°	Elbow Pronation	0.5°
Hip Flexion	5°	Hip Flexion	85°
Hip Abduction	12°	Hip Abduction	11°
Hip External Rotation	−0.5°	Hip External Rotation	−0.5°
Knee flexion	10°	Knee flexion	20°
Ankle Plantar Flexion	3.6°	Ankle Plantar Flexion	3.6°
Standing lift stretched arms		*Lying on the back*	
Thorax flexion-extension	0°	Backrest inclination	90°
Thorax lateral bending	0°	Legrest inclination	90°
Thorax axial rotation	0°	Footrest linear y position of	

Glenohumeral Flexion	30°	Model 1	0.139 m
Glenohumeral Abduction	10°	Model 2	0.097 m
Glenohumeral External Rotation	0°	Model 3	0.096 m
		Model 4	0.128 m
Elbow Flexion	60°	Model 5	0.050 m
Elbow Pronation	0°	Thorax lateral bending	0°
Hip Flexion	5°	Thorax axial rotation	0°
Hip Abduction	12°	Glenohumeral Flexion	2°
Hip External Rotation	−0.5°	Glenohumeral Abduction	5°
Knee flexion	10°	Glenohumeral External Rotation	−14°
Ankle Plantar Flexion	3.6°		
		Elbow Flexion	2°
		Hip Abduction	0.5°
		Elbow Pronation	50°
		Hip Flexion	2°
		Hip External Rotation	0.05°
		Knee flexion	5°
		Ankle Plantar Flexion	−10°

A.6 Results

Below are additional figures of results which are excluded from the main document but are relevant for reference purposes.

A.6.1 Validation: progression

Figure A.1 and Figure A.2 show the comparison of the L4/L5 IDP between the five simulated models and literature data [103] during basic motions. Each set of three diagrams represents one of the two configurations missing in the validation results section.

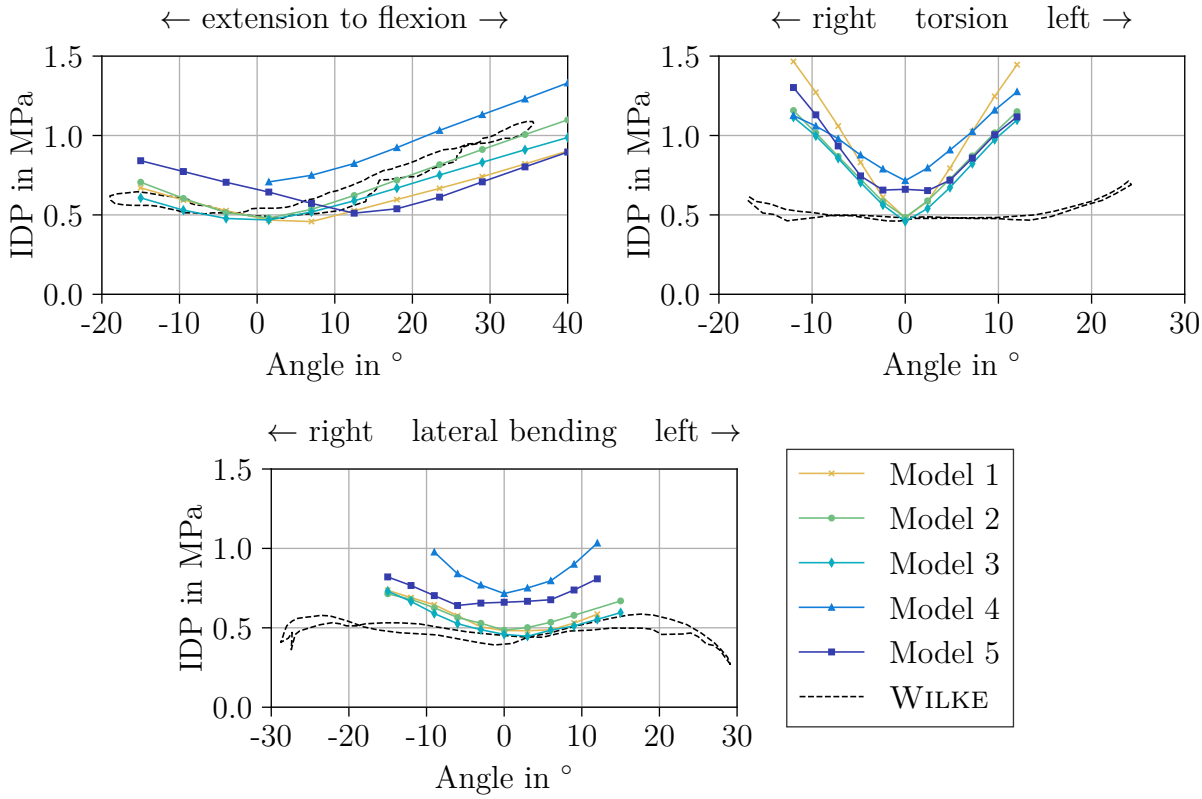

Figure A.1: Comparison of the L4/L5 IDP during basic motions between simulation and literature data [103]. The models are configured with a linear disc stiffness, ligaments calibrated in groups, no facet capsular ligament, an active contact between facet surfaces and FDK. This corresponds to the model configuration in the second sensitivity study.

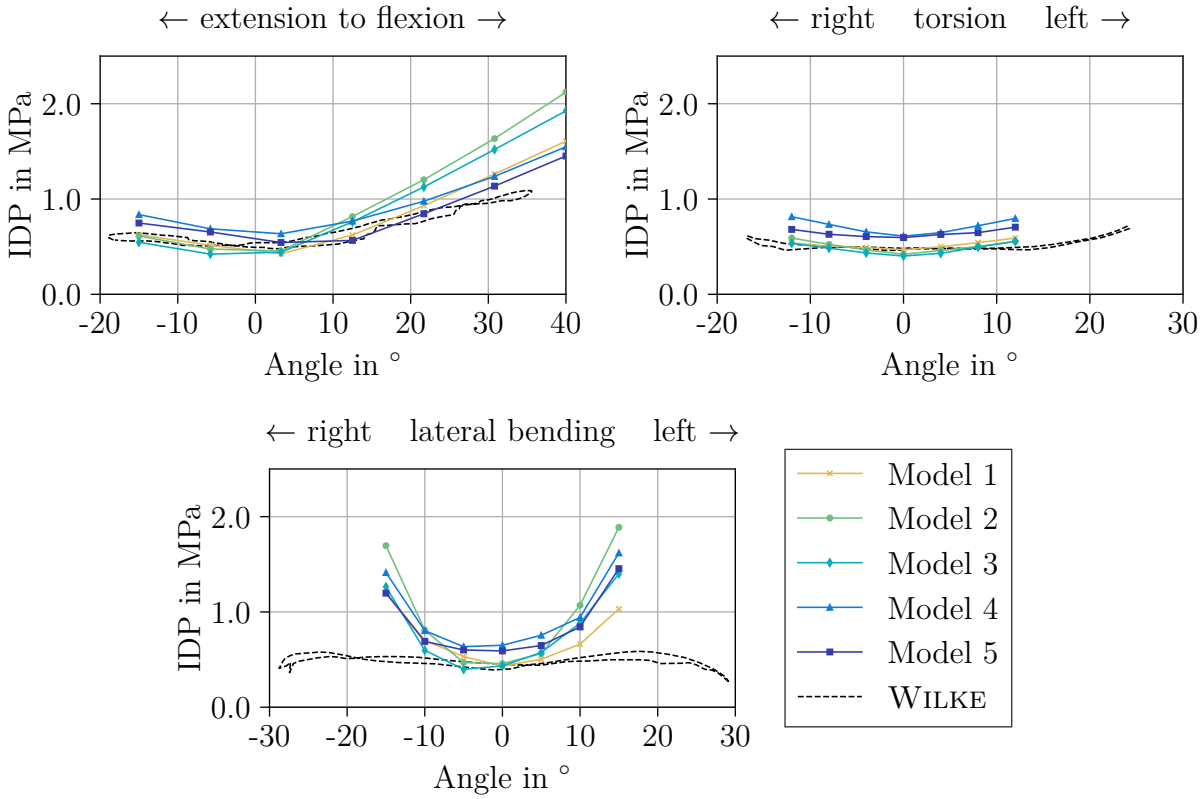

Figure A.2: Comparison of the L4/L5 IDP during basic motions between simulation and literature data [103]. Configuration of the models correspond to the third study with an activated spine rhythm. It includs individual calibration of ligament elements, a non-linear disc stiffness with active scaling, surface contact between facets and the FCL was activated.

A.6.2 Validation: relative differences

The following two figures depict the validation of relative differences of IDP between various postures for the two additional model configurations which are not included in the results section.

Figure A.3 depicts the relative changes of IDP at the L4/L5 level for the configuration used in the second sensitivity study. It uses a linear disc stiffness, ligaments calibrated in groups, no facet capsular ligament, an active contact between facet surfaces and the FDK solver.

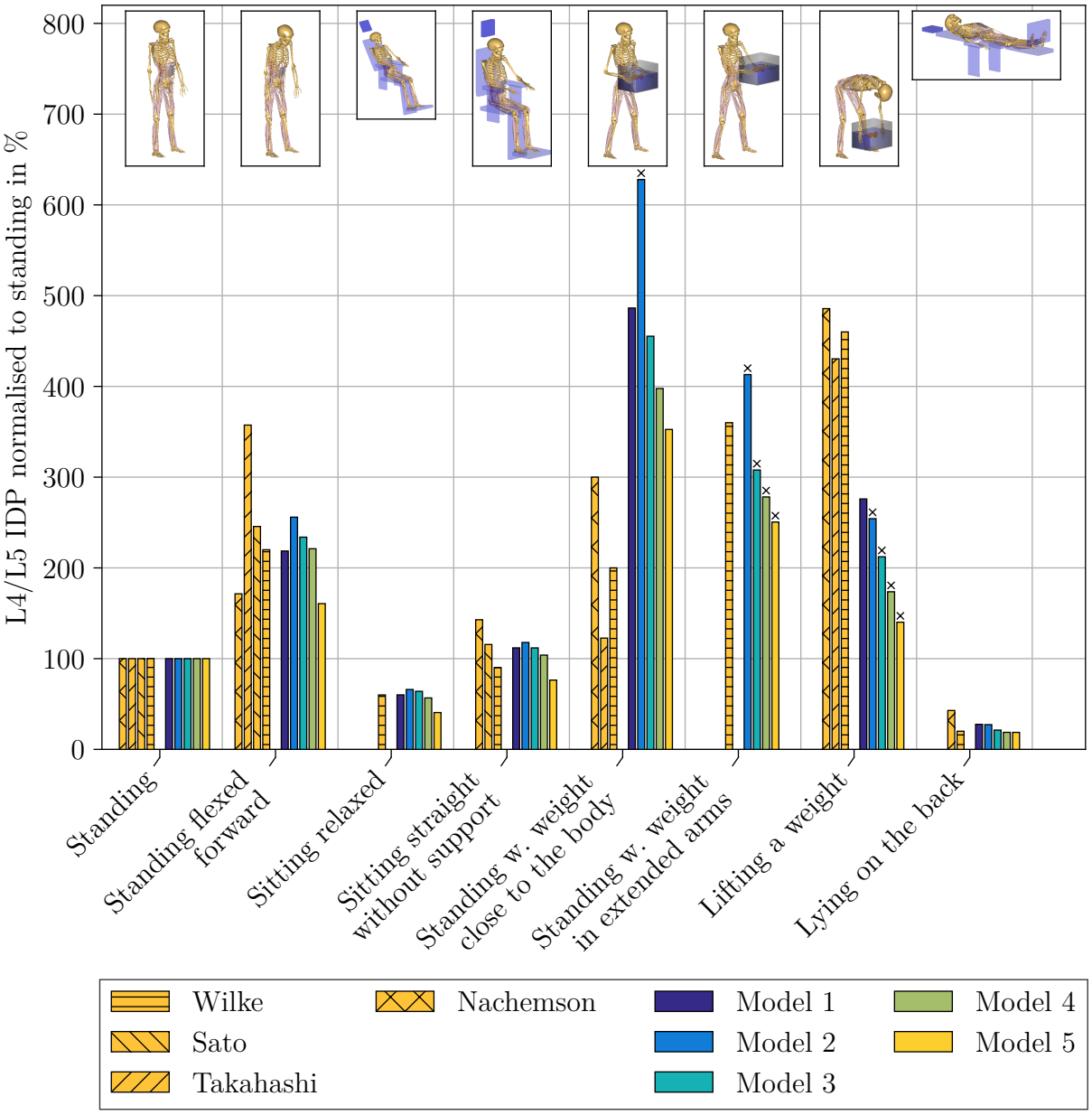

Figure A.3: Relative changes of the IDP for configuration one (Table 4.8).

Figure A.4 illustrates the relative differences of IDP for the configuration used in the case study. It includes a non-linear disc stiffness, ligaments calibrated individually, an active surface contact between facets and the facet capsular ligament. The kinematics of the lumbar spine are computed with the spine rhythm.

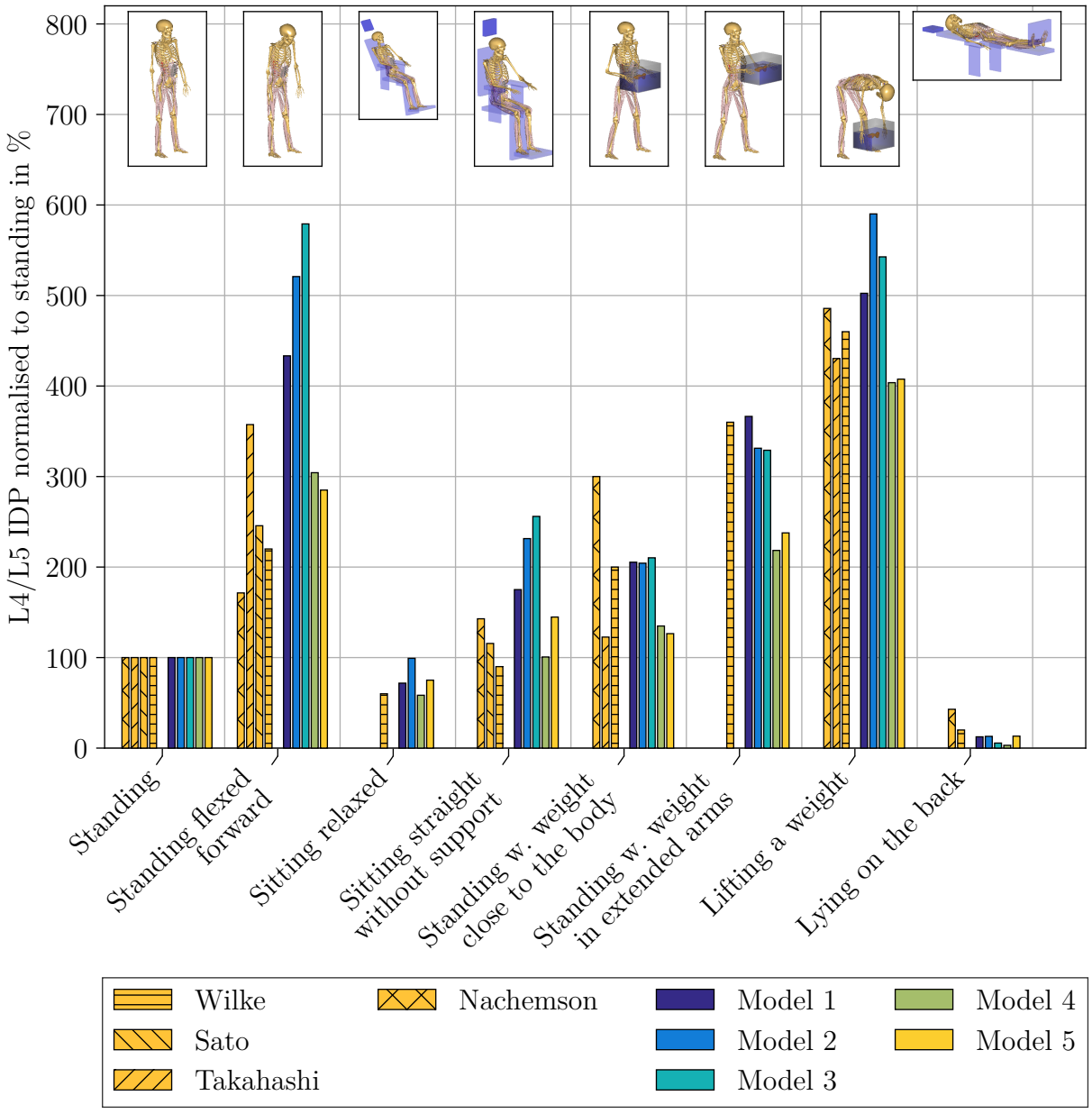

Figure A.4: Relative changes of the IDP for configuration three (Table 4.8).

A.6.3 Study 3: disc forces

Table A.4 lists the loading of all lumbar discs in percent for all model-motion combinations. The list differentiates between a healthy and an atrophic multifidus muscle group. Furthermore, results of both kinematic options are included.

Table A.4: Lumbar disc loading in percent when referencing a fully degenerated disc to its intact state. Listed are values of every lumbar level and all motions with the models in two configurations: first with healthy (H) multifidus muscles and second with atrophic (A) ones.

FDK		T12/L1		L1/L2		L2/L3		L3/L4		L4/L5	
		H	A	H	A	H	A	H	A	H	A
Model 1	Standing	104	104	104	104	103	103	101	101	83	83
	Flexion	98	97	95	94	94	93	95	94	96	94
	Lateral bending	102	103	102	103	103	103	103	103	89	89
	Axial rotation	96	98	96	99	96	99	96	98	76	75
Model 2	Standing	101	101	100	101	100	100	100	100	84	84
	Flexion	99	99	95	95	95	94	95	94	94	92
	Lateral bending	103	103	103	103	103	103	103	104	89	90
	Axial rotation	95	95	94	94	94	94	94	95	79	84
Model 3	Standing	99	99	100	100	100	100	100	101	91	92
	Flexion	99	99	95	95	96	95	96	95	95	94
	Lateral bending	100	98	100	99	101	101	103	103	93	96
	Axial rotation	95	93	94	92	93	91	95	94	88	87
Model 4	Standing	108	108	109	108	108	108	105	105	83	83
	Flexion	98	98	97	98	98	98	96	98	95	98
	Lateral bending	107	107	107	107	108	108	108	107	93	92
	Axial rotation	98	98	98	98	98	97	97	96	76	78
Model 5	Standing	97	97	96	96	96	96	96	96	79	79
	Flexion	99	98	96	95	96	95	97	96	97	97
	Lateral bending	–	–	–	–	–	–	–	–	–	–
	Axial rotation	96	96	95	94	95	94	95	95	83	83
Spine rhythm		T12/L1		L1/L2		L2/L3		L3/L4		L4/L5	
		H	A	H	A	H	A	H	A	H	A
Model 1	Standing	100	103	100	104	99	103	98	100	98	101
	Flexion	106	119	112	128	112	129	111	128	114	139
	Lateral bending	109	109	109	110	111	112	109	113	109	114
	Axial rotation	102	106	103	106	101	105	100	103	99	103
Model 2	Standing	106	111	105	108	105	107	103	105	102	104
	Flexion	106	115	113	123	113	123	114	123	118	131
	Lateral bending	120	120	118	120	120	121	121	120	118	119

	Axial rotation	100	101	100	100	99	99	98	98	95	96
Model 3	Standing	97	98	100	101	103	103	105	107	104	107
	Flexion	107	103	117	114	117	114	119	117	117	119
	Lateral bending	122	126	117	120	114	113	119	117	107	109
	Axial rotation	98	100	101	101	102	100	102	100	97	98
Model 4	Standing	104	99	104	100	106	101	102	101	103	103
	Flexion	103	127	102	124	102	122	103	125	104	127
	Lateral bending	111	112	108	112	108	111	109	112	105	110
	Axial rotation	102	107	101	105	100	105	97	100	97	101
Model 5	Standing	102	101	105	105	106	107	106	108	109	111
	Flexion	107	113	107	113	106	113	110	118	111	118
	Lateral bending	–	–	–	–	–	–	–	–	–	–
	Axial rotation	103	106	108	110	111	115	108	114	107	115